

**A Fundamental Study on the Surface Binding Isotherms
of Carbon Dots Bound with Heavy Metal Ions In View of
Its Potential as Innovative Optical Sensing Receptors**

By

Ng Yann Huey

A thesis submitted in fulfillment
of the requirements for the degree of
Master of Science by Research

Faculty of Engineering, Computing and Science,
Swinburne University of Technology Sarawak Campus,
Malaysia

2016

Abstract

Carbon dots (CDs) as an emerging nanomaterial has attracted tremendous research attention due to their superior properties. Intensive research studies have been focusing on exploring the potential of CDs for various applications. CDs are especially being widely investigated on their potential for chemical sensing. Although it is generally mentioned that better interaction between surface functionalized CDs and targeted analytes will lead to more obvious change in optical signal, it has not been proven yet until now. This research project was conducted to produce CDs from sustainable organic precursors via simple acid hydrolysis and thermal pyrolysis method. The CDs synthesized from α -cellulose via acid hydrolysis approach were found to exhibit two different fluorescence emissions under different synthetic conditions. The properties of these two CDs were investigated and the results showed that the CDs emitting blue photoluminescence (PL) were comparatively more stable than the green emitting CDs. CDs synthesized via thermal pyrolysis of α -cellulose was isolated and proceed further by functionalization with Tris(hydroxymethyl)aminomethane (TRIS). The TRIS-functionalized CDs were found responsive positively towards cobalt (II) ions, (Co(II)) where significant fluorescence quenching was observed in its presence. The binding isotherms study using spectroscopic technique had proven that better interaction between surface functionalized CDs and targeted metal ions resulted in better binding affinity, hence led to significant change in optical signal. In addition, interface study of CDs produced from L-glutamic acid through thermal carbonization and its potential as metal ion sensing receptors was investigated. The CDs were then surface functionalized with chitosan and the results showed that chitosan functionalized CDs exhibited enhanced sensitivity towards mercuric (II) ions, (Hg(II)) compared to the bare CDs. In summary, CDs were successfully synthesized from both α -cellulose and L-glutamic acid via facile acid carbonization and/or thermal pyrolysis method. Surface functionalization was found to enhance the sensitivity and selectivity of CDs towards metal ions sensing. The correlation between binding affinity resulted from binding interaction towards change in optical signal was established. The findings can be potentially used as reference for future development of CDs as metal ions sensing receptors.

Acknowledgement

Foremost, I would like to express my sincere appreciation to my principal coordinating supervisor, Dr. Ng Sing Muk for his persistent guidance and inspiring motivation throughout my study. His continuous support and immense knowledge steered me in the right direction especially when I ran into trouble spots. Besides, I would also like to express my genuine gratitude to my co-supervisors, A/Prof. Dr. Chin Suk Fun and Prof. Dr. Pang Suh Cem for their insightful comments and encouragement during my research.

I would like to further extend my gratitude to Dr. Paul Neilsen, Dr. Irine Ginjom, Dr. Hwang Siaw San and A/Prof. Dr. Peter Morin Nisson for sharing their experiences and valuable advice. My heartfelt thanks also go to the Biosafety officer, Ms. Chua Jia Ni as well as all the science laboratory staffs: Ms. Nurul Arina, Ms. Cinderella, Ms. Marciana Jane and Mdm. Dayang Rafika for their gracious assistance.

In addition, special thanks also go to the awesome bunch of friends cum lab mates for stimulating discussions and inspirations. They have make life a lot more fun and I cherish the joyful and unforgettable moments that we have had together.

I would also like to acknowledge the Ministry of Higher Education Malaysia for providing Fundamental Research Grant Scheme (Ref: FRGS/2/2013/SG06/SWIN/03/1) to support the study and make this dissertation possible.

Last but not least, I would like to express my deepest appreciation to my family for providing me with loving encouragement and unfailing support throughout my years of study. This accomplishment would not have been possible without them.

Declaration

I, Ng Yann Huey, higher degree research student of Master of Science by Research from Faculty of Engineering, Computing and Science (FECS), Swinburne University of Technology Sarawak Campus hereby declare that this dissertation is original and contains no material which has been accepted for the award to the candidate of any other degree or diploma, except where due reference is made in the text of the examinable outcome. To the best of my knowledge, this thesis contains no material previously published or written by another person except where due reference is made in the text of the examinable outcome; and where the work is based on joint research or publications, discloses the relative contributions of the respective workers or authors.

(NG YANN HUEY)

As the principal coordinating supervisor, I hereby acknowledge and certify that the above mentioned statements are legitimate to the best of my knowledge.

(DR. NG SING MUK)

Conference Presentations

1. Ng, YH, Chin, SF, Pang, SC & Ng, SM 2015, 'Synthesis of green carbon dots as potential mercuric(II) ions sensing probe', *28th Regional Symposium of Malaysia Analytical Sciences (SKAM28), Ipoh, Malaysia, August 17 – August 20, 2015.*
2. Ng, YH, Chin, SF, Pang, SC & Ng, SM 2016, 'Interface study on carbon dots using fluorometric technique and its potential as metal ions sensing receptors', *EUROPT(R)ODE XIII, Graz, Austria, March 20 – March 23, 2016.*

Conference Award

1. 'The Best Poster for Content', *28th Regional Symposium of Malaysia Analytical Sciences (SKAM28), Ipoh, Malaysia, August 17 – August 20, 2015.*

Table of Contents

Abstract.....	I
Acknowledgement.....	II
Declaration.....	III
Conference Presentations	IV
Conference Award	IV
List of Figures	IX
List of Tables.....	XIV
List of Abbreviations.....	XV
Chapter 1 Introduction	1
1.1 Research Background.....	1
1.2 Research Motivations and Challenges.....	3
1.3 Research Objectives	4
1.4 Research Approaches.....	5
1.5 Organization of Thesis	6
Chapter 2 Literature Review	8
2.1 Executive Summary.....	8
2.2 Luminescence	9
2.2.1 Photoluminescence	9
2.2.2 Chemiluminescence	11
2.3 Instrumental Analysis.....	13
2.3.1 Fluorescence Spectroscopy	13
2.3.2 Ultraviolet and Visible Spectroscopy	14
2.4 Carbonaceous Materials.....	17
2.5 Synthesis of CDs	19
2.5.1 Top-Down Approach.....	19
2.5.2 Bottom-Up Approach.....	21

2.6 Properties of CDs	22
2.6.1 Chemical structure and composition.....	22
2.6.2 Absorbance and photoluminescence.....	23
2.6.3 Up-conversion Luminescence and Electrochemiluminescence	25
2.6.4 Photoluminescence mechanism	26
2.6.5 Quantum Yield (QY)	29
2.7 Post-Synthetic Strategies	30
2.8 Applications of CDs	32
2.8.1 Bio-imaging/Bio-labelling	32
2.8.2 Theranostics	34
2.8.3 Bio-sensing.....	36
2.8.4 Photocatalysis	38
2.8.5 Chemical Sensing	40
Chapter 3 Synthesis of Carbon Dots.....	43
3.1 Executive Summary.....	43
3.2 Introduction.....	44
3.3 Experimental Design.....	45
3.3.1 Materials and Reagents.....	45
3.3.2 Instrumentations	46
3.3.3 Synthesis of CDs via Acid Hydrolysis of α -Cellulose	47
3.3.4 Isolation of Acid hydrolysed CDs Sample	47
3.3.5 Synthesis and Isolation of CDs (Thermal Carbonization)	48
3.3.6 Thermal Carbonization of L-Glutamic Acid	48
3.4 Results and Discussion	49
3.4.1 Acid hydrolysis of α -Cellulose.....	49
3.4.1.1 Optical Properties.....	49
3.4.1.2 PL properties during carbonization.....	52

3.4.1.3 Characterizations of CDs	57
3.4.1.4 Effect of pH and CDs Isolation	59
3.4.2 Thermal Carbonization of α -Cellulose	62
3.4.2.1 Characterization of CDs	62
3.4.2.2 Effect of Pyrolysis Conditions	65
3.4.2.3 Effect of pH	69
3.4.3 Thermal Carbonization of L-Glutamic Acid	70
3.4.3.1 Effect of Pyrolysis Conditions	70
3.4.3.2 Characterization of CDs	73
3.5 Conclusions	78
Chapter 4 Interface Study on Carbon Dots and Its Potential as Metal Ions	
Sensing Receptors	80
4.1 Executive Summary	80
4.2 Introduction	81
4.3 Experimental Design	82
4.3.1 Materials and Reagents	82
4.3.2 Instrumentations	83
4.3.3 Surface Modification of CDs	83
4.3.4 Metal Ions Sensing Potential	84
4.4 Results and discussion	85
4.4.1 Potential of CDs _{Green} as Metal Ions Sensing Receptors	85
4.4.1.1 Assay for Hg(II) Ions Detection	85
4.4.1.2 Detection Assay on Real Water Samples	87
4.4.2 Potential of CDs _{Blue} as Metal Ions Sensing Receptors	90
4.4.2.1 Detection Assay for Fe(III) Ions	90
4.4.3 Interface Study of Bare CDs _{Glu} and Interaction with Chitosan	92
4.4.3.1 Surface Modification with Chitosan	92

4.4.3.2 Interference Study.....	96
4.4.4 Surface Functionalization of CDs ₂₅₀ with TRIS.....	98
4.4.4.1 Interaction between CDs ₂₅₀ and TRIS.....	98
4.4.4.2 Potential in Metal Ions Sensing.....	99
4.5 Conclusions.....	102
Chapter 5 Binding Isotherms of Carbon Dots.....	103
5.1 Executive Summary.....	103
5.2 Introduction.....	104
5.3 Experimental Design.....	105
5.3.1 Materials and Reagents.....	105
5.3.2 Spectroscopic Determination of Binding Isotherms.....	105
5.3.3 Encapsulation of CDs.....	105
5.4 Results and discussion.....	106
5.4.1 Binding Isotherms Analysis.....	106
5.4.1.1 Absorption and Stoichiometry of Co(II)-CDs ₂₅₀ /TRIS Complex.....	106
5.4.1.2 Stern-Volmer Analysis.....	110
5.4.1.3 Double Log Regression Model.....	112
5.4.1.4 Modified Scatchard Method.....	114
5.4.2 CDs Immobilization on Alginate Beads.....	117
5.5 Conclusions.....	120
Chapter 6 Further Works and Conclusions.....	121
6.1 Executive Summary.....	121
6.2 Project Summary.....	121
6.3 Project Limitations.....	122
6.4 Further Works.....	123
References.....	124

List of Figures

Figure 2.1: Jablonski diagram illustrates typical light absorption and emission processes.	9
Figure 2.2: Schematic diagram of essential components of a fluorescence spectrophotometer.....	14
Figure 2.3: Possible electron transitions between molecular orbitals.....	15
Figure 2.4: Three different types of CDs that are structurally distinct (Adopted from [15])......	18
Figure 3.1: CDs synthesized from α -cellulose via sulphuric acid hydrolysis approach under (a) visible light and (b) UV light exposure.	49
Figure 3.2: The (a) absorption, (b) optimum excitation and (c) emission spectrum of CDs _{Green} prepared by acid hydrolysis approach. Inset illustrates that emission of CDs _{Green} is independent on the excitation wavelength.....	50
Figure 3.3: The (a) absorption, (b) optimum excitation and (c) emission spectrum of CDs _{Blue} obtained by sulphuric acid hydrolysis method. Inset illustrates that emission of CDs _{Blue} is independent on the excitation wavelength.....	50
Figure 3.4: Variation of fluorescence intensity of CDs synthesized at 50 °C monitored at (a) 500 nm and (b) 456 nm.	52
Figure 3.5: Variation of fluorescence intensity monitored at (a) 500 nm and (b) 456 nm for CDs prepared at 4 °C, 24 °C and 70 °C.....	53
Figure 3.6: 3-dimensional scan of CDs prepared by incubation at 50 °C for 1.5 hours.....	55
Figure 3.7: CDs synthesized by mixing the reactants at (a) 4 °C for 10 minutes incubation and subsequently at 24 °C, and (b) 24 °C without incubation at 4 °C.	56
Figure 3.8: Fluorescence intensity of (a) CDs _{Blue} and (b) CDs _{Green} monitored at emission wavelengths of 456 nm and 500 nm, respectively.....	57

Figure 3.9: FTIR absorption spectra of (a) untreated α -cellulose, (b) CDs _{Green} and (c) CDs _{Blue}	58
Figure 3.10: Variation of fluorescence intensity of CDs _{Blue} and CDs _{Green} in aqueous solutions of different pH values.	60
Figure 3.11: TEM image of CDs _{Blue} synthesized from α -cellulose via acid dehydration method.	61
Figure 3.12: The (a) absorbance, (b) excitation and (c) emission spectrum of CDs synthesized from α -cellulose via thermal carbonization. Inset: Photograph of ultrapure water (left) and CDs (right) under exposure of UV light.....	62
Figure 3.13: FTIR absorption spectrum for (a) untreated α -cellulose and (b) CDs carbonized in furnace at 250 °C for 30 minutes.	63
Figure 3.14: Photostability measurement of CDs ₂₅₀ monitored at 435 nm upon excitation at 346 nm for 60 minutes.	64
Figure 3.15: Photographs of (a) untreated α -cellulose and the products after thermal pyrolysis at different temperatures of (b) 200 °C, (c) 225 °C, (d) 250 °C, (e) 275 °C, (f) 300 °C, (g) 350 °C and (h) 400 °C.....	65
Figure 3.16: Emission of CDs carbonized at different temperatures monitored at 435 nm upon excitation at 346 nm. Inset: Emission spectrum of CDs synthesized at different temperatures.	66
Figure 3.17: Emission of CDs synthesized from α -cellulose treated at 250 °C in furnace at different time variation monitored at 435 nm.	68
Figure 3.18: (a) Variation of fluorescence intensity and (b) fluorescence emission spectrum of CDs ₂₅₀ in aqueous solutions of different pH values.....	69
Figure 3.19: Schematic diagram of CDs formation from L-glutamic acid.	70
Figure 3.20: Photographs of CDs synthesized by thermal pyrolysis of L-glutamic acid at different temperature under (a) visible light and (b) UV exposure.....	71

Figure 3.21: Variation of fluorescence intensity monitored at 440 nm when excited at 365 nm for CDs prepared at different temperatures. ...	72
Figure 3.22: The (a) absorbance, (b) excitation and (c) emission spectrum of CDs _{Glu} synthesized by thermal pyrolysis of L-glutamic acid.....	73
Figure 3.23: (a) Fluorescence emission spectra of CDs _{Glu} excited at increasing excitation wavelength from 330 nm to 410 nm; (b) Contour plot of fluorescence spectrum of CDs _{Glu}	74
Figure 3.24: Fluorescence emission spectrum of CDs _{Glu} suspended in ultrapure water and sodium acetate/acetic acid buffer with pH5.43.....	76
Figure 3.25: Plot of integrated fluorescence intensity versus absorbance for quantum yield determination of CDs _{Glu} (red line) using quinine sulphate (blue line) as standard.....	76
Figure 3.26: Photostability measurement of CDs _{Glu} monitored at 440 nm upon excitation at 365 nm for 60 minutes.	77
Figure 4.1: The normalized fluorescence intensity of CDs _{Green} recorded at 500 nm in the presence of different metal ions at concentration of 16.08 μM . The line represents the baseline of initial intensity in the absence of metal ions.	85
Figure 4.2: Photographs of CDs _{Green} incubated with different metal ions taken under (a) visible light and (b) UV exposure.	86
Figure 4.3: The effect of quenching on the fluorescence intensity of CDs _{Green} in the presence of Hg(II) ions at different concentrations monitored at 500 nm.....	87
Figure 4.4: Stern-Volmer plot shows the dependence of F_0/F_x on the concentrations of Hg(II) ions within the range of 0 - 160 μM	88
Figure 4.5: Relative intensity of CDs _{Blue} at 500 nm in the presence of different metal ions at concentration of 400 μM	90
Figure 4.6: Stern-Volmer plot shows the dependence of F_0/F_x on the concentrations of Fe(III) ions within the range of 80-1960 μM	91

Figure 4.7: Absorption, fluorescence excitation and emission spectrum of bare CDs_{Glu} and CDs_{Glu}/CS	93
Figure 4.8: Schematic diagram of functionalization of bare CDs_{Glu} with chitosan for $Hg(II)$ ions detection.	93
Figure 4.9: Fluorescence emission spectra of (a) bare CDs_{Glu} and (b) CDs_{Glu}/CS in the presence of different concentration of $Hg(II)$ ions.	94
Figure 4.10: Stern-Volmer plot of (a) bare CDs_{Glu} and (b) CDs_{Glu}/CS at different concentrations of $Hg(II)$ ions in the range of 20-2080 μM	94
Figure 4.11: Relative intensity of bare CDs_{Glu} and CDs_{Glu}/CS in the presence of different metal ions at concentration of 330 μM	96
Figure 4.12: Photograph of (a) bare CDs_{Glu} and (b) CDs_{Glu}/CS incubated with various interfering metal ions under UV exposure.	97
Figure 4.13: Absorption spectra of CDs_{250} in the presence of different concentration of TRIS solution.	98
Figure 4.14: Various fluorescence intensity ratio $(F_o - F_x)/F_o$ of the solutions of CDs_{250} and $CDs_{250}/TRIS$ in the presence of different metal ions.	99
Figure 4.15: Stern-Volmer plot shows the dependence of F_o/F_x on the concentrations of $Co(II)$ ions within the range of 0-1870 μM	100
Figure 5.1: Absorption spectra of $CDs_{250}/TRIS$ in the presence of $Ni(II)$ ions at different concentrations. Inset: Absorption spectra of different concentrations of $Ni(II)$ ions.	107
Figure 5.2: Absorption spectra of $CDs_{250}/TRIS$ in the presence of different concentrations of $Co(II)$ ions. Inset: Absorption spectra of different concentrations of $Co(II)$ ions.	107
Figure 5.3: Mole ratio plot for the interaction of $Co(II)$ ions with TRIS.	109
Figure 5.4: Stern-Volmer plot for binding of $CDs_{250}/TRIS$ to $Co(II)$, $Ni(II)$ ions and ultrapure at different concentrations.	110

Figure 5.5: Different types of bonding formed between TRIS and Co(II) ions [254].	111
Figure 5.6: Plot of $\log_{10} (F_0 - F_x)/F_x$ against $\log_{10} [Q]$.	113
Figure 5.7: Modified Scatchard plot for the interaction of Co(II) and Ni(II) ions with CDs ₂₅₀ /TRIS system.	115
Figure 5.8: Chemical structures of D-mannuronic acid and L-guluronic acid.	117
Figure 5.9: Schematic presentation of preparation of CDs ₂₅₀ encapsulated alginate beads.	118
Figure 5.10: Photographs of air-dried (a) plain alginate beads and (b) CDs ₂₅₀ encapsulated alginate beads under visible light; (c) plain alginate beads and (d) CDs ₂₅₀ encapsulated alginate beads under UV exposure.	119

List of Tables

Table 2.1:	List of several typical chromophores (Adopted from [38]).	16
Table 2.2:	List of CDs for fluorescence detection of Hg(II) ions.	41
Table 2.3:	List of CDs for fluorescence detection of some compounds.	42
Table 3.1:	Summary of the properties of different types of CDs.	78
Table 4.1:	Detection of Hg(II) ions in real water sample spiked with known concentrations of Hg(II) ions.	89
Table 4.2:	Analytical performance of CDs _{Glu} and CDs _{Glu} /CS for Hg(II) ions detection.	95
Table 4.3:	Summary of the analytical potentials of the different CDs sensing systems.	101
Table 5.1:	Quenching parameters for binding interaction between CDs ₂₅₀ /TRIS with Co(II) and Ni(II) ions.	116

List of Abbreviations

AFP	Alpha-fetoprotein
Ag ₃ PO ₄	Silver orthophosphate
ATP	Adenosine triphosphate
BPEI	Branched polyethylenimine
CDs	Carbon dots
CDs ₂₅₀	Carbon dots synthesized by thermal pyrolysis of α-cellulose
CDs ₂₅₀ /TRIS	Tris(hydroxymethyl)aminomethane functionalized carbon dots
CDs _{Blue}	Blue emitting carbon dots
CDs _{Glu}	Carbon dots synthesized by thermal pyrolysis of L-glutamic acid
CDs _{Glu} /CS	Chitosan functionalized carbon dots
CDs _{Green}	Green emitting carbon dots
CEE	Crosslink enhanced emission
CNDs	Carbon nanodots
CNTs	Carbon nanotubes
Co(II)	Cobalt ions
CQDs	Carbon quantum dots
CS	Chitosan
CuAc ₂	Copper (II) acetate
CuDTC ₂	Bis(dithiocarbamate)copper (II)
DCD	Dicyandiamide
DMF	Dimethylformamide
DOX	Doxorubicin
dsDNA	Double stranded DNA
ECL	Electrochemiluminescence
EDX	Energy dispersive X-ray spectroscopy
EGFP	Enhance green fluorescent protein
Fe(III)	Iron (III) ions
Fe ₂ O ₃	Iron (III) oxide
Fe ₃ O ₄	Magnetite
FIA	Flow injection analysis
FITC	Fluorescein isothiocyanate

FRET	Fluorescence resonance energy transfer
FTIR	Fourier transform infrared
FWHM	Full width at half maximum
GO	Graphene oxide
GQDs	Graphene quantum dots
Hg(II)	Mercuric ions
HOMO	Highest occupied molecular level
HPLC	High performance liquid chromatography
HRTEM	High resolution transmission electron microscope
IgG	Immunoglobulin G
IUPAC	International Union of Pure and Applied Chemistry
K ₂ S ₂ O ₈	Potassium persulphate
K _A	Binding/ association constant
K _{SV}	Stern-Volmer constant
LOD	Limit of detection
LOD	Limit of detection
LSCM	Laser scanning confocal microscopy
LUMO	Lowest unoccupied molecular level
mSiO ₂	Mesoporous silica nanoparticles
<i>n</i>	Number of binding site
Ni(II)	Nickel ions
NMR	Nuclear magnetic resonance
PAMAM	Polyamidoamine
PDs	Polymer dots
PEG	Polyethylene glycol
PEI	Polyethylenimine
PL	Photoluminescence
PMT	Photomultiplier tube
PPEI-EI	Poly(propionylethyleneimine-co-ethyleneimine)
QDs	Quantum dots
QY	Quantum yield
R ²	Coefficient of determination
RGD	Arginyl-glycyl-aspartic acid

ROS	Reactive oxygen species
Ru	Ruthenium
SEM	Scanning electron microscope
ssDNA	Single stranded DNA
SWCNTs	Single-walled carbon nanotubes
TEM	Transmission electron microscope
TiO ₂	Titanium dioxide
TNT	2,4,6-trinitrotoluene
TRIS	Tris(hydroxymethyl)aminomethane
UV	Ultraviolet
UV-Vis	Ultraviolet and visible
XRD	X-ray diffraction
ZnO	Zinc oxide
ZnPc	Zinc phthalocyanine
ZnS	Zinc sulphide

Chapter 1 Introduction

1.1 Research Background

Carbon dots (CDs) is a fascinating class of fluorescent nanomaterials that have gained tremendous research attention over the past few years. CDs were first serendipitously discovered by researchers during electrophoretic purification of single-walled carbon nanotubes (SWCNTs) by arc-discharge methods [1]. Ever since this discovery, great efforts have been paid on developing different synthetic approaches to obtain CDs. This include laser ablation [2], acid dehydration [3], hydrothermal carbonization [4] and electrochemical synthesis [5] which can be classified into 2 categories: top-down and bottom-up approaches.

CDs can be easily produced in large scale from various inexpensive starting precursors. This includes diverse organic precursors ranging from environmental wastes such as fruit peels and biomass wastes to analytical grade chemicals, for example, bovine serum albumin, ammonium citrate and chitosan [6-11]. CDs obtained from these organic precursors via different synthetic methods possess distinct physiochemical and optical properties. CDs with full photoluminescence (PL) colour such as blue, green, yellow and red have been reported [12, 13].

Typically, CDs are nanosized carbon nanoparticles with typical dimension less than 10 nm [14]. CDs have excellent water solubility due to the presence of carboxylic acid moieties at their surface. Notably, CDs can serve as a promising alternative to the traditional semiconductor quantum dots (QDs) owing to their tunable PL, resistance to photobleaching and ease of functionalization. CDs also exhibited robust chemical inertness and highly photostable. Unlike the toxic metal-based QDs, CDs exhibited relatively non toxicity and highly biocompatibility properties that have made them suitable candidates for a wide range of applications especially in biological fields [14]. Owing to the key merits mentioned above, CDs have been widely used for biological applications such as bioimaging and biolabelling, drug and gene delivery as well as biosensors for disease detection. Moreover, CDs have also found application as photocatalysts and chemical sensors for environmental monitoring.

Although the exact PL mechanism for CDs is still remained controversies, several mechanisms have been proposed. The suggested PL mechanisms of CDs include the armchair and zigzag edges of CDs, surface and molecule states, radiative recombination of excitons, quantum confinement effect as well as the crosslink enhanced emission (CEE) effect [15].

CDs are a promising nanomaterial that can be developed as sensitive probe for heavy metal ions detection. Contamination of heavy metals in the environment has been a global issue for decades due to the adverse effects on organisms and human health. The emission of heavy metals into the environment can be induced by natural sources such as weathering of rocks and volcanic eruptions [16-19]. Besides natural sources, anthropogenic activities that also contributed to the release of heavy metals include mining, metal processing in refineries, nuclear power stations as well as a variety of materials processing plants such as plastics, textiles and microelectronics [20-22]. Due to the hazardous effects of heavy metals, a rapid and sensitive practical detection method is highly desired.

The surface of CDs can be altered by surface modification to promote better interaction with targeted analytes for various applications. Surface passivation or sometimes known as surface functionalization involves the introduction of a thin layer of desired functional groups on the surface of CDs [23]. The capping agents can be chemicals or biological compounds depending on the intended applications.

It is generally believed that the binding of surface modified CDs with analytes can lead to the change in fluorescence properties. A general assumption is often made that stronger interaction between surface functionalized CDs with targeted analytes leads to more significant change in optical signal. However, it is still lacking in study on this aspect. Therefore, the effect of surface modification on CDs and its influence on surface interaction between CDs and metal ions that lead to change in fluorescence signal are worth investigation.

1.2 Research Motivations and Challenges

CDs can generally be produced from various starting precursors that are rich in carbon. Agriculture based countries such as Malaysia can produce considerable huge amount of carbon rich biomass wastes. Hence, one of the motivations of the research is to turn side products or wastes with low economic values into valuable CDs. Employment of renewable resources and adoption of green chemistry in CDs production in this study is considered as more economical and contributed towards a sustainable future.

One of the major challenges in this field of study is that the fluorescence origin of CDs remains unresolved until now. Although the exact mechanism is not yet to be fully understood, some studies have tentatively suggested the origin to be caused by the quantum size effect, different types of edges such as zigzag and armchair, radiative recombination of excitons as well as defect state emission [15]. More research is desired to further clarify and unveil the exact fluorescence mechanism of CDs.

Up till now, CDs have been commonly reported to emit at shorter wavelengths in blue region as well as emission at slightly longer wavelength such as green and yellow regions. However, the synthesis of CDs emitting at even longer wavelengths towards the red region is rarely reported and it is still remain a challenge. More in-depth study is required to fully realized and produce CDs that can emit at the full range of visible spectrum to maximize its applications in different fields. In addition, immobilization of CDs on matrixes is still remained to be explored. Successful immobilization will bring a step closer towards the practical applications of CDs as portable nanodevices for rapid and sensitive sensing applications.

Although considerable research have been focusing on fabrication of CDs through surface modification with various capping agents and utilize the surface modified CDs as metal ions sensing receptors, there is lacking of prediction guideline to evaluate the final sensing outcomes of surface functionalized CDs. This is where the research comes in with motivation to establish the correlation between change in optical signal and binding affinity of the surface

functionalized CDs with metal ions. This study can serve as a good platform to unveil some of these missing pieces of information although not all, which can later contribute to the development of CDs as robust applications in various fields.

1.3 Research Objectives

The research project embarked the aim of establishing the correlation between binding affinity and optical properties of surface functionalized CDs bound with targeted metal ions as a reference model that can be utilized for optical sensing applications in the future. The experimental study was designed to fulfill the following objectives:

- a. Synthesize and characterize a new class of CDs from economical and sustainable sources of carbon such as α -cellulose and L-glutamic acid as starting materials via simple acid hydrolysis and thermal pyrolysis approaches.
- b. Surface modification of the isolated CDs employing chitosan and Tris(hydroxymethyl)aminomethane (TRIS) as functionalization agents and its utilization for detection of metal ions that showed positive response towards the system.
- c. Investigation and extraction of the binding parameters of the interaction between surface modified-CDs and targeted analytes using spectroscopic analysis.
- d. Establishment of a relationship between binding affinities with the change in optical properties of the surface modified CDs as reference model for future development of CDs as metal sensing receptors.

1.4 Research Approaches

Early stage of the study involved reviewing journal articles from major databases (Elsevier Publisher, Royal Chemical Society Library, Wiley Publisher, Taylor & Francis Group Publisher, etc.) to gather information, followed by detailed research planning and proper experimental design. Sourcing of materials and apparatuses was also done after selection of materials and techniques.

Several research directions have been identified in order to fulfill the objectives of the study. First research direction involves the synthesis and isolation of CDs produced from sustainable carbon precursors under optimized synthesis conditions. The next direction involved modification of CDs surface with selected capping agents by physical absorption and investigated its metal ions sensing potential.

The next approach is analyzing data collected from different systems using available tools and software. The highlight of the research which is to establish the binding isotherms of surface functionalized CDs that correlates optical signal change and binding affinity were then identified by employing well-established mathematical models. The last approach of the study involved summing up the project and writing up.

1.5 Organization of Thesis

This thesis consists of six chapters with the following layout.

Chapter 1: Introduction

The first chapter of the thesis provides a general overview on the research background by giving a brief introduction on the current state of research in the field of CDs. Motivations behind the study and challenges that remained to be explored currently in this research area are also highlighted. Aim and objectives to be achieved in this study are included as part of this chapter. Research approaches in order to fulfill the objectives are also stated.

Chapter 2: Literature Review

The second chapter covers the basic concepts and mechanism of photoluminescence (PL), chemiluminescence and electrochemiluminescence (ECL). Instrumental analysis includes fluorescence spectroscopy and ultraviolet and visible (UV-Vis) spectroscopy and overview of carbonaceous materials. The detailed reviews on CDs synthesis (top-down and bottom-up approaches), properties (structure and composition, absorbance and photoluminescence, electrochemiluminescence, photoluminescence mechanism and quantum yield), post-synthetic strategies as well as applications of CDs (bioimaging/biolabelling, theranostics, biosensing, photocatalysis and chemical sensing) are also included in this chapter.

Chapter 3: Synthesis of Carbon Dots

This chapter provides a detailed description on the synthesis of CDs by acid hydrolysis and thermal pyrolysis using α -cellulose and glutamic acid as starting materials. The materials, reagents and instrumentations used are listed. The detailed protocols of CDs synthesis and isolation are provided. Besides, the physiochemical properties of the different types of CDs obtained are also discussed and summarized in this chapter.

Chapter 4: Interface Study on Carbon Dots and Its Potential as Metal Ions Sensing Receptors

The fourth chapter explores on the interface study of the bare CDs and surface functionalized CDs. The acid hydrolysed CDs obtained from α -cellulose are tested against various metal ions without further surface modification. The CDs synthesized from thermal carbonization of L-glutamic acid and α -cellulose are surface functionalized with chitosan and Tris(hydroxymethyl)aminomethane (TRIS), respectively. Their potential as metal ions detection probes are described in this chapter.

Chapter 5: Binding Isotherms of Carbon Dots

This chapter highlights the binding isotherms study using CDs obtained from α -cellulose via thermal carbonization approach as study model. Spectroscopic study that is employed to establish the relationship between CDs and TRIS as well as the relationship between the developed system towards its specific detection of cobalt ions (Co(II)) are described in detail. Several standard analysis methods such as mole ratio method, Stern-Volmer analysis, double log regression and modified Scatchard methods are also explored. Immobilization of CDs in alginate gel beads is also explored and discussed in detail.

Chapter 6: Further Works and Conclusions

The last chapter of the thesis concludes overall findings of the study by providing a project summary. Besides, some project limitations identified throughout the study are also outlined. Further works to address the project limitations that remain to be further explored are also provided.

Chapter 2 Literature Review

2.1 Executive Summary

Luminescence can be generally referred to all forms of light emission from a source. Photoluminescence (fluorescence and phosphorescence) and chemiluminescence (including electrochemiluminescence) are two different types of luminescence that can be distinguished by the types of energy transition involved. The concepts and mechanism of these two common types of luminescence will be described in this chapter. Instrumental analysis employing both fluorescence spectroscopy and UV-Vis spectroscopy for the measurement of fluorescence and absorbance respectively are also mentioned.

An overview of carbonaceous materials including a detailed literature review on the newly emerging CDs is provided. This covers the synthesis of CDs which can be categorized into top-down and bottom-up approaches. The physiochemical and optical properties of CDs including the chemical structure and compositions, absorbance and photoluminescence, upconversion and electrochemiluminescence as well as quantum yield are discussed.

Besides, several post-synthetic strategies to adjust the properties of CDs are also mentioned. CDs that possess unique properties are widely explored for applications in various fields. The literature review on the applications of CDs in the area of bio-imaging/ bio-labelling, theranostics, bio-sensing, photo-catalysis and chemical sensing are also provided in this chapter.

2.2 Luminescence

2.2.1 Photoluminescence

The phenomenon of light emission from electronically excited states of any substance is known as luminescence [24]. Emission of light is usually a response due to an input of energy. Hence, different types of luminescence can be distinguished by the types of energy transition involved. When the energy is supplied by absorption of photons from ultraviolet (UV) irradiation, the light emitted is known as photoluminescence (PL) [24]. Fluorescence and phosphorescence are two specific types of PL.

Jablonski diagram as shown in Figure 2.1 illustrates the typical light absorption and emission processes. The singlet ground, first and second electronic states are denoted as S_0 , S_1 and S_2 , respectively. Whereas triplet excited states is depicted as T . The different vibrational energy levels at each of the electronic levels are denoted as 0, 1 and 2 accordingly. Vertical lines are used to show the transition between states to illustrate the direct light absorption nature.

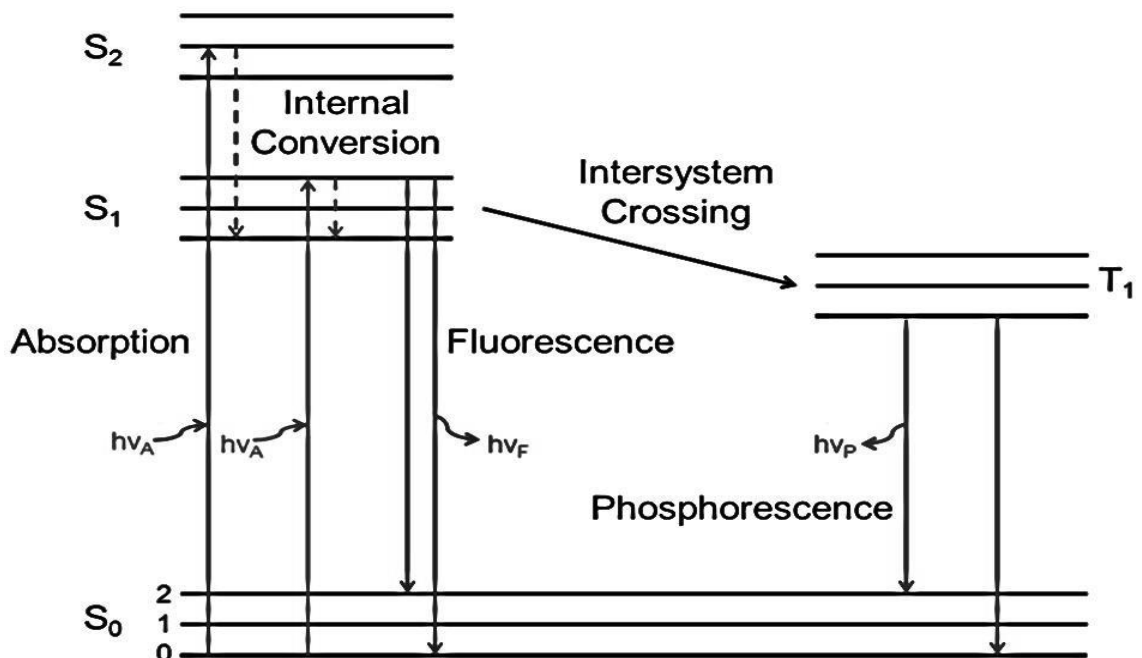


Figure 2.1: Jablonski diagram illustrates typical light absorption and emission processes.

An assumption that radiant energy can only be absorbed in definite unit or *quanta* is made, and hence the following Equation 1 is proposed to determine the energy of photon.

$$E = hv = hc/\lambda \quad \textbf{(Equation 1)}$$

where E depicts the energy, h ($= 6.626 \times 10^{-27}$ ergs) is the Planck's constant, ν is the frequency, c ($= 2.9979 \times 10^{10}$ cm/s) depicts the light velocity and λ is the related wavelength [25].

Fluorescence is the emission of light from excited singlet states. This means absorption of photon is in the singlet ground state that promoted to a singlet excited state. This electron in the excited orbital will pair up with the electron in the ground state orbital in opposite spin and consequently return to the ground state and emit photons of lower energy. The typical emission rates and fluorescence lifetime are 10^8 s^{-1} and approximately 10 ns, respectively [26]. Emission rate is refer to the number of photon emitted per second [27]. Fluorescence lifetime of a fluorophore can be defined as the average value of time spent in the excited state [26].

Unlike fluorescence emission, phosphorescence emission will continue from seconds to minutes after the excitation radiation is ceased [24]. In triplet excited states, the electron in the excited orbital has the same spin orientation as the ground state electron; hence these two electrons are not paired. Transition to the ground state is forbidden and molecule in the lowest vibrational energy level of an excited triplet state relaxes to the ground state by intersystem crossing [26]. Intersystem crossing can be referred to the radiationless transfer between electronic states of different multiplicity, for instance, between singlet and triplet states. Whereas, radiationless transfer between electronic states of the same multiplicity such as between singlet states is known as internal conversion [24]. Due to the intersystem crossing, emission rate is typically slower (10^3 to 10^0 s^{-1}) and the phosphorescence lifetime can be ranging from milliseconds to seconds or even longer [26].

2.2.2 Chemiluminescence

Chemiluminescence is another type of luminescence that involves the emission of light due to chemical reactions [28]. The energy level of chemiluminescence is identical to that in fluorescence, but different mode of excitation. Transition of electrons from ground state to excited state is induced by chemical reaction that produces sufficient amount of energy. Vibrational and rotational changes in molecules are often associated with this energy transition. Chemiluminescence is observed when the excited electrons subsequently relax to ground state by releasing photons [29]. There is no need to have an excitation light source.

Emission of chemiluminescence is highly sensitive to environmental factors such as temperature, solvent, ionic strength, pH and the presence of other species [30]. However, it has been widely adopted as detection method because the advantages far outweigh the disadvantages. Chemiluminescence can be measured with relatively simple instrumentations, low detection limits and wide dynamic ranges [30].

Compounds such as luminol, acridinium derivatives and coelenterazine that exhibit chemiluminescence property have been used for different applications. Chemiluminescence has been employed as detection method in various fields such as high performance liquid chromatography (HPLC), flow injection analysis (FIA) and capillary electrophoresis. In addition, immunoassays based on chemiluminescence have also been broadly developed for enzyme, protein, hormones and antibodies detection over the past few decades [29].

Electrochemiluminescence (ECL) also known as electrogenerated chemiluminescence. This occurs by electron transfer reactions of highly reactive species generated electrochemically that induces the generation of emitting excited states which subsequently leading to the emission of light [31]. In other words, ECL is induced electrochemically instead of chemical reactions. Some examples of molecules that exhibited ECL are ruthenium, osmium, rhenium, etc. [32].

ECL has been employed as a powerful tool for detection and quantification of chemical, biochemical and biological substances [33]. In the presence of ECL luminophore such as $\text{Ru}(2,2'\text{-bipyridine})_3^2$ (commonly known as $\text{Ru}(\text{bpy})_3^2$), application of a voltage to an electrode will induce light emission that be measured as ECL [31]. Ruthenium is one of the most widely studied ECL species due to its electrochemical properties and quantum yield [34].

Furthermore, ECL has been developed for commercial application in immunoassay and DNA analyses for detection of a wide range of proteins over the past few decades [31]. Application of ECL technology offers several distinct advantages. Liquid reagent can be used in ECL measurement due to the use of highly stable non-isotopic label. Besides, ECL detection offers high quality assay with enhanced sensitivity and rapid result turnaround. ECL measurement requires only relatively short incubation and handling time and can be used for large measuring range. This ECL technology is also applicable for detection of solid analytes [32].

2.3 Instrumental Analysis

2.3.1 Fluorescence Spectroscopy

Fluorescence excitation and emission spectra are measurable with a fluorescence spectrophotometer or spectrofluorometer. The wavelength distribution of an emission measured at a fixed excitation wavelength is called the emission spectrum. On the other hand, the dependence of emission intensity measured at a single emission wavelength upon scanning the excitation wavelength is the excitation spectrum [26].

In general, three basic components of a fluorescence spectrophotometer include a light source, a sample holder and a detector. Light source that is commonly used in fluorescence spectrometry have spectral output as energy continuum over a wide range or a series of discrete lines. Mercury lamp and tungsten-halogen lamp are examples of commonly employed light sources. Fluorescence is usually measured at 90° because this angle detect only stray light scattered by the sample, hence minimize interference due to the excitation light. Photomultiplier tubes (PMTs) are often employed as detectors for the commercial fluorescence instruments [25].

A PMT vacuum tube composed of a thin film of metal known as photocathode and a series of dynodes. Ejection of electrons from photocathode that held at a high negative potential can be induced by incident photons. Dynodes also held negative potentials that decrease along the dynode chains. The potential difference between photocathode and first dynode causes acceleration of the ejected photoelectron towards first dynode and leads to ejection of more electrons upon collision with the first dynode. This process continues down the dynode chain until a current pulse arrives at the anode. Higher voltage causes higher amplification as a result of the increased number of electrons ejected [26].

In addition, fluorescence instruments are usually equipped with excitation and emission monochromators to select specific wavelength. Optical filters can be used and placed into the light path to direct the light as waveguide. In some cases, filter is used to isolate a desired wavelength in the excitation beam as

well as remove scattered light from the emission channel [26]. Figure 2.2 shows the schematic diagram of the essential components of a fluorescence spectrophotometer.

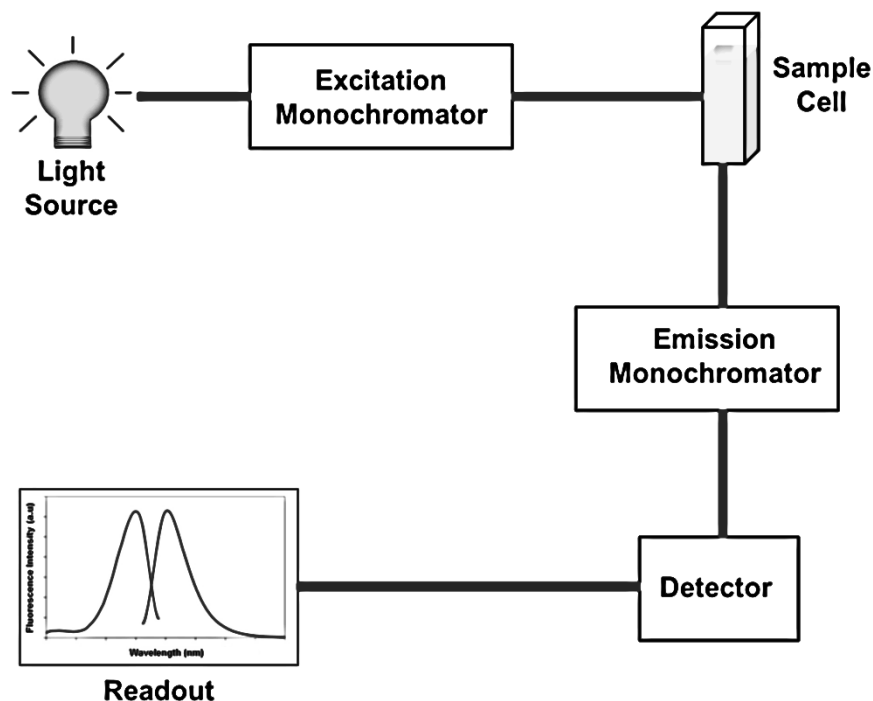


Figure 2.2: Schematic diagram of essential components of a fluorescence spectrophotometer.

2.3.2 Ultraviolet and Visible Spectroscopy

Ultraviolet and visible (UV-Vis) spectroscopy is an essential tool that has been widely applied to study a wide range of biological and chemical substances. UV-Vis spectral region provides information on the transition of electronic energy [35, 36]. Absorption is a process where radiation frequency corresponds closely to the energy difference of the transition between two energy states. This process leads to resonance excitation, change in electron density distribution and electronic transition from highest occupied molecular level (HOMO) to the lowest unoccupied molecular level (LUMO) [37].

The energy level in UV-Vis spectrum is corresponding to the electron density orbitals. Most σ to σ^* absorptions occur in the vacuum-ultraviolet region (< 200 nm) whereas $\pi \rightarrow \pi^*$ and $n \rightarrow \pi^*$ absorptions occur in the near UV/visible

region [38]. Figure 2.3 illustrates possible electron transitions between typical molecular orbitals. Referring to Figure 2.3, HOMO is depicted as π or n while LUMO is depicted as π^* .

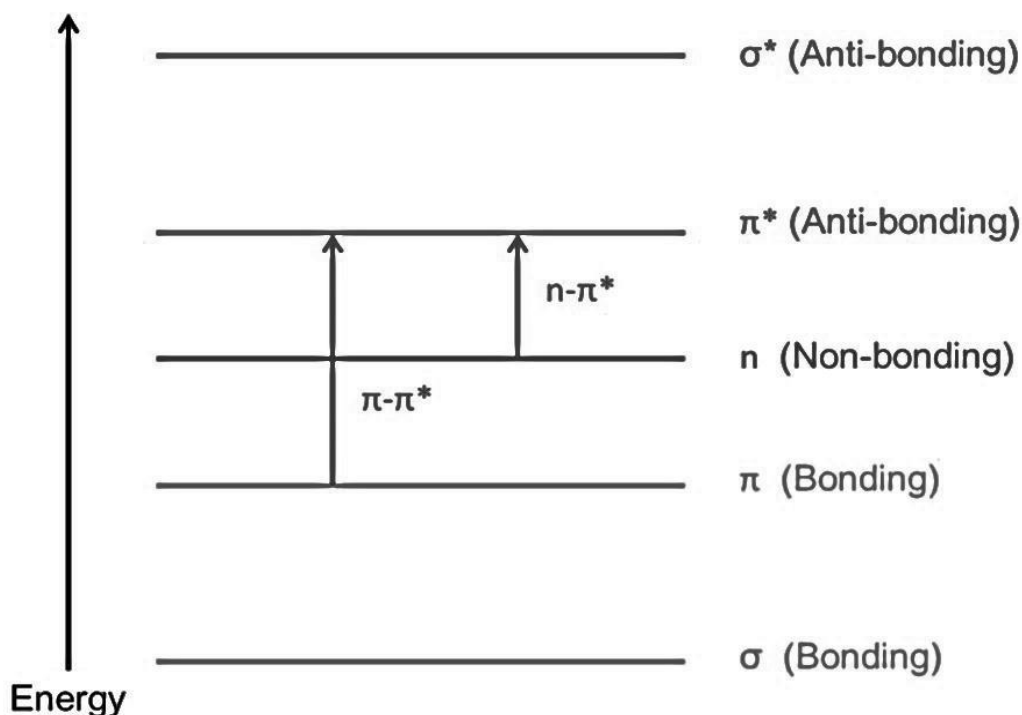


Figure 2.3: Possible electron transitions between molecular orbitals.

Absorbance, A can be defined as the amount of radiation absorbed by a solution. Beer-Lambert law also known as Beer's law stated that absorbance is dependent on the molar absorptivity, ϵ which is also known as molar absorption coefficient and concentration, c of the attenuating species. The radiation path length, l through cell is usually fixed at 1 cm. Beer's law can be written as follows:

$$\text{Log} (I_0/I) = A = \epsilon cl \quad \text{(Equation 2)}$$

From Equation 2, a linear relationship is obtained by taking the logarithm of the ratio of the non-absorbing incident beam, I_0 to the transmitted intensity, I . A standard calibration graph of absorbance versus concentration needs to be constructed in order to determine the concentrations of unknown analytes using the Beer's law [38].

In addition, the absorption bands obtained in UV-Vis spectrum can provide some information about the molecular structure and functional groups present in a sample [39]. UV-Vis spectroscopy can be employed as a quick and inexpensive method to elucidate the structure of certain organic compounds which absorb in the region (180-700 nm) of UV-Vis spectrum.

Chromophores are chemicals that can confer colour on a substance while auxochromes are chemicals that can modify the colour produced by chromophore but do not produce colour on its own. This in turn indicated that compounds that composed of chromophores and auxochromes are most likely coloured. Chromophores have characteristic molar absorptivities and absorb at specific wavelengths which can be identified using a UV-Vis spectrophotometer as shown in Table 2.1 [38].

Table 2.1: List of several typical chromophores (Adopted from [38]).

Chromophore	Typical Compound	Electronic Transition	Wavelength (λ_{\max} , nm)	Molar Absorptivity (ϵ , $\text{m}^2 \text{mol}^{-1}$)
$>\text{C}=\text{C}<$	Ethene	$\pi \rightarrow \pi^*$	180	1300
$>\text{C}=\text{O}$	Propanone	$\pi \rightarrow \pi^*$	185	95
		$n \rightarrow \pi^*$	277	2
	Benzene	$\pi \rightarrow \pi^*$	200	800
			255	22
$-\text{N}=\text{N}-$	Azomethane	$n \rightarrow \pi^*$	347	1
$-\text{N}=\text{O}-$	Nitrosobutane	$n \rightarrow \pi^*$	665	2

2.4 Carbonaceous Materials

Carbonaceous materials are well known for decades. It can be defined as materials with structures that are mainly composed of elemental carbon. Carbon can exist in different forms and allotropes. Diamonds and graphite are two of the best known examples that can be found naturally [40]. A great variety of carbonaceous materials such as activated carbon, graphene oxide (GO), carbon nanotubes (CNTs) and many more have attracted considerable research interests due to their unique properties.

The fluorescent CDs have recently recognized as a new member of carbonaceous nanomaterials. CDs were first serendipitously discovered by Xu *et al.* during electrophoretic purification of SWCNTs fabricated by arc-discharge method in 2004 [1]. Since then, research studies exploring on different synthesis approaches, fluorescence properties and utilizing the CDs for various potential applications have been triggered. CDs are a class of fluorescent carbon nanoparticles that consists of graphene quantum dots (GQDs), carbon nanodots (CNDs) and polymer dots (PDs). The three different types of CDs are illustrated in Figure 2.4 which can be distinguished by their distinct inner structure and surface chemical groups [15].

GQDs are anisotropic with larger lateral dimension as compared to the height. They can be made of either single or several layers of graphene with attached chemical groups. CNDs are spherical carbon nanoparticles that can be further classified into two different kinds. CNDs are carbon nanoparticles without crystal lattice, while the one with crystal lattice is known as carbon quantum dots (CQDs). The other type of CDs that can be prepared from linear polymer or monomers in which the carbon core attached to the polymer chains is known as PDs [15]. Although the fluorescent carbon nanoparticles can be categorized into several kinds, CDs which is the general term for the various kinds of nanosized carbon materials will be used in this study.

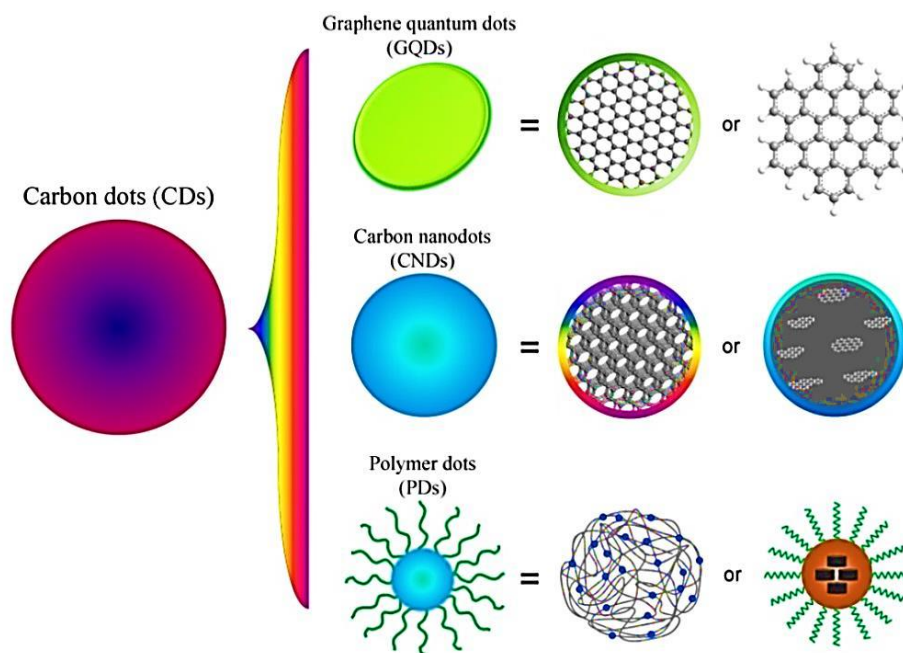


Figure 2.4: Three different types of CDs that are structurally distinct (Adopted from [15]).

2.5 Synthesis of CDs

Over the past few years, many methods have been developed to produce CDs from various carbon sources. Synthesis of CDs can be generally classified into two main routes: top-down and bottom-up approaches. Top-down approaches usually involve cleaving or breaking down of large carbonaceous materials such as nanodiamonds, carbon nanotubes, graphite and activated carbon to obtain CDs. Bottom-up approach primarily involves pyrolysis or carbonization of organic molecular precursors into CDs [41].

2.5.1 Top-Down Approach

Synthesis of CDs via top-down routes can be implemented via different methods such as chemical, electrochemical or physical techniques [41]. Commonly employed top-down methods include acidic oxidation, hydrothermal and solvothermal method, electrochemical exfoliation and microwave-assisted technique. Oxidation treatment in the presence of strong acid solutions is a widely adopted chemical method for the production of CDs. CDs were successfully synthesized from different kinds carbon precursors such as soot [42], sago starch [43], carbon fibers [44] and activated carbon [45] via acidic exfoliation and oxidation. Acidic dehydration and oxidation is a method that can be implemented for large scale synthesis of CDs. It was also reported that more smooth edges could be produced with properly controlled oxidation treatment [46]. However, the difficulty to thoroughly remove the excess acidic solutions after carbonization process is a commonly encountered problem. The utilization of strong acidic solutions may lead to the production of CDs with defective graphitic structures [41].

Hydrothermal synthesis usually involves cleavage and deoxidation of carbon precursors into colloids CDs using strong alkali solutions such as ammonia and sodium hydroxide. Pan *et al.* were the first who demonstrated the hydrothermal synthesis of CDs from GO sheets [47]. The method was then further improved by Pan *et al.* to obtain well crystallized CDs with strong green fluorescence [48]. Solvothermal methods are usually performed in conjunction with sonication, followed by carbonization at high temperature. This method was reported by Zhu

et al. employing GO sheets as starting precursor for the production of CDs using dimethylformamide (DMF) as solvent [49].

Electrochemical exfoliation involves the use of high redox potential to generate hydroxyl and oxygen radicals through oxidation of water. The hydroxyl and oxygen radicals generated can act as effective electrochemical “scissors” that play an important role in cleavage reaction to release CDs [50]. Li *et al.* first demonstrated the production of CDs via electrochemical method. CDs with uniform sizes were isolated from electrochemical reaction of graphene film as working electrode in phosphate buffer solution [51]. Electrochemical synthesis of CDs is relatively simple and the resultant CDs can be doped with heteroatoms in the one-step synthesis [52].

Microwave irradiation is a convenient and rapid physical method for the preparation of CDs. CDs with high product yield can be prepared in a relatively short reaction time. Therefore, such method has been widely adopted for the synthesis of CDs. Liu *et al.* reported one-step production of hydrophilic CDs emitting green fluorescence from sucrose in the presence of diethylene glycol as reaction medium. The synthesis process is relatively quick and can be completed within one minute [53]. Mitra *et al.* demonstrated the preparation of hydrophobic CDs emitting blue and green fluorescence depending on the excitation wavelength from poloxamer via simple microwave assisted method [54].

The different methods in the top-down approach offer the advantages of simple operation and facilitate large scale production. CDs synthesized via such methods often possess oxygen-containing functional groups, rendering the CDs to be water soluble and can be easily functionalized and passivated for various applications. In contrary, extreme harsh conditions especially in the presence of strong acidic solutions could interrupt the aromatic carbon framework, hence producing CDs with defective graphitic structures. In addition, non-selective chemical cleavage may results in the synthesis of CDs with inconsistent morphology and size distribution [55, 56].

2.5.2 Bottom-Up Approach

Bottom-up approaches involve the employment of organic molecules as starting precursors for the synthesis of CDs. Bottom-up routes enable the production of CDs with more uniform size distributions, homogenous morphology and shape and well-defined properties [57]. It is achieved by step-wise chemical fusion of small molecules such as the one with aromatic moiety [41]. Yan *et al.* have demonstrated the synthesis of CDs with uniform size through stepwise solution chemistry [58]. In this study, the formation of large colloidal CDs containing 168, 132 and 170 conjugated carbon atoms was due to the oxidative condensation of aryl groups of the carbon precursor. The resultant CDs was stabilized by covalent attachment of 2',4',6'-trialkyl phenyl groups to the edges of the graphene moieties.

Simple thermal combustion technique was also performed for the production of CDs from organic precursors such as citric acid [56], L-glutamic acid [59], ascorbic acid [60] and glycerol [61]. Other than simple pyrolysis, Tang *et al.* pioneered the CDs synthesis from glucose precursor via microwave-assisted hydrothermal method [62]. The glucose molecules were first dehydrated, following by growth of CDs at the spherical surface with increasing heating time. Wang *et al.* reported one-step synthesis of multicolour CDs from pyrolysis of epoxy-enriched polystyrene photonic crystal through a rapid plasma-induced method [63]. The CDs obtained were amphiphilic, rendering them soluble in water and most organic solvents.

Another interesting bottom-up method was demonstrated by Lu *et al.* who prepared CDs with well-defined size on ruthenium (Ru) surface using a spherical fullerene molecule, C₆₀ as starting precursor [64]. In this study, surface vacancies formed in Ru single crystal as a result of strong interaction between C₆₀ molecules and Ru. C₆₀ molecules were then embedded in the Ru surface. CDs were eventually formed through Ru-catalysed cage opening of C₆₀ as a result of diffusion and aggregation of carbon cluster produced when the embedded molecules were treated at elevated temperatures.

2.6 Properties of CDs

QDs have received wide attention due to their high brightness and good photostability [65]. However, the metal-based QDs are toxic and hence limit their applications in biological aspects. Alternative fluorescent nanomaterials that possess the desired characteristics of QDs and at the same time, less toxic and more biocompatible are highly needed. CDs recently emerge as a new class of carbon nanomaterials and triggered intensive research activities. CDs can be categorized into 3 kinds, namely GQDs, CNDs and PDs. The superior properties of CDs have made it a promising alternative to replace the use of toxic QDs. Some unique properties of CDs as universal fluorophores are discussed as follows.

2.6.1 Chemical structure and composition

Different kinds of CDs can be differentiated through their distinct structures. GQDs resemble single or a few graphene layers with typical morphology of either circular or elliptical [55]. CNDs are quasispherical nanoparticles with typical diameter less than 10 nm [14]. Moreover, CNDs can be amorphous or nanocrystalline with sp^2 carbon clusters [66]. High resolution transmission electron microscope (HRTEM) and X-ray diffraction (XRD) revealed that both GQDs and CNDs possess graphitic in-plane lattice spacing of 0.18 – 0.24 nm and 0.334 nm graphitic inter-layer spacing [41]. PDs possess similar chemical and fluorescent properties as CNDs. The crystal carbon cores of CDs are usually unobvious. PDs possess lower carbonization degree than CNDs with cross-linked polymer chains that passivate and stabilize the carbon cores. [67].

Often the surfaces of CDs are attached to polymer chains or chemical functional groups such as hydroxyl, epoxy or ether, carbonyl and carboxylic acid groups [15]. Nuclear magnetic resonance (NMR) measurements were employed by Wang *et al.* to identify the presence of sp^2 carbon. The results showed that carbon atoms in CDs were sp^2 hybridized with unsaturated sp^3 carbon atoms [68]. Ray *et al.* found that CDs obtained from candle soot had a nanocrystalline core of graphitic sp^2 carbon atoms with peripheral carboxylic or carbonyl functionalization [66].

The core of CDs are generally composed of carbon (C), hydrogen (H), nitrogen (N), oxygen (O) and some doped elements. Yu *et al.* stated that purified CDs have significantly higher oxygen content compare to that of raw candle soot [69]. Elemental analysis of CDs showed that purified CDs compose of 36.8% C, 5.9% H, 9.6% N and 44.7% O whereas raw candle soot contain 91.7% C, 1.8% H, 1.8% N and 4.4% O. The presence of carbonyl groups in the purified CDs contributed partially to the high oxygen content.

Functional groups present on the surface of CDs can be characterized using fourier transform infrared (FTIR) spectroscopy. The FTIR spectra obtained by Hu *et al.* revealed that the stretching vibrations of C=O in conjunction with asymmetric and symmetric stretching vibrations of C-O-C in carboxylate groups were detected in CDs produced in polyethylene glycol (PEG_{200N}) [70]. Tan *et al.* reported that the FTIR spectrum of CDs produced by thermal pyrolysis of sago waste indicated the presence of alcohol or phenol -OH group, stretching vibrations band of alkyl C-H bond, carboxylic acid and amide C=O bond and aromatic C-H bond [7]. From the above reported studies, it is observed that carboxylic moieties are commonly present on the surface of CDs.

2.6.2 Absorbance and photoluminescence

All kinds of CDs possess similar optical properties despite their variation in structures. CDs typically display strong absorption band the in UV region of 260-320 nm, with a tail extending into the visible range. Due to the $\pi - \pi^*$ transition of C=C bonds, CDs are effective in photon-harvesting in the region of short wavelength [14]. In addition, shoulder peak can sometimes be observed in GQDs in the range of 270-390 nm. It was claimed that the shoulder peak is most likely attributed to the $n - \pi^*$ transition of C=O bonds [71]. Surface passivation and the presence of surface functional groups on CDs can also contribute to the absorption characteristics at UV-Vis range. It was stated that the position of absorption band can be altered by the oxygen content variation of CDs [72].

PL is one of the most fascinating features of CDs. Emission wavelength and intensity of CDs is generally found dependent on the excitation wavelengths. Up till now, full PL emission colours have been reported. The excitation dependence behaviour of CDs have made it a useful tool in multi-colour imaging applications [12, 13]. Although the mechanisms of the tuneable PL properties of CDs still remain unclear, quantum confinement effects are suggested to contribute to the tuneable PL properties of CDs [41]. The full width at half maximum (FWHM) for CDs is relatively low [73, 74]. However, the bandwidth of CDs PL emission is broader when compared with that of semiconductor QDs. The wide peak can be attributed to the inhomogeneous chemical structure and lack of size uniformity [61]. As compared to the conventional organic fluorophores, CDs possess excellent photostability which permits long term real-time imaging. No blinking or reduce in fluorescence intensity was observed even after the CDs were exposed to continuous excitation under UV [75]. CDs were also highly durable against photobleaching [49].

Some factors that will affect the optical properties of CDs include ionic strength of the aqueous, pH and types of solvent used to suspend CDs. Jia *et al.* demonstrated that the maximum emission of the CDs produced from ascorbic acid showed red shifted from 441 nm to 550 nm with increasing pH. It was suggested that pH change may induce electronic transition changes of $\pi - \pi^*$ and $n - \pi^*$ in graphite nanodomains [60]. Sun *et al.* found that PL of CDs has shifted in different solvents [76]. It was conjectured that the solvent effect is due to either attachment of solvent or formation of different emissive traps on CDs surface [77, 78]. However, there is exception in some cases where Xue *et al.* realized that there was neither obvious change in fluorescence intensity nor shift in emission wavelength could be observed for the CDs synthesized from peanut shells. The CDs obtained were found stable in pH ranging from 3 to 12 [79].

2.6.3 Up-conversion Luminescence and Electrochemiluminescence

In addition to the normal fluorescence (sometimes also known as down-conversion fluorescence), up-conversion luminescence of CDs are also reported. Up-conversion fluorescence is the emission of photon/fluorescence at shorter wavelength than the excitation wavelength. Up-conversion fluorescence is particularly useful for in vivo imaging of biological samples because bio-imaging at longer wavelength allows improved deep-tissue penetration and low background interference [23]. The up-conversion fluorescence of CDs was first realized by Cao *et al.* who observed CDs emitted visible light upon excitation at 800 nm using a femtosecond pulsed laser. It was suggested that this up-conversion emission is attributed to multiphoton active process [80]. Following that, Li *et al.* also reported up-converted PL property in CQDs prepared by alkali-assisted electrochemical method [81].

Shen *et al.* later speculated that up-conversion fluorescence is due to anti-Stokes PL which involves the process of relaxation of electrons to σ orbital from high energy state (LUMO) when the electrons in π orbital are excited by low-energy photons [82]. Besides, Jia *et al.* stated that the CDs synthesized from ascorbic acid via low-temperature aqueous heating in the presence of copper (II) acetate (CuAc_2) displayed up-conversion luminescence [60]. Up-conversion luminescence has also observed in CDs prepared by Salinas-Castillo *et al.* through microwave-assisted pyrolysis of citric acid in the presence of polyethylenimine (PEI) [83]. In a more recent study, Wen *et al.* argued that the up-conversion luminescence is actually the normal fluorescence excited by radiation of light leaked from the second diffraction in monochromators of fluorescence spectrophotometer. The so-called up-conversion luminescence due to the leaking light radiation can be eliminated by inserting a long-pass filter in the excitation pathway of the spectrophotometer [84].

As mentioned previously, ECL has been widely adopted as a robust detection method due to the advantages such as high sensitivity, wide concentration working range and improved selectivity due to the absence of background signal induced by emission of interfering species during detection process [85]. Zhu *et al.* have reported ECL property in CDs prepared by microwave pyrolysis

of PEG-200 and saccharide. The ECL mechanism is suggested to involve the oxidized state (R^+) and reduced state (R^-) of CDs formed with potential cycle. Relaxation of excited state (R^*) of CDs that is formed by electron transfer annihilation of the two oppositely charged carriers to ground state via a radiation pathway by emitting a photon, thus emission of ECL [73].

Zheng *et al.* also demonstrated that water-soluble carbon nanocrystals obtained from graphite rod by electrochemical method exhibited ECL properties [86]. Besides, ECL of GQDs was also reported by Li *et al.* [87]. The GQDs exhibited two different PL colours (greenish-yellow and blue) were found to show ECL behaviour in the presence of potassium persulphate ($K_2S_2O_8$). At the same time, a novel ECL sensor based on the intense ECL behaviour of the obtained GQDs for detection of cadmium ions [$Cd(II)$] was developed. More recently, Xiong *et al.* have fabricated N-doped CDs with ECL activity and utilize the CDs as ECL biosensor for intracellular lead ions [$Pb(II)$] sensing [88]. Comparable to semiconductor QDs, CDs also exhibit ECL properties making them a potential tool for various analytical applications.

2.6.4 Photoluminescence mechanism

Intensive research has been focusing on unveiling the PL mechanism of CDs. Although the exact PL mechanism of CDs is still remains controversial, several generally accepted tentative mechanisms have been proposed. PL mechanism may derive from intrinsic state emission (quantum size effect, zigzag edges and recombination of localized electron-hole pairs) and defect state emission which can be induced by surface energy traps [71]. Some of these PL mechanisms will be discussed in this section.

GQDs exhibit different types of edges such as armchair and zigzag edges resulting from cutting of graphene sheets along different crystallographic directions [15]. Radovic and Bockrath claimed that zigzag sites were carbene-like and commonly with triplet ground state while armchair sites were carbene-like and commonly with singlet ground state [89]. The different type of edges is vital in determining the electronic, magnetic and optical properties [15]. Pan *et al.* proposed that the blue luminescence of GQDs synthesized through

hydrothermal method might be originated from free zigzag sites with a carbene-like triplet ground state [4]. HRTEM images by Kim *et al.* revealed that GQDs with circular/elliptical morphology consisted of both zigzag and armchair edges whereas polygonal GQDs consisted mostly of armchair edge [90].

The presence of functional groups on GQDs surface can lead to the formation of defect or surface states on GQDs. Surface states are energy levels between π and π^* states of C=C which is suggested contributing to the PL of GQDs. A series of emissive traps could result from the functional groups with different energy levels [91]. Sun *et al.* were the first who tentatively proposed that PL of CDs might be attributed to the presence of surface energy traps [75]. Later, Zhou *et al.* further developed the PL mechanism proposed by Sun *et al.* and suggested that the mechanism was due to the radiative recombination of excitons from CDs of various sizes and a distribution of different emissive trap sites [74]. When electrons on the ground-state valence band are excited into the conduction energy band due to absorbance of energy greater than the band-gap energy, an exciton (negative electrons and positive holes pair) will be produced. The annihilation of the exciton through emission of a photon is known as radiative recombinant [92].

Pan *et al.* proposed that relaxation of photo-excited electrons through $\pi - \pi^*$ transition into sp^2 energy levels will induce blue emission which was probably due to quantum confinement effect. Whereas, relaxation into surface states will give rise to emission at longer wavelength which could be related to the hybrid structure of oxygen functional groups and graphene core [93]. Other than oxygen functional groups, amine-based groups also contributed to the surface state in GQDs. Zhang *et al.* reported that the yellow luminescence from GQDs was attributed to the modified hydrazine group attached on GQDs [94].

Quantum confinement effect of conjugated π -domains in GQDs was claimed to be the true intrinsic PL mechanism in cases where GQDs exhibit perfect graphene core and less surface functional groups [15]. Quantum confinement effect can be referred to nanosized particles with diameter smaller than the exciton radius, causing the charge carriers to become spatially confined and leading to the rise in energy levels [95]. Li *et al.* convincingly showed that the PL

of CQDs synthesized from one-step alkali-assisted electrochemical method was attributed solely to the quantum-sized graphitic structure of CQDs. The CQDs obtained possessed size-dependent PL [81].

Unlike surface state where the PL origin was formed by hybridization structure of functional groups and carbon core, PL induced by molecule state is due solely to the organic fluorophore attached on the surface or interior of the carbon backbone [15]. Giannelis's group conjectured that besides surface defects, the formation of several different fluorophore within the carbon network might also be contributed to the PL of CQDs [96]. Later, this group found out that pyrolysis at 180 °C produced CNPs with intense PL and high quantum yield. Pyrolysis at 230 °C initiated the formation of carbon core and the PL of CNDs produced is attributed to the presence of both molecular fluorophore and carbon core. PL of CNDs obtained at even higher temperature is claimed to exclusively arise from carbon core [97].

Zhu *et al.* discovered that PL of PDs was attributed to the CEE effect using branched polyethylenimine (BPEI) as model. PEI possessed secondary and tertiary amine as potential fluorophore. The PL of PDs is found to be temperature-dependent where PL would be quenched to certain extent at high temperature. The high temperature was claimed to aggravate and decrease the vibration and rotation of the amine-based PL origin, increased the non-radiative process and hence enhanced the PL of non-conjugated PDs [98].

2.6.5 Quantum Yield (QY)

PL quantum yield (QY) is particularly important for the characterization of a fluorophore. QY is defined as the ratio of the number of photon emitted to the number of photon absorbed [99]. Determination of QY is usually done by comparative method of Williams *et al.* which involves the use of well-established reference standard with known literature QY value [100]. QY can then be calculated based on Equation 3 as shown below by employing UV-Vis and fluorescence spectroscopy.

$$Q = Q_R \frac{I}{I_R} \frac{A_R}{A} \frac{n^2}{n_R^2} \quad \text{(Equation 3)}$$

where QY and QY_R denoted as photoluminescence quantum yield of sample and reference standard respectively; I is the integrated intensity, A is the absorbance value and n is the literature refractive index. The reference standard chosen should absorb at the same wavelength and emit at similar region as the test sample. This is based on the assumption that reference standard and test sample absorb at the same wavelength have the same number of photon. Some examples of most commonly used reference standards with well reported QY include quinine sulphate, fluorescein and rhodamine [101].

During the early discovery of CDs, QY of bare CDs is relatively low with typical QY of less than 10% [41]. Progress in CDs research revealed that QY of CDs varies with different synthetic routes and surface chemistry. Moreover, QY can be enhanced significantly via surface passivation of CDs. Zhai *et al.* were able to produce CDs with QY of 30.2% via one-step microwave-assisted pyrolysis of citric acid in the presence of different amines without further surface modification. It was claimed that the doping of N element in the core of CDs can increase the QY up to 50%. It was also observed that the QY value can be increased with increasing N content in the CDs [102].

Dong *et al.* also found that the QY of N-doped CDs (16.9%) and N,S-co-doped CDs (73.0%) exhibited higher QY when compared to the O-doped CDs (5.3%). It was suggested that co-doping with sulphur (S) atoms can enhance doping of

Nitrogen (N) atoms in CDs through a cooperative effect [103]. In another study by Ding *et al.*, the QY of N,S-CDs produced from α -lipoic acid by one-pot hydrothermal method was calculated to be 54.4% with strong blue fluorescence. The C=N and C-N bonds in the form of polyaromatic structures were found to play significant role in enhancing the QY of the N,S-doped CDs. At the same time, the synergistic role of co-doped S for N doping of CDs was confirmed [104]. Qu *et al.* managed to obtain N-doped GQDs with QY as high as 94% using citric acid as carbon source and ethylene diamine as N source under optimized hydrothermal reaction conditions [105].

2.7 Post-Synthetic Strategies

Several post-synthetic strategies have been developed and employed to tune the properties of CDs. Post synthetic strategies are required in order to obtain CDs with defined and desired properties for various applications. Surface functionalization or modification by attachment of chemical moieties, tuning the oxidation degree and polymer passivation is one of the post-synthetic strategies that is typically employed to tune the properties of CDs. Doping with heteroatoms can also effectively adjust the intrinsic properties of CDs.

CDs can be innovatively functionalized with desired ligand such as small molecules, surfactants, dendrimers, polymers and biomolecules on the surface interface. Attachment of chemical moieties can be achieved via desired functional groups such as carboxyl and amine groups on the CDs surface. Introduction of surface functional groups on CDs often leads to shift in fluorescence emissions. For instance, substitution of carboxyl groups with alkylamine lead to blue-shift in the green emission wavelength of GQDs [106]. Furthermore, Tetsuka *et al.* have managed to control the PL colour of GQDs from blue to yellow by tuning the degree of amine functionalization. Tetsuka *et al.* showed that this can be done by precisely adjusting the initial concentration of ammonia and temperature during the synthesis of GQDs via amino-hydrothermal treatment [107].

Oxygenated functional groups on CDs surface render the hydrophilic property and hence exhibit excellent water solubility. Moreover, these functional groups can act as surface emissive traps and lead to radiative recombination contributing to the PL as mentioned previously. Therefore, tuning the degree of oxidation can change the PL of CDs as a result of alteration of localized sp^2 clusters and structural defects [71, 108]. Li *et al.* reported that chemical reduction of green emitting GQDs with sodium borohydride, $NaBH_4$ shifted the green PL to blue and at the same time significantly enhanced the QY [87]. In addition, Zhu *et al.* found that higher degree of surface oxidation led to red-shift in emission due to the presence of more surface defects [109].

Polymer passivation involves the formation of a thin insulating layer on CDs surface by attachment of polymeric materials [23]. Polymer passivation is a commonly adopted technique to improve the QY of CDs [41]. Shen *et al.* reported that GQDs surface passivated by PEG exhibited two times higher PL QY than that of bare GQDs [110]. Wang *et al.* also suggested that variation in the degree of surface passivation by PEG_{1500N} might result in different PL QY and lifetime [111]. Anilkumar *et al.* also suggested that crosslinking of CDs with PEG_{1500N} can possibly stabilize the soft shell of functional molecules and lead to reinforcement of CDs structure, hence improve optical performance [112].

Doping CDs with heteroatoms is often employed to fine-tune the CDs. Heteroatoms doped on CDs can be inherited from carbon source during synthesis [41]. Yang *et al.* successfully demonstrated the synthesis of N-doped CDs via one-pot hydrothermal treatment of ammonium citrate. The resultant N-doped CDs exhibited bright blue PL, short fluorescence lifetime, sensitive towards pH and stable at high salt concentration [10]. Sun *et al.* developed the strategy of synthesizing CDs co-doped with S and N atoms through sulphuric acid carbonization and etching of hair fiber [76]. Another interesting doping example is reported by Anilkumar *et al.* who successfully produced carbon-based “quantum” dots. CDs doped with semiconductors zinc sulphide (ZnS) or titanium dioxide (TiO_2) were obtained via passivation of CDs by a combination of surface-doping with semiconductors and organic functionalization. The semiconductors CDs exhibited enhanced QY up to 78% [113].

2.8 Applications of CDs

Owing to the remarkable physiochemical properties of CDs, intensive research studies have been carried out to discover the potential of CDs for various applications. Post synthetic strategies as mentioned previously are employed to obtain CDs with desired characteristics and properties. Applications of CDs in biological and chemical fields such as bio-imaging/ bio-labelling, theranostics, photo-catalysis, bio-sensing and chemical sensing will be discussed as follows.

2.8.1 Bio-imaging/Bio-labelling

Unlike QDs, CDs are biocompatible and relatively non-toxic based on current biological findings. Sun *et al.* were among the pioneers that evaluated the utilization of CDs for bio-imaging and bio-labelling [75]. The CDs were synthesized via laser ablation of carbon target and treated with nitric acid prior to surface passivation with polyethylene glycol (PEG_{1500N}) and poly(propionylethyleneimine-co-ethyleneimine) (PPEI-EI) for biolabeling/bioimaging of *Escherichia coli* and Caco-2 cells. This work later triggered comprehensive research activities on cellular uptake of CDs for bio-imaging applications. Some cell types that have been studied for bio-imaging include human lung cancer (A549) cells [114], cervical cancer cells (HeLa) [48], human breast cancer (MCF-7) cells [115] and liver hepatocellular cancer (HepG2) cells [116].

Shang *et al.* showed that GQDs could also be useful for human neural stem cell (hNSCs) labelling. The results revealed that the cellular uptake of GQDs was concentration- and time-dependent via endocytosis mechanism [117]. Wet chemistry derived functionalized GQDs by Kumar *et al.* were found localized into the cytoplasmic region of human hepatic cancer (HuH-7) cells. The PL of the functionalized GQDs were found stable under different pH conditions and makes it a potential candidate for in vivo imaging [118]. Although majority of the studies showed the uptake of CDs into cell membrane and cytoplasm, there are reports on the localization of CDs in the nucleus. The CDs synthesized by Ray *et al.* through nitric acid oxidation of carbon soot were able to enter the nucleus of the cells without further functionalization [66].

Besides in vitro cellular labelling and imaging, Zheng *et al.* demonstrated that CDs can be potentially used as fluorescent tags for real time molecular tracking in live cells [119]. GQDs were found to readily conjugate with large number of proteins, at the same time retaining their functionalities. In their study, insulin-conjugated GQDs were used for real-time dynamic tracking of insulin receptors in adipocytes to study the distribution, internalization and recycling of insulin receptors. For the first time, the results revealed that apelin and TNF α were the two cytokines that oppositely regulate the internalization and recycling of insulin receptors in adipocytes.

The non-toxic CDs also possess great potential for application in fluorescence imaging in vivo. Yang *et al.* demonstrated for the first time the utilization of CDs obtained from laser ablation for in vivo optical imaging. PEG-passivated CDs and ZnS-doped CDs were injected subcutaneously, intradermally and intravenously into mice. The results showed that the CDs remained strongly fluorescent in vivo with both one- and two-photon excitations [120]. He *et al.* intravenously injected CDs attached with arginyl-glycyl-aspartic acid (RGD) peptide into mice for in vivo imaging of HeLa tumour. Intense fluorescence was observed at the tumour site and in the bladder using a 405 nm laser as a light source [121].

In addition, CDs extracted from instant coffee was demonstrated useful as fluorescence probe for fish tagging. CDs were incorporated into the fish feed for adult guppy fish. In vivo imaging showed that the CDs could be directly applied for fish imaging with low toxicity [122]. Using a genetic worm model named *Caenorhabditis elegans*, Yuan *et al.* have homogenously labelled the sigmoid worm with CDs and the fluorescence was clearly detected using laser scanning confocal microscopy (LSCM) [123]. Another interesting application of CDs is demonstrated by Ghosh *et al.* that have used CDs to image the life cycle of fruit flies. All developmental stages of fruit flies from eggs to adulthood were successfully recorded by optical fluorescence microscopy imaging without showing obvious toxic effects [124].

CDs have also been used for fluorescence labelling and staining of bacteria, fungi and plant cells. Mandal and Parvin have demonstrated rapid detection and staining of bacteria using CQDs as fluorescent marker. Fluorescence microscope showed that the CQDs were only uptake into the cell membrane of bacteria [125]. Metha *et al.* also used water soluble CDs as fluorescent probes for cellular imaging of bacteria and yeast cells [126]. Moreover, Jin *et al.* have fabricated pH-sensitive CDs via simple hydrothermal treatment of threonine. It was reported that the CDs can be readily used to stain plant pathogenic fungal cells for fluorescent imaging [127]. Confocal microscopy by Wang *et al.* showed that staining of intact onion epidermal cells was possible by using CDs as fluorescent dye [59].

2.8.2 Theranostics

The relatively non-toxic and biocompatible CDs have triggered considerable research activities that explore on its potential uses in theranostics which combine diagnosis and therapy [128]. Doxorubicin (DOX) is a broadly used anthracycline medication for cancer chemotherapy. DOX can effectively induce cell death by causing DNA damage and inhibit nucleic acid synthesis in cell nucleus [129]. PEG encapsulated CDs within mesoporous silica nanoparticles (mSiO₂) have been prepared from glycerol. The PEG-encapsulated CDs were then loaded with DOX and incubated with HeLa cells to monitor drug release in vitro [130]. Wang *et al.* also reported similar study using CDs obtained from commercial beer for breast cancer cell imaging and DOX delivery [131].

Besides, in vivo study using A549 xenograft nude mice have also been assessed. DOX-conjugated CDs were intravenously injected into the tumour-bearing mice and the therapeutic efficacy was investigated. The DOX-CDs could be a promising nano-carrier due to its sustained drug release behaviour with enhanced therapeutic effect [129]. In another study, the bio-distribution, clearance and tumour uptake of fluorescence dye ZW800-attached CDs were tracked ex vivo and in vivo using mice model. CDs rapidly excreted from the body after injection through different routes. Different blood clearance patterns were observed for the different injections with clearance rate ranked as intravenous > intramuscular > subcutaneous [132].

Photodynamic therapy is one of the therapeutic approaches mainly for superficial tumours which involves localization and accumulation of photosensitizers in tumour tissue. Singlet oxygen species or reactive oxygen species (ROS) are formed when the photosensitizers are irradiated with specific wavelength and lead to cell death [23]. Photosensitizers are highly hydrophobic light-sensitive molecules that are involved in photodynamic therapy [133]. Choi *et al.* have fabricated folic acid-functionalized PEGylated CDs to deliver photosensitizer zinc phthalocyanine (ZnPc) for both in vitro and in vivo bio-imaging and targeted photodynamic therapy. In vivo cell death can be effectively induced with a combination of targeted delivery of ZnPc and irradiation [133].

Christensen *et al.* studied the effect of CDs on the generation of singlet oxygen and ROS in vitro [134]. The results revealed that CDs were able to scavenge free radicals and generate ROS upon external radiation, making them promising candidates as antioxidants and prooxidants. CDs as antioxidants was also demonstrated by Yang *et al.* who prepared CDs via microwave treatment of garlic and tested against oxidative stress in macrophages that play an important role in initiating and developing inflammatory response [135]. The multi-coloured garlic CNDs could be effectively taken up by macrophages and reduce cells inflammation as a result of antioxidative effect towards macrophages.

CDs have also been explored for their applications in radiotherapy. Kleinauskas *et al.* reported that CDs can also be used as radiosensitizers for radiotherapy treatment of cancer. The cytotoxicity effect of CNDs encapsulated with silver shell was investigated in human prostate cancer cell (DU145) in vitro. The cells viability was significantly reduced upon exposure to radiation in the presence of silver-coated CDs. The silver-coated CDs were claimed to enhance the radiation effect and hence could be used as sensitizers in the cancer cells for phototherapy and radiotherapy treatment [136]. Radio sensitizers are substances that designed to make tumour cells more vulnerable to radiation [137]. Besides, Wang *et al.* showed that the synthesized nanostructured particles comprising of CDs, magnetite (Fe_3O_4) and gold could regulate the release of DOX, and at the same time possess enhanced photothermal effect for cancer therapy [138].

Besides drug delivery, there have been studies on utilizing CDs as nano-carriers for gene delivery and tracking. Liu *et al.* have fabricated PEI functionalized CDs (CD-PEI) through one-pot microwave assisted pyrolysis of glycerol and BPEI with molecular weight of 25000 g/mol (PEI25k). Gene expression of plasmid DNA in COS-7 (African green monkey kidney cells) and HepG2 cells was successfully mediated by CD-PEI as gene vector [139]. In more recent study, Hu *et al.* have prepared BPEI-based CDs by hydrothermal reaction and investigated their potential for gene delivery. Agarose electrophoresis assay indicated that the CDs will react with DNA to form complex. Successful gene delivery was observed when the enhanced green fluorescent protein (EGFP) gene as the reporter gene was expressed in cells using CDs as gene carrier [140].

2.8.3 Bio-sensing

CDs with exceptional PL properties and biocompatibility can also be designed as biosensors to detect a wide range of biomolecules such as glucose, protein, nucleic acid, intracellular pH, antibodies, etc. CDs as biosensors can also be potentially apply as disease detection system. For instance, Qin *et al.* have demonstrated practical application of CDs as potential glucose biosensor to detect glucose in human blood serum based on electrochemical method [141]. Shen *et al.* have also synthesized fluorescent boronic acid modified CDs to detect blood glucose. Fluorescence of the CDs could be selectively quenched by glucose. The CDs was claimed to have “inert” surface and make them highly resistant to interference from different biomolecules [142].

CDs as intracellular pH sensors have also been reported in several studies. Du *et al.* designed a fluorescence resonance energy transfer (FRET) based CDs nano-sensor for intracellular pH sensing and mapping [143]. The fluorescein isothiocyanate (FITC) dye was first covalently attached to CDs. The change in pH would affect the structural and spectral conversion of the FITC moieties. In another study, fluorescence intensity of N-doped GQDs obtained from citric acid and dicyandiamide (DCD) increased with pH increased from 2 to 9. Cell cytotoxicity assay revealed that the GQDs were highly biocompatible, hence a good fluorescent pH indicator to monitor intracellular pH of live cells [144].

Xu *et al.* have presented the first assay exploiting aptamer as target binder for protein detection. The aptamer-functionalized CDs exhibited high specificity towards thrombin with a detection limit of 1.0 nM [145]. Thrombin is a highly specific endoprotease enzyme that acts as blood clotting factor and plays an important role in pathologic processes such as leukemia and liver disease [146, 147]. Moreover, CDs have also been utilized as effective fluorescent sensor for nucleic acid detection [148]. CDs was first attached to single-stranded DNA (ssDNA) labelled with fluorescent dye through π - π interaction, resulted in fluorescence quenching of the dye. When the ssDNA attached to CDs hybridized with its target to form double-stranded DNA (dsDNA), dye fluorescence was recovered due to the release of ssDNA from CDs surface.

Alpha-fetoprotein (AFP) is a serum that associated with a number of liver diseases in adults [149]. Hence, rapid and sensitive detection is desired. The nanocrystal nanocomposites consisting polyamidoamine (PAMAM)-capped CDs and gold (Au) prepared by Gao *et al.* were designed as immobilized matrix for immunosensing of AFP. The nanocomposites were highly sensitive towards AFP with detection limit of 0.025 pg/ml [150]. Lu *et al.* also synthesized GQDs exhibited ECL as ultrasensitive biosensor to detect adenosine triphosphate (ATP), which is the “energy currency” in organisms that is crucial for most enzymatic activities [58]. The developed ECL GQDs sensor exhibited excellent analytical performance in the range of 5.0×10^{-12} to 5.0×10^{-9} mol/L [151].

Furthermore, Zhao *et al.* have demonstrated sensitive detection of human immunoglobulin G (IgG) through regulated interaction between graphene and GQDs [152]. A CDs-based ratiometric fluorescent sensor for intracellular detection of hydrogen sulphide was also reported [153]. CDs and chitosan hybrid film for dopamine sensing [154]; synthesis of hybrid fluorescent probe based on CDs and hydroethidine for specific determination of superoxide anion in live cells [155]; and synthesis of amino-functionalized CDs for melamine detection based on FRET with shorter analysis time and rapid detection [156] have also been developed. These intensive reports on determination of biological compounds based on CDs indicate that CDs can be potentially utilized as biosensor with rapid and sensitive detection for practical applications.

2.8.4 Photocatalysis

The semiconductor, titanium dioxide (TiO_2) that possess long-term thermodynamic stability, strong oxidizing power and relative non toxicity has made it one of the most widely used photocatalyst. However, photocatalytic activity of TiO_2 is limited under visible light due to its inefficiency utilization of visible light as irradiation source [91]. CDs are found to be a potential substitute photocatalysts due to its capability of harnessing light at long wavelength and energy exchange with solution species [23]. Therefore, recent studies have been exploring in integration of CDs with semiconductors to produce photocatalysts that are able to utilize both UV and visible light.

Kang's group has prepared iron (III) oxide (Fe_2O_3) functionalized CDs ($\text{Fe}_2\text{O}_3/\text{CQDs}$) composites for photodegradation of toxic gas-phase benzene and methanol [157]. Under visible light irradiation, the $\text{Fe}_2\text{O}_3/\text{CQDs}$ composites were found exhibited significantly enhanced degradation efficiency for both benzene and methanol degradation. The CQDs were used as electron reservoir to trap electrons. Besides, the CQDs exhibited upconversion PL property that allow absorption of light at longer wavelength, then emit shorter wavelength light. The $\pi - \pi$ interaction between CQDs and benzene was found useful for benzene enrichment on the surface of $\text{Fe}_2\text{O}_3/\text{CQDs}$ composites. Kang's group has also prepared CQDs modified with silver orthophosphate (Ag_3PO_4). The synthesized $\text{CQDs}/\text{Ag}_3\text{PO}_4$ and $\text{CQDs}/\text{Ag}/\text{Ag}_3\text{PO}_4$ can act as high performance photocatalyst for photodecomposition of methyl orange under visible light irradiation [158].

In another study, CQDs modified P25 TiO_2 ($\text{CQDs}/\text{P25}$) composites were fabricated by hydrothermal method for photocatalytic hydrogen (H_2) production. The $\text{CQDs}/\text{P25}$ composites were found to enhance photocatalytic H_2 production under both UV-Vis and visible light. It was proposed that upon UV light irradiation, the CQDs in $\text{CQDs}/\text{P25}$ composites served as electron reservoirs for efficient separation of electron-hole pairs of P25. This was achieved by trapping the photoinduced electrons and led to improved photocatalytic activity. Under irradiation of visible light, the CQDs acted as photosensitizers to facilitate the transfer of photoexcited electrons to P25.

Yu *et al.* claimed that π -conjugated CDs displayed improved photocatalytic activity compared to that of physically adsorbed to semiconductor [159]. Hu *et al.* have investigated the effect of different surface groups on the photocatalytic activity of CDs. Among the surface groups investigated, it was evidenced that chlorine-capped CDs exhibited highest degradation rate, followed by oxygen-capped CDs and nitrogen-capped CDs being the slowest [160].

CDs have also been reported as potential photosensitizers in solar cells. Zhang *et al.* have prepared hybrid nano-spheres of N-doped CQDs and TiO_2 (NCQDs/ TiO_2) and investigated the photocatalytic activity by degradation of Rhodamine B and conversion of benzyl alcohol under irradiation of visible light. The NCQDs/ TiO_2 nanocomposites were found to enhance the photocatalysis activity. Moreover, it was revealed that utilization of NCQDs/ TiO_2 as sensitizers in dye-sensitized solar cells display improved performance [161]. CQDs functionalized with different surface groups were demonstrated to be good sensitizers to sensitize zinc oxide (ZnO) nano-rods to visible light as solid-state nanostructured solar cells. The different functional groups on CQDs surface were found to affect the performance of the solar cells [162].

In more recent study, Wang *et al.* have also reported the development of CDs based solar cells. The N-doped CDs were first prepared by facile pyrolysis of citric acid as the carbon source and ammonia as the source of nitrogen. Higher current density could be induced by the N-doped CDs when compared with the N-free CDs. The N-doped CDs that exhibited enhanced visible light absorption were then integrated with porous TiO_2 for QDs solar cells. The N-doped CDs were used as sensitizers in the solar cells and found to improve the efficiency of the solar cells. The developed "green" CDs-based QDs solar cells was claimed to have the best power conversion efficiency so far [163].

2.8.5 Chemical Sensing

Chemical sensing is one of the applications of CDs that have captivated great research attention. Fluorescence response of CDs as sensing system can be generally classified into fluorescence turn-off, fluorescence turn-on, FRET and ratiometric. Considerable studies have been reported on utilizing CDs as sensitive sensing receptors to detect a wide range of heavy metal ions that are detrimental to human health. Along with sensing of metal ions, CDs have also been utilized as fluorescent sensing receptors for chemical detection of anions as well as chemical and biological molecules in aqueous solution.

Initial stage of research involves exploring CDs as direct fluorescence sensors for metal ions detection. For instance, CDs can be used as direct selective fluorescence sensing receptors for lead ions (Pb(II)) [9], tin ions (Sn(II)) [164], silver ions (Ag(I)) [165], mercury ions (Hg(II)) [2], and iron (III) ions (Fe(III)) [166]. Over the past few years, research in the application of CDs for metal ions sensing evolved around enhancing the sensitivity and specificity of CDs through different strategies such as surface functionalization and doping of CDs. For instance, Dong *et al.* prepared BPEI-functionalized CQDs for copper ions (Cu(II)) detection with detection limit as low as 6 nM [167]. Chen *et al.* also reported the fabrication of N and S co-doped CDs for Fe(III) detection with excellent sensitivity [168].

In more recent study, attempts have been made to fabricate CDs into nano-devices with enhanced sensitivity and selectivity. A paper based sensor strips was prepared by Gupta *et al.* for ultrasensitive and highly sensitive detection of Pb(II) ions. The paper strips were prepared by immobilizing CDs obtained via microwave-assisted carbonization of biological media onto cellulose based filter paper. The LOD in aqueous solution was determined to be 106-110 pM [169]. Wang *et al.* have fabricated a fluorescent sensing interface using β -amino alcohol functionalized CDs for selective Cu(II) detection [170].

Although majority of the reported studies are based on fluorescence turn-off mechanism, fluorescence turn-on studies are also demonstrated. A fluorescent turn-on CDs sensor for selective detection of Hg(II) ions based on

bis(dithiocarbamate)copper(II) conjugated CDs (CuDTC₂-CDs) was developed. CuDTC₂ would first quench the CDs fluorescence upon functionalization. The fluorescence of the functionalized CDs could be recovered in the presence of Hg(II) ions [171]. Hg(II) ions are one of the most studied metal ions among the varieties of metal ions due to their adverse effects on the environment and human health. Table 2.2 summarizes the varieties of CDs-based chemical sensors for the detection of Hg(II) ions in recent studies.

Table 2.2: List of CDs for fluorescence detection of Hg(II) ions.

Probe	QY (%)	Read Out	LOD (nM)	Linear Range (μM)	Real Sample	Reference
CDs	82.4	Turn off	201	0-80	Lake water, cattle's urine	[172]
CDs	-	Turn off	17	2-22	Pool water	[173]
CDs	36	Turn off	20	0-50	Tap water	[174]
CDs	35.4	Turn off	1.65	0-10	Tap water	[175]
CDs	-	Turn off	630	0-20	-	[176]
CDs	42.5	Turn off	7.3	0.05-5	Tape water, lake water	[177]
CDs	-	Turn off	80	0.16-2	-	[178]
CDs	17.2	Turn off	1.37	0-30	Mineral water, tap water, ground water	[179]
CDs/Zn(OH) ₂	-	Turn off	0.2	0-0.40	Tap water	[180]

Detection of anions using CDs based fluorescence system has also been reported. A CDs-based system to detect Cu(II) ions and sulphide (S²⁻) anions have been developed. In this system, fluorescence of CDs was quenched upon binding of Cu(II) ions to ligands on CDs surface. Subsequent adding of S²⁻ anions led to fluorescence enhancement due to dissociation of Cu(II) from CDs surface to form stable CuS complex [181]. In another study, presence of Hg(II) provoked CDs fluorescence quenching while fluorescence could be recovered upon addition of I⁻ anions [182]. Static quenching of tryptophan doped CDs was also observed in the presence of peroxyntiride (ONOO⁻) anions [183].

Besides metal ions and anions, CDs detection of compounds are also reported. Zhang *et al.* have employed microwave-assisted pyrolysis carbonization to obtain N-rich CDs as dual sensing probe for 2,4,6-trinitrotoluene (TNT). TNT can effectively quench the fluorescence of N-rich CDs through charge transfer based on strong TNT-amino interaction. Electrochemical detection of TNT using CDs modified glassy carbon electrode was found exhibited even more sensitive response compared to fluorescent detection [184]. Cayuela *et al.* also prepared N-doped CDs as fluorescence sensors that could be used to effectively detect nitroaromatic explosives through fluorescence quenching mechanism [185]. In addition, fluorescence sensing of some other compounds developed based on CDs system is summarized in Table 2.3.

Table 2.3: List of CDs for fluorescence detection of some compounds.

Probe	Analyte	QY (%)	Read Out	LOD (nM)	Linear Range (μM)	Real Sample	Reference
CDs	Guanine	16	Turn on	6.7	0.013-0.27	Urine, DNA	[186]
CDs	Tetracycline	-	Turn off	5.48	0.02-14	Milk	[187]
CDs	Ammonia	5.28	Turn off	1.76×10^5	-	-	[188]
CDs	Curcumin	25.4	Turn off	84.8	0.2-10	Urine	[189]
CDs	Tartrazine	10.37	Turn off	73	0.25-32.5	Food	[190]
CDs	Glutathione	17.2	Turn off	6700	0-50, 50-100	-	[191]
CDs	Dopamine	67	Turn on	1×10^{-4}	1×10^{-6} - 1	Human serum	[192]
CDs	Thiamine	2.8	Turn on	280	10-50	Vitamin capsule	[193]

Chapter 3 Synthesis of Carbon Dots

3.1 Executive Summary

In search for a sustainable starting precursor for the synthesis of CDs, cellulose as one of the most abundant and renewable resources found naturally has been chosen to be used as carbon source in this study. Facile acid-assisted hydrolysis approach using sulphuric acid is used to dehydrate and carbonize α -cellulose into CDs. In order to compare the physiochemical properties of CDs synthesized via different methods and precursors, thermal pyrolysis in high temperature furnace is also employed for the synthesis of CDs from α -cellulose and L-glutamic acid. Synthesis conditions of both approaches are optimized to obtain CDs with best fluorescence properties where the fluorescence excitation and emission are the highest. The morphology and optical properties of the CDs obtained from these different methods are performed and reported in this study.

CDs exhibiting different fluorescence emission and distinct properties have been successfully synthesized from the two different approaches. This chapter provides a brief overview on current state of CDs synthesis using acid dehydration method. The experimental procedures, analytical results and relevant discussions are also included in this chapter. Finally, a brief summary is included at the end of the chapter to conclude the findings.

3.2 Introduction

Since the accidental discovery of CDs by Xu *et al.* in 2004 [1], attention have been paid on developing new approaches to prepare CDs from diverse organic precursors. Simple aqueous solution route to synthesize CDs by acid dehydration and oxidation method was pioneered by Peng and Trivas-Sejdic. Sulphuric acid as strong dehydrating and oxidizing agent was first used to dehydrate carbohydrates into carbonaceous materials. Subsequent treatment with nitric acid can further break down the carbonaceous materials into CDs. CDs emitting blue fluorescence were finally obtained by passivation with amine-terminated compounds [3]. Following that, Chandra *et al.* have synthesized CDs exhibiting green fluorescence by employing sucrose as starting precursor and phosphoric acid as oxidizing agent through microwave-assisted acid exfoliation [194].

Qiao *et al.* demonstrated the synthesis of CDs with bright blue fluorescence by nitric acid treatment of different activated carbon sources. The fluorescence emission of the CDs was found to be dependent on the excitation wavelengths [45]. Furthermore, it was reported that heteroatoms can be doped into the CDs as a concurrent effect of acid dehydration synthesis to modify the optical properties. The Energy Dispersive X-ray Spectroscopy (EDX) spectrum reported by Sachdev *et al.* has revealed that CDs obtained by microwave assisted sulphuric acid dehydration of chitosan composed of carbon, oxygen, nitrogen and sulphur elements where the sulphur was originated from sulphuric acid [195].

Peng *et al.* managed to obtain CDs emitting at blue, green and yellow fluorescence in large scale by carbonizing and oxidizing carbon fibers in a mixture of concentrated sulphuric acid and nitric acid solution. The CDs with different emission colour were obtained at different temperatures, revealing that reaction temperature plays an important role in controlling the size of the carbon nanoparticles [196]. In another study, Bhunia *et al.* investigated the effects of different dehydrating agents as well as altering the reaction temperature and time for the synthesis of CDs. CDs exhibiting different fluorescence colours such as blue, green, yellow and red fluorescence were obtained. It was claimed

that acid dehydration using sulphuric acid is most likely to produce CDs emitting blue and green fluorescence whereas concentrated phosphoric acid based carbonization of carbohydrates is more favorable for the production of CDs emitting yellow and red fluorescence [197].

Although considerable research have been reported on CDs synthesis via acid dehydration approach, direct comparison of the CDs reported from various studies is inappropriate due to different starting precursors and/or synthesis parameters. In this study, the effect of reaction temperature and time during the synthesis of CDs through acid carbonization using only sulphuric acid will be investigated. α -cellulose will be used as the starting materials for CDs synthesis. Moreover, simple thermal pyrolysis of the same α -cellulose and L-glutamic acid in high temperature furnace will also be employed to produce CDs. Synthesis conditions such as reaction time and temperature will be optimized to obtain CDs with optimum fluorescence properties. The properties of the different types of CDs obtained will be systematically compared and analyzed.

3.3 Experimental Design

3.3.1 Materials and Reagents

All reagents used in this study were of analytical grade. α -cellulose was purchased from Sigma Aldrich. Concentrated sulphuric acid (98%) was purchased from RCI Labscan Chemicals. Sodium hydroxide in pellet form was purchased from Hudson Chemicals. L-glutamic acid was purchased from R&M Chemicals and acetone was purchased from Bendosen. Sodium acetate and glacial acetic acid purchased from R&M Chemicals and RCI Labscan, respectively were used to prepared buffer solution with pH 5. All chemicals were used as received without further purification unless otherwise stated. Ultrapure water obtained from Milipore Mili-Q Advantage-A10 and Milipore Elix-5 water purification system (~ 18.2 M Ω .cm, 25°C) was used throughout the study.

3.3.2 Instrumentations

Fluorescence measurements were recorded using fluorescence spectrophotometer (Cary Eclipse Varian). In brief, CDs sample was diluted with ultrapure water and transferred into a quartz cuvette of 4 clear sides with a path length of 1.0 cm. The settings of excitation and emission wavelengths were altered accordingly to obtain optimum fluorescence excitation and emission of CDs prepared in different synthesis conditions. UV-Vis absorption spectra were obtained using UV-Visible spectrophotometer (Varian Cary 50). The absorbance of samples was recorded within the range of 200 nm to 800 nm. Ultrapure water was used as reference for the absorbance measurement. Laboratory furnace (Carbolite ELF 11/14B) was used for synthesis of CDs by thermal carbonization method. A pH meter (Mettler Toledo SevenEasy) was used for adjustment of pH and water bath (Memmert WNB 14) was used to control the temperature. Vacuum concentrator (Labconco Acid-Resistant CentriVap Concentrator) was used to remove excess solvent during isolation of CDs. Freeze dryer (Labconco FreezeZone 6) was used for CDs isolation by lyophilize CDs sample to remove excess water in CDs sample. Scanning Electron Microscope (SEM) (JEOL JSM-6930 LA) operated at zeta potential of 10kV was used to characterize the physical properties of CDs obtained. In brief, sample for SEM imaging was prepared by dispensing 10 μl of CDs sample onto a 1.0 x 1.0 cm^2 platinum plate and left to dry. Besides, Transmission Electron Microscope (TEM) was also used to characterize the CDs sample by drying approximately 5 μl of CDs sample on TEM copper grid prior to imaging. Fourier Transform Infrared (FTIR) (Perkin-Elmer) was used to characterise the organic functional groups present on CDs surfaces.

3.3.3 Synthesis of CDs via Acid Hydrolysis of α -Cellulose

The method of acid hydrolysis of organic precursor for the synthesis of CDs was adopted with slight modification from Chin *et al.* who synthesized CDs from starch nanoparticles [43]. In general, α -cellulose weighed 0.04 g was dispersed in 1.0 ml ultrapure water. The dispersion was dripped dropwise into 3.0 ml of chilled concentrated sulphuric acid (98%). It was observed that the α -cellulose suspension dissolved once added into concentrated sulphuric acid. The mixture was briefly swirled to obtain homogenous solution, followed by incubation at different temperatures ranging from 4 °C to 70 °C. The samples incubated at different temperatures were monitored over a period of prefixed time. The resulting brownish solutions indicated the formation of CDs. The as-synthesized CDs samples were then diluted with ultrapure water and filtered through 0.22 μ m syringe filter to remove large carbon residues. Sodium hydroxide solution was used to neutralize and adjust the pH of the CDs samples.

3.3.4 Isolation of Acid hydrolysed CDs Sample

For CDs isolation, salting out method using acetone as solvent was employed to remove the sodium sulphate salt formed after neutralization. Equal volume of acetone was added to the neutralized CDs solution and mixed vigorously. The solution was then left to stand at 4 °C for minimum 2 hours to promote crystallization of salts. The CDs that suspended in the acetone supernatant were then pipetted into new vials. The presence of acetone in the supernatant solution containing CDs was eliminated by vacuum concentration. The setting of vacuum concentrator was fixed at 50 °C heating time for 50 minutes. After the removal of acetone, the CDs solution was concentrated by lyophilization overnight in freeze dryer to remove excess water. The isolated CDs samples in dry form were then kept in clean vials, sealed airtight and store in -20 °C until use for further characterization.

3.3.5 Synthesis and Isolation of CDs (Thermal Carbonization)

Besides acid hydrolysis, thermal carbonization was also employed to obtain CDs for comparison study. CDs were prepared by pyrolysis of α -cellulose in a laboratory furnace (Carbolite ELF 11/14 B). In the typical synthesis, accurately 1.0 g of α -cellulose was weighed into a crucible and carbonized in furnace at a fixed temperature for 30 minutes. Optimized synthetic temperature was obtained by carbonizing α -cellulose at different temperature ranging from 200 to 400 °C. After pyrolysis process, the resulting product was left cool to room temperature before suspended in 20 ml ultrapure water. The suspension was centrifuged at 4,000 rpm for 10 minutes to remove bulk particles and the supernatant was then filtered through 0.22 μ m syringe filter. The CDs solution was then lyophilized for 18 hours in freeze dryer (Labconco FreeZone 6) and kept at -20 °C until used.

3.3.6 Thermal Carbonization of L-Glutamic Acid

L-glutamic acid was also used as another carbon source for the synthesis of CDs by thermal pyrolysis in furnace. In typical synthesis, 0.5 g of L-glutamic acid was weighed into a crucible and carbonized in high temperature furnace. Reaction temperature was optimized for optimum CDs production. The carbonized product was then left to cool at room temperature and suspended in 20 ml ultrapure water, followed by filtration through 0.22 μ m syringe filter to remove large undissolved particles, and used for further study.

3.4 Results and Discussion

3.4.1 Acid hydrolysis of α -Cellulose

3.4.1.1 Optical Properties

In this study, it was found that CDs emitting two different fluorescence colours can be isolated during different stages of carbonization of α -cellulose using concentrated sulphuric acid. CDs emitting bright green and blue fluorescence obtained from acid hydrolysis of α -cellulose are clearly shown in Figure 3.1 under the exposure of UV light.

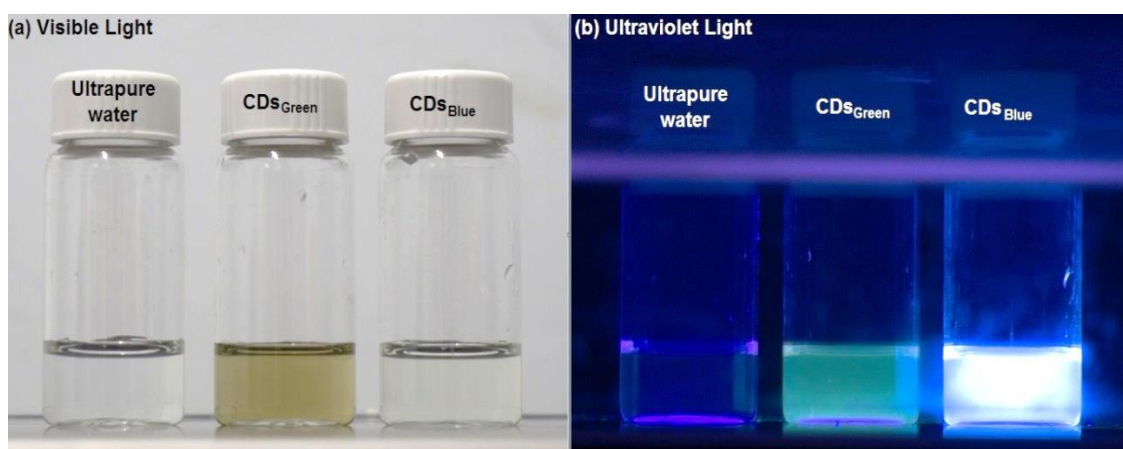


Figure 3.1: CDs synthesized from α -cellulose via sulphuric acid hydrolysis approach under (a) visible light and (b) UV light exposure.

This is the first evidence that the α -cellulose has been converted into CDs since other ingredients involved for the synthesis showed no or low fluorescence. Accordingly, the emission intensity can be correlated as semi-quantitative indicator for the CDs concentration, where higher intensity will reflect the presence of more CDs and vice versa. The CDs emitting green fluorescence is depicted as CDs_{Green} whereas CDs emitting blue fluorescence is depicted as CDs_{Blue}. CDs_{Green} was recorded to have an emission band with peak wavelength at 500 nm when being excited at the optimum wavelength of 450 nm (Figure 3.2), whereas CDs_{Blue} showed a band with peak wavelength at 456 nm upon excitation at the optimum wavelength of 357 nm (Figure 3.3).

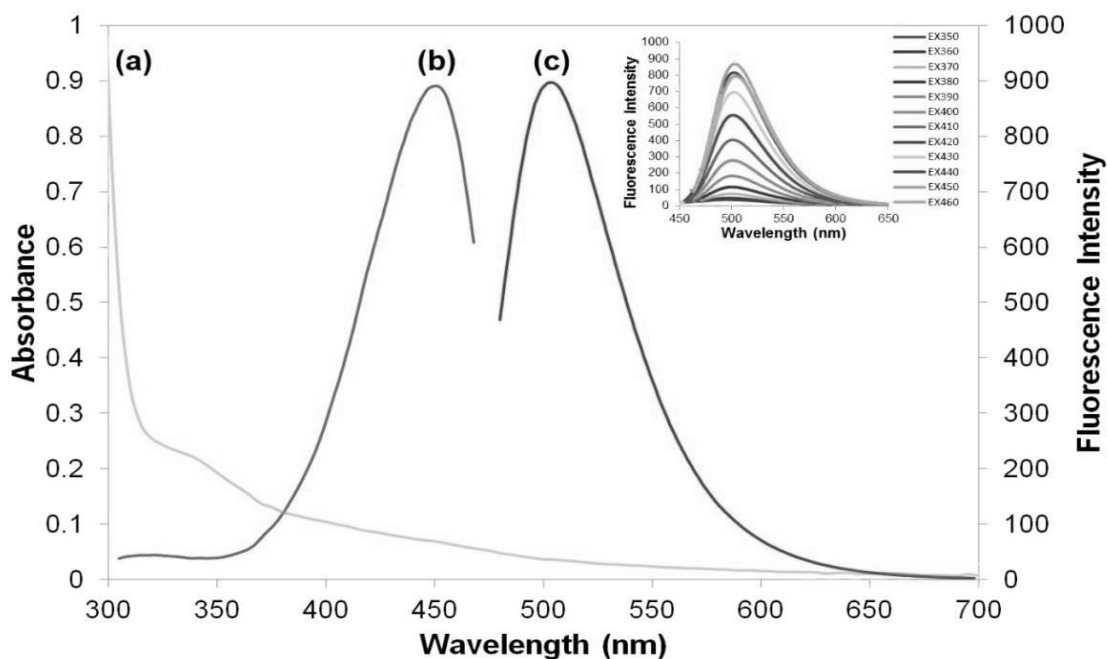


Figure 3.2: The (a) absorption, (b) optimum excitation and (c) emission spectrum of $\text{CDs}_{\text{Green}}$ prepared by acid hydrolysis approach. Inset illustrates that emission of $\text{CDs}_{\text{Green}}$ is independent on the excitation wavelength.

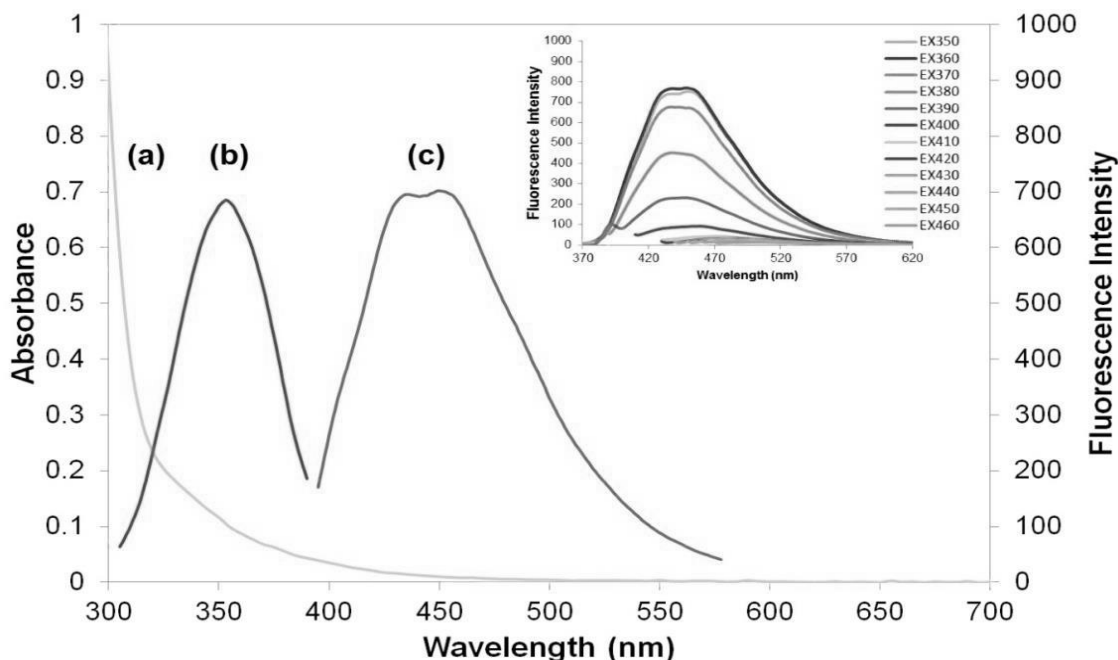


Figure 3.3: The (a) absorption, (b) optimum excitation and (c) emission spectrum of CDs_{Blue} obtained by sulphuric acid hydrolysis method. Inset illustrates that emission of CDs_{Blue} is independent on the excitation wavelength.

FWHM of emission band is typically adopted as a measure of homogeneity of a system where narrow FWHM indicates a homogenous system whereas wide FWHM indicates a heterogenous system. The FWHM of the emission band for $\text{CDs}_{\text{Green}}$ was ~ 65 nm where this relatively narrow FWHM suggested that the $\text{CDs}_{\text{Green}}$ produced were uniform in size [56]. However, the FWHM of CDs_{Blue} was found to be ~ 92 nm which was slightly wider when compared to $\text{CDs}_{\text{Green}}$. The FWHM of CDs_{Blue} was observed to associate with a small shoulder peak. The small shoulder peak was suggested to be caused by either the transmission property of the CDs itself or the presence of trace impurities in the surrounding of the CDs [198]. Moreover, both the as-prepared $\text{CDs}_{\text{Green}}$ and CDs_{Blue} have portrayed an excitation-independent behaviour. In other words, there was only change in intensity of the fluorescence emission but no shift in the emission wavelengths when the excitation wavelength was adjusted within the range of 350-460 nm at an interval of 10 nm. This excitation-independent emission has suggested less types of surface defect present on the CDs surface and the as-synthesized CDs obtained were more homogenous in size [199].

The UV-vis absorption of both $\text{CDs}_{\text{Green}}$ and CDs_{Blue} were recorded using ultrapure water as solvent blank for the measurement. Figure 3.2 shows the typical absorption spectrum of $\text{CDs}_{\text{Green}}$ exhibited a weak UV-vis absorption shoulder peak at around 340 nm. The weak absorption band is ascribed to the presence of aromatic π orbitals [200, 201]. For CDs_{Blue} , the UV-Vis absorption spectrum was relatively featureless. There was no obvious absorption peak can be seen as shown in Figure 3.3, instead a wide absorption band is observed in the absorption spectrum. The broad absorption band may be attributed to broad size distribution of CDs or distribution of different emissive sites on CDs [6, 202].

3.4.1.2 PL properties during carbonization

During the synthesis of CDs, it was realized that the fluorescence of CDs_{Green} was slowly shifted towards the blue region when left overnight at room temperature. This led to the suggestion that CDs_{Green} could eventually be converted into CDs_{Blue} at ambient condition continuously. Thus, it will be interesting to further on the study to understand more on conversion kinetics. To achieve this, it is known that the kinetic of CDs formation is greatly affected by the synthesis temperature. In this scenario, changing the temperature during the carbonization process could eventually change the formation kinetics. Different solutions containing similar mixture content of α -cellulose and concentrated sulphuric acid were incubated separately in controlled temperature of 4, 24, 50 and 70 °C. Formation of brown to dark brown solutions of all the samples indicated the formation of CDs. During the carbonization process in sulphuric acid solutions, the fluorescence emission at 456 and 500 nm was monitored simultaneously upon excitation at 357 and 450 nm, respectively for a period of 4.5 to 5 hours. The result reveals that temperature applied during the synthesis process exerts significant effect on the formation of CDs and eventually led to the production of CDs with distinct fluorescence emission. The kinetic study of CDs formation performed at 50 °C was shown in Figure 3.4.

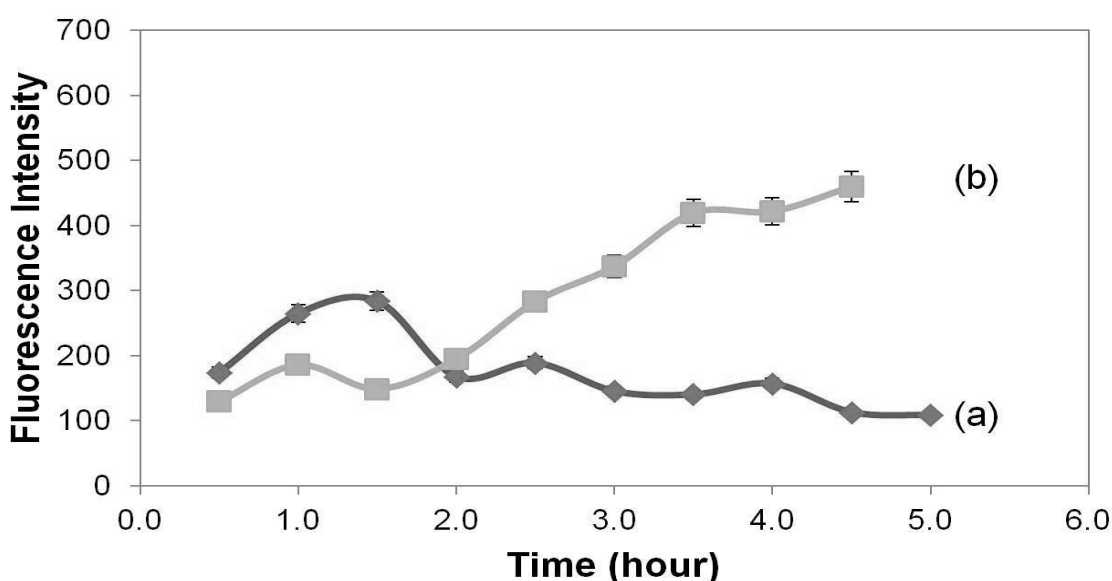


Figure 3.4: Variation of fluorescence intensity of CDs synthesized at 50 °C monitored at (a) 500 nm and (b) 456 nm.

The temperature of 50 °C was chosen to monitor the kinetics of CDs formation because both CDs_{Green} and CDs_{Blue} were co-existed at such temperature. When the temperature of the synthesis process was fixed at 50 °C, it was observed that the fluorescence of CDs monitored at green spectral region (500 nm) decreased gradually. Concurrently, fluorescence intensity of CDs monitored at blue spectral region (456 nm) increased continuously. This result is in agreement with the previous observation where the fluorescence of CDs_{Green} would eventually shift to the blue spectral region. The formation kinetics could be altered by adjusting the synthesis temperature from 4 °C to 70 °C.

The variation of fluorescence emission intensity of CDs synthesized at 4, 24 and 70 °C monitored at 500 nm upon 450 nm excitation and emission at 456 nm upon excitation at 357 nm are shown in Figure 3.5 (a) and (b), respectively.

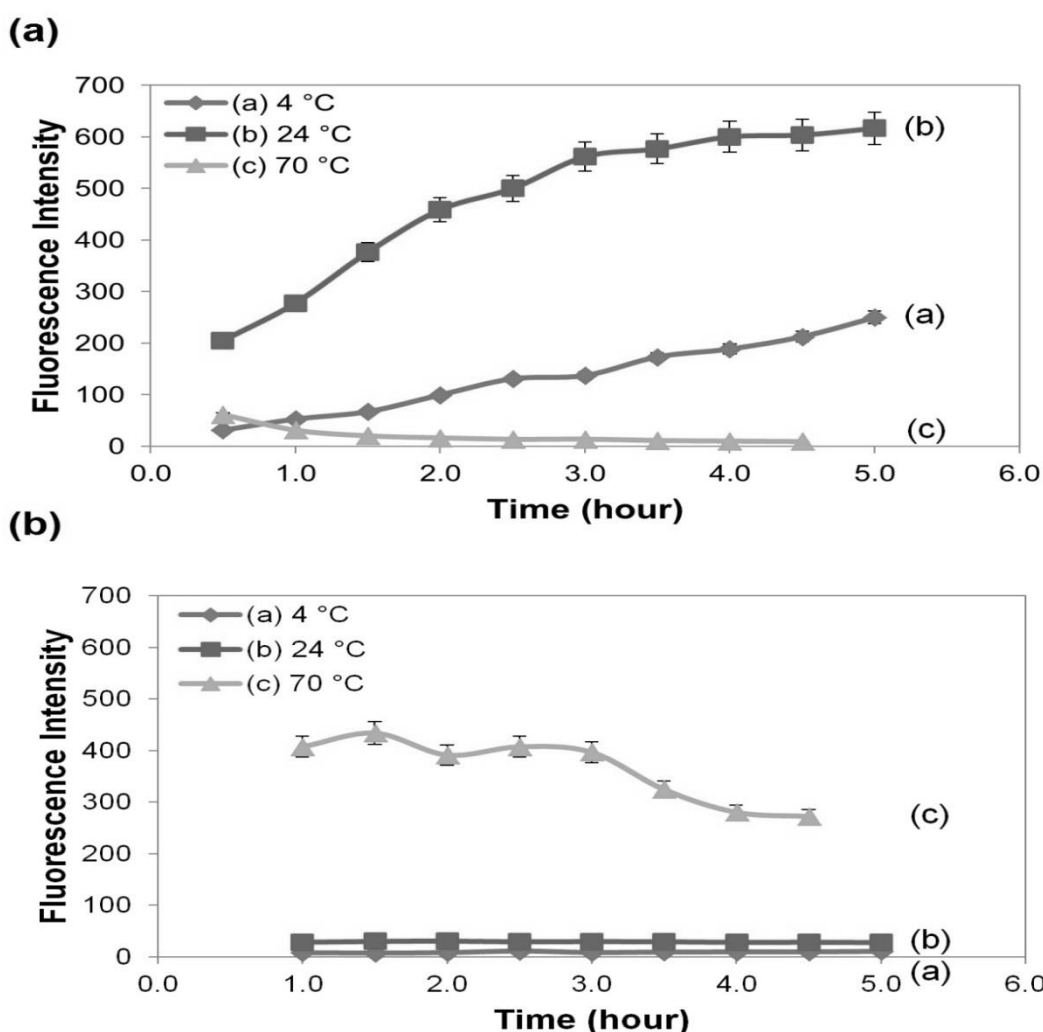


Figure 3.5: Variation of fluorescence intensity monitored at (a) 500 nm and (b) 456 nm for CDs prepared at 4 °C, 24 °C and 70 °C.

The result reveals that synthesis process at lower temperature promoted the formation of CDs_{Green} while higher temperature was more favourable for the formation of CDs_{Blue}. This concept was clearly demonstrated with the gradual increase in fluorescence at 500 nm was recorded over the period of 5 hours when sulphuric acid hydrolysis was performed at 4 °C. At this temperature, no fluorescence emission was detected at 456 nm, indicating only CDs_{Green} were present at that instant. The fluorescence intensity of CDs_{Green} increased gradually at 24 °C when compared to that of 4 °C, but no fluorescence could be detected at 456 nm. On the other hand, sulphuric acid hydrolysis of α -cellulose incubated at 70 °C showed intense fluorescence emission at 456 nm, but no fluorescence emission can be detected at 500 nm, indicating only CDs_{Blue} were being produced. This result shows that 24 °C promotes the effective formation of CDs_{Green} whereas 70 °C was too vigorous for CDs_{Green} formation. Hence, this result further confirmed that temperature is an important parameter that will affect the formation kinetics of CDs. Further incubation at such temperature (70 °C) will eventually lead to decrease in blue fluorescence intensity of CDs_{Blue} (456 nm). Prolong incubation at high temperature was suggested to induce excessive carbonization that will eventually result in complete carbonization and distortion of the graphitic structure of CDs which in turn leads to the formation of bare CDs which possess no PL properties [92].

Figure 3.6 illustrates the 3-dimensional scan of CDs isolated from sample incubated at temperature of 50 °C for 1.5 hours. This is the intermediate setting of this study. The figure clearly shows that CDs_{Green} and CDs_{Blue} are co-existed at this particular synthetic condition. Hence, this study has demonstrated that CDs with different PL properties can be prepared by precisely control the synthesis parameters such as reaction temperature and time during carbonization process. Reaction temperature has altered the carbonisation kinetics, and led to the formation of different kinds of CDs with unique emission spectra profiles. These results strongly suggested that reaction temperature played an important role in the PL of CDs. This result is in good agreement with the findings by Peng *et al.* who emphasized that PL of CDs can be tailored by simply adjusting the reaction temperature [44].

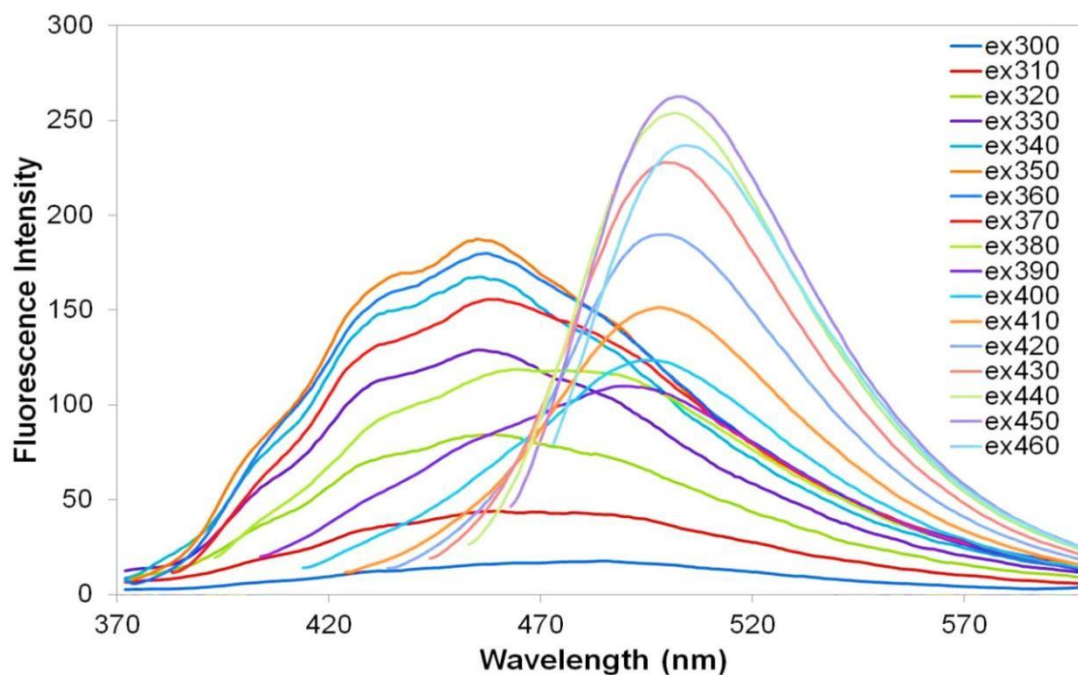


Figure 3.6: 3-dimensional scan of CDs prepared by incubation at 50 °C for 1.5 hours.

Additionally, Hsu and Chang have proposed a four-stage mechanism for the formation of CDs, which involved dehydration of precursors, polymerisation of intermediates or aromatisation, nucleation, and crosslinking that promotes particles growth [203]. Similarly, the concept is suggested to be applicable to this study. α -cellulose will be first dehydrated by sulphuric acid to form reactive intermediates that are further proceeded with polymerization of these intermediates units. At low temperature, the dehydration and polymerisation processes were expected to be slower and would not favour the next nucleation process to form the CDs. The intermediates instead crosslink with the existing nuclei and eventually promoted the growth of the particles. Due to this reason, CDs with growing size were reported to emit at longer wavelength [196]. This matched with the fluorescence profile of CDs obtained at low temperature that possesses fluorescence emission at longer wavelength. As the temperature during CDs synthesis increased, the active hydrolysis in the presence of acid as strong dehydrating and oxidizing agent could rapidly produce intermediates at higher concentration. This would in turn cause active nucleation to occur and eventually results in the formation of smaller particles and blue-shifted the fluorescence emission towards the region with shorter wavelength.

In order to validate the suggested explanations on the observed FL trend, a test was performed by mixing the reactants at low temperature (4 °C) and maintained the temperature for 10 minutes before warming the mixture to 24 °C. This allowed slower rate of hydrolysis to occur during the initial stage of reaction, followed by faster growth rates at elevated temperatures. The results obtained clearly showed that such approach had promoted the final intensity of CDs_{Green} by at least 25% as compared to the batch of CDs sample that was synthesised at fixed temperature of 24 °C (Figure 3.7). There was no fluorescence recorded within the blue range at this stage.

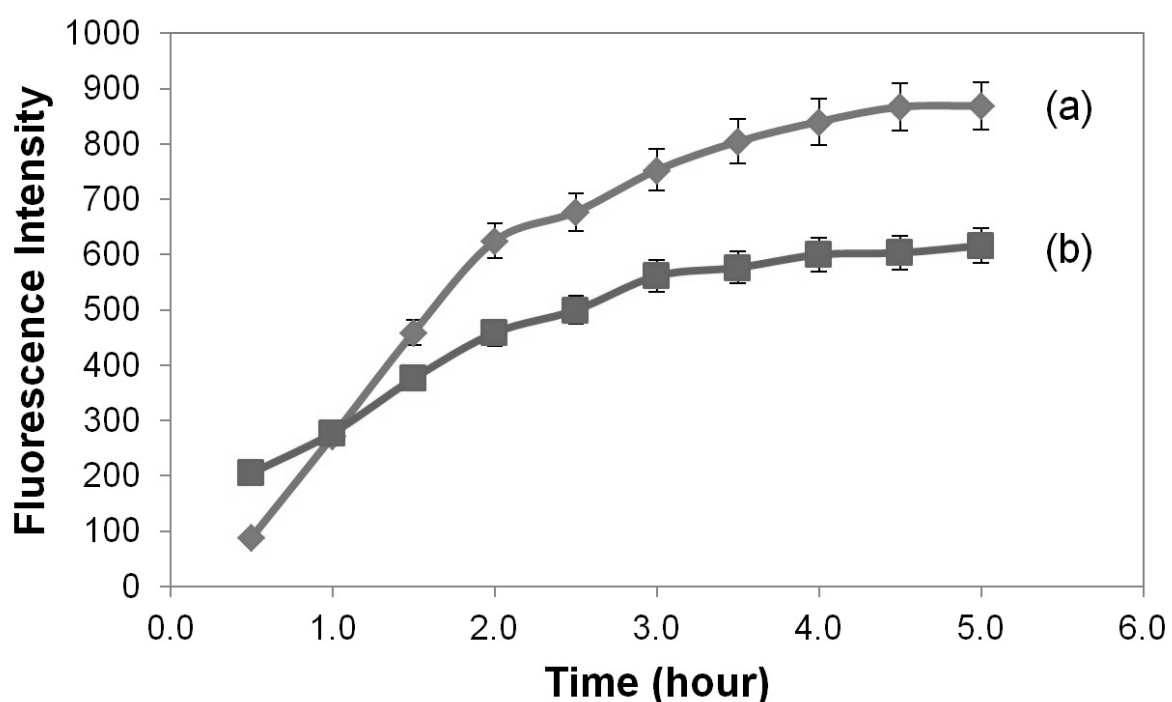


Figure 3.7: CDs synthesized by mixing the reactants at (a) 4 °C for 10 minutes incubation and subsequently at 24 °C, and (b) 24 °C without incubation at 4 °C.

3.4.1.3 Characterizations of CDs

CDs are generally known to have high photostability with potential applications in various fields. In order to determine the photostability at room temperature of the as-prepared CDs_{Green} and CDs_{Blue}, both samples were exposed to UV light at their respective optimum excitation wavelengths for 75 minutes. The fluorescence intensity of CDs_{Green} and CDs_{Blue} were measured every 5-minutes interval at 500 and 456 nm respectively. As indicated in Figure 3.8, the fluorescence emission of CDs_{Green} was found to have decreased by 23.22% over 75 minutes. This result suggests that the as-prepared CDs_{Green} were comparatively less stable than CDs_{Blue}. On the other hand, the fluorescence emission of CDs_{Blue} showed a slight decrease in fluorescence intensity of approximately 1.86% from its initial intensity upon continuous excitation in the UV range. This indicates that CDs_{Blue} possessed higher photostability when compared to CDs_{Green} and hence a more suitable candidate for practical applications. The decreased in fluorescence intensities could be a result of photobleaching which is a photo-induced chemical destruction process that eventually leads to fluorescence decay of fluorophores upon continuous exposure to UV irradiation [204].

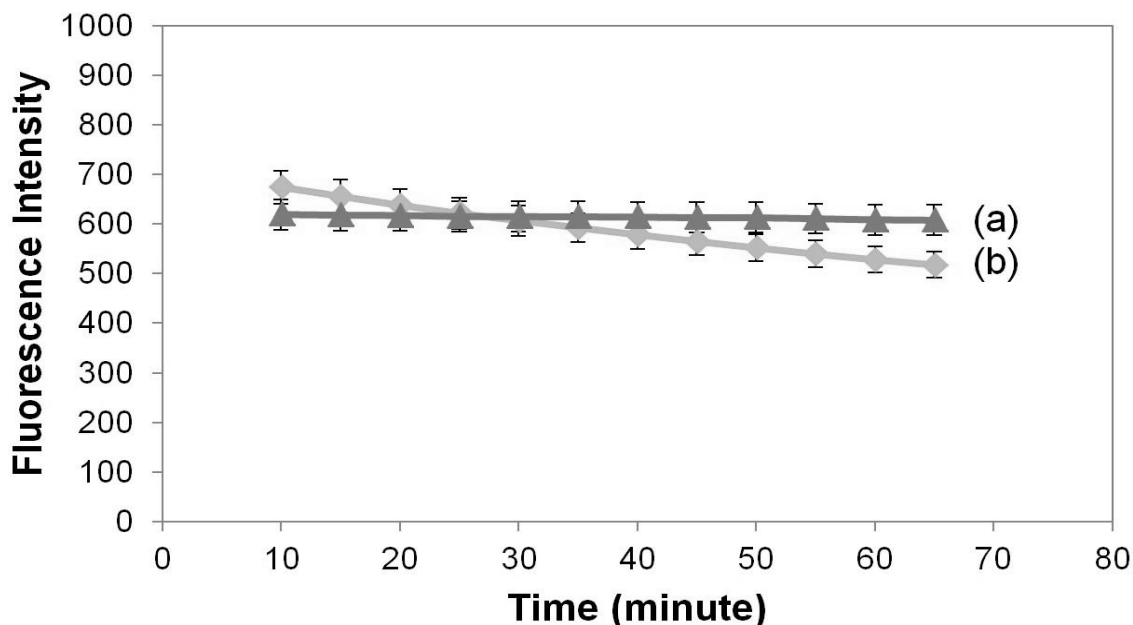


Figure 3.8: Fluorescence intensity of (a) CDs_{Blue} and (b) CDs_{Green} monitored at emission wavelengths of 456 nm and 500 nm, respectively.

The relative QY of both CDs_{Green} and CDs_{Blue} were also determined by comparison to the typical quinine sulphate standard, with literature represented QY value of 54%. The QY values of CDs_{Green} and CDs_{Blue} were calculated to be 6.4% and 4.0% respectively. These QY values were comparable with most of CDs systems reported in the literature [205, 206]. Furthermore, FTIR was used to characterize the organic functional groups that are present on the surface of CDs. The FTIR spectrum of the untreated α -cellulose, CDs_{Green} and CDs_{Blue} are shown in Figure 3.9 (a), (b) and (c), respectively.

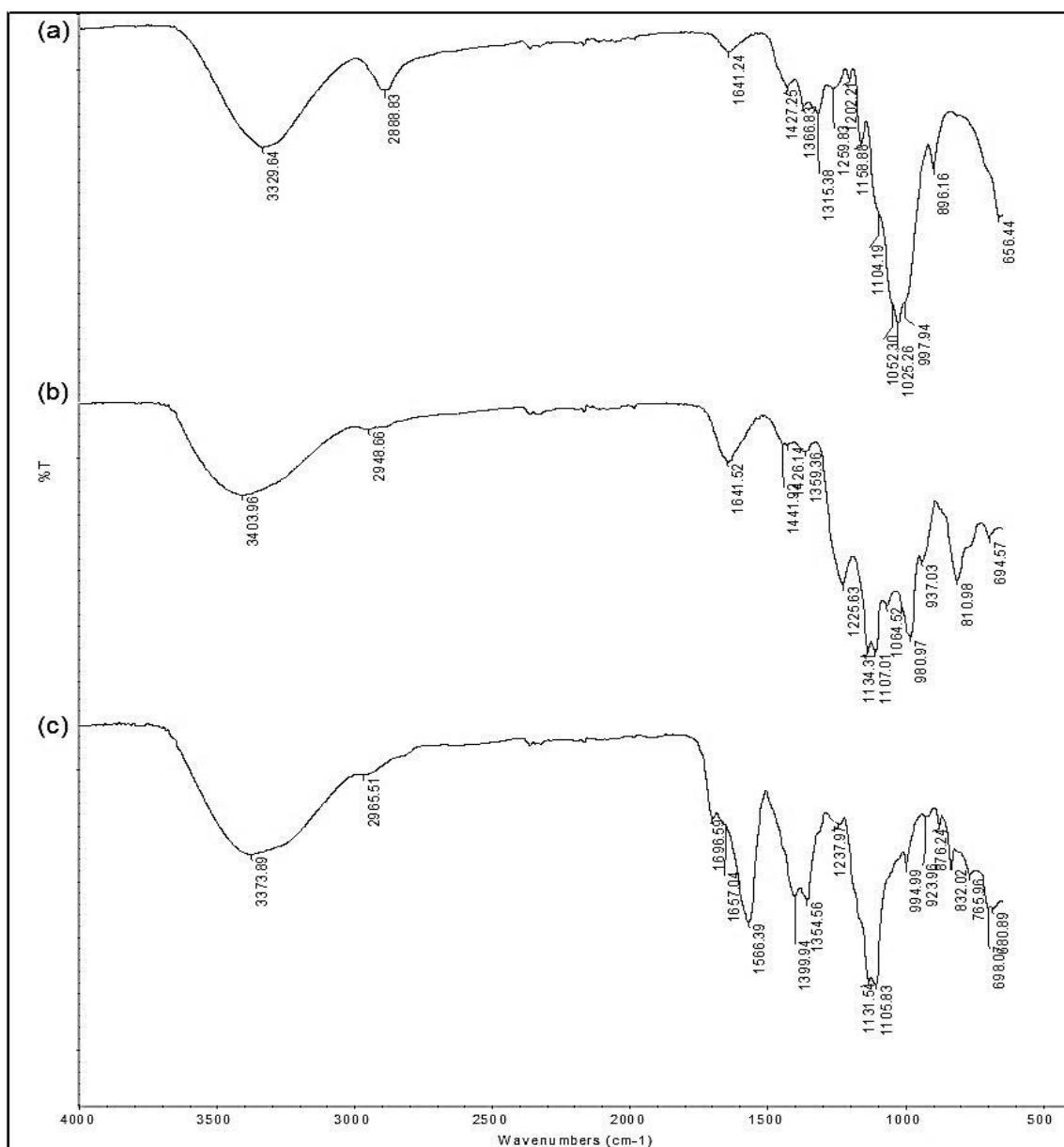


Figure 3.9: FTIR absorption spectra of (a) untreated α -cellulose, (b) CDs_{Green} and (c) CDs_{Blue} .

The stretching vibration of O-H, C-H, C-O and C-O-C could be found in untreated α -cellulose at 3329, 2888 cm^{-1} , 1158 and 1025 cm^{-1} , respectively. Similarly, these vibration stretches were also found present in both $\text{CDs}_{\text{Green}}$ and CDs_{Blue} , suggesting the presence of alcohol or phenol, alkyl and carboxylic acid on the CDs surface. Besides, the FTIR spectrum of CDs_{Blue} also clearly shows that the stretching vibration of $-\text{CH}_2-$ at 1399 cm^{-1} was more distinct when compared to the untreated α -cellulose and $\text{CDs}_{\text{Green}}$. This indicates that CDs_{Blue} had undergone higher carbonization degree than $\text{CDs}_{\text{Green}}$ using the FTIR spectrum of the untreated α -cellulose as reference. Therefore, resulting in more alkyl groups as the structures of CDs_{Blue} were broken down further.

3.4.1.4 Effect of pH and CDs Isolation

The effect of pH on the fluorescence of CDs was investigated. Acid hydrolysis approach could possibly induce oxidation of the surface interfaces of CDs during the carbonization process. The functional group of carboxylic has been reported to form on the CDs surface after treatment with acid [207]. Since the initial pH of the CDs sample was strongly acidic, 100 μl of the CDs solution was first diluted with 3 ml of ultrapure water. Sulphuric acid with concentration of 1.0 M and sodium hydroxide solutions with concentrations of 1.0 M and 10.0 M were then used to adjust the pH of the diluted CDs solutions. In order to standardize the condition and to minimize the effect of dilution for accurate comparison between samples, the series of CDs solutions with desired pH were topped up with ultrapure water to a final volume of 3.7 ml. Addition of minimal amount of water would also dilute the concentration of salt formed during the neutralization process and minimize its possible interference on the PL. The resulting pH and the fluorescence intensity were recorded.

The solution pH was found greatly affecting the PL intensity of both $\text{CDs}_{\text{Green}}$ and CDs_{Blue} as shown in Figure 3.10. Both types of CDs showed strong fluorescence under acidic condition at $\text{pH} < 3$. However, the bright PL was significantly quenched with increasing pH. The $\text{CDs}_{\text{Green}}$ showed a very narrow pH-dependent range with no fluorescence observed as pH values increased beyond pH 3. The low pH stability of $\text{CDs}_{\text{Green}}$ could be attributed to fluorescence degradation induced by the increasing charges on the surface

interface as a result of deprotonation. This was further supported by the evidence that the recovery of fluorescence was not possible even when the pH value was readjusted back to below pH 3. The pH effect indicates that the surface of $\text{CDs}_{\text{Green}}$ exhibited acidic sites that are associated with the green fluorescence because PL quenching was observed at higher pH [208, 209].

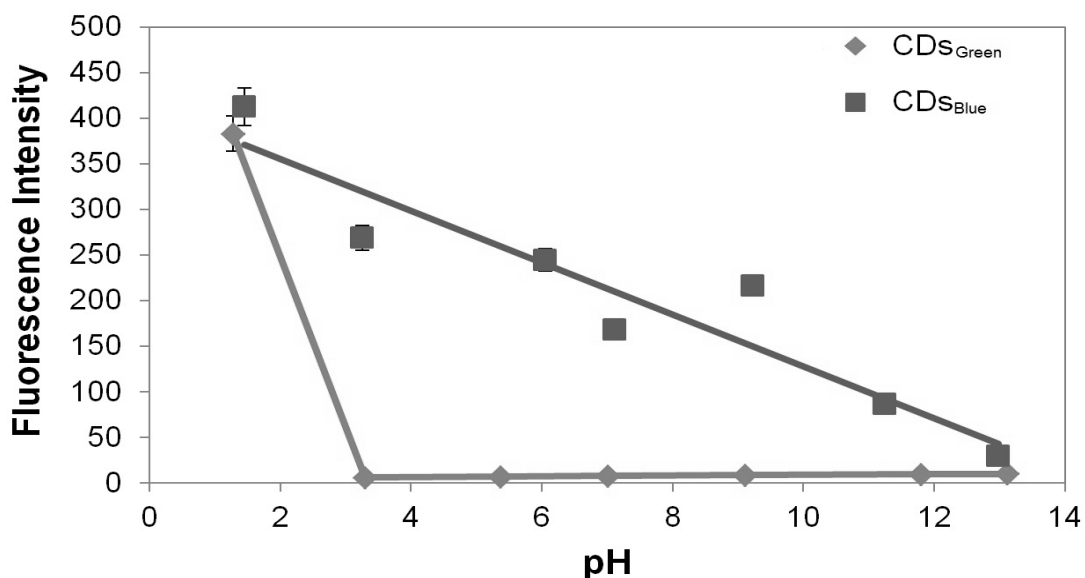


Figure 3.10: Variation of fluorescence intensity of CDs_{Blue} and $\text{CDs}_{\text{Green}}$ in aqueous solutions of different pH values.

As for the CDs_{Blue} , the pH dependent range was wider than that of $\text{CDs}_{\text{Green}}$. It was observed that the PL intensity of CDs_{Blue} decreased gradually with increasing pH. Furthermore, CDs_{Blue} were more stable and the fluorescence can be recovered when pH was tuned back to acidic condition. Our findings concurred with results reported recently by Wang *et al.*, who demonstrated that the fluorescence showed a decrease in intensity from its maximum at pH 3 when pH was shifted to the basic range [210]. The increase of pH value indicates the increase in negative charges species in the surrounding solution. This could lead to the deprotonation of the CDs surface, hence disturbing the electronic configuration of the interfaces and the fluorescence properties of CDs can be altered subsequently. The highly electronegative surface could also attract counter ions present in the system and led to the formation of particles aggregates. The close contact between particles could eventually promote non-radiative pathway for the relaxation of excited electrons, as reflected in the drop of fluorescence intensity observed in this study.

Due to the extremely pH sensitive properties, isolation of CDs_{Green} is still remained a challenge. However, CDs_{Blue} have been successfully isolated for TEM imaging using salting out approach. Crystallization of sodium sulphate salt formed from neutralization reaction between sulphuric acid and sodium hydroxide can be promoted in the presence of acetone. After neutralization of the CDs_{Blue} solution to pH 7, equal volume of acetone was added to promote crystallization of the sodium sulphate salts. The solution was mixed vigorously prior to incubation at 4 °C to promote salt nucleation and crystal growth. In the water phase, the acetone in the supernatant solution containing the CDs was collected and then the acetone was removed using vacuum concentrator. The CDs_{Blue} were then concentrated by lyophilisation to remove excess water and sent for TEM imaging. The yield of CDs_{Blue} from α -cellulose was calculated to be 29.58% w/w. The TEM image of CDs_{Blue} as shown in Figure 3.11 revealed that CDs_{Blue} synthesized from acid dehydration of α -cellulose are homogenously distributed in nanometer range, mostly spherical with diameter of 10-20 nm.

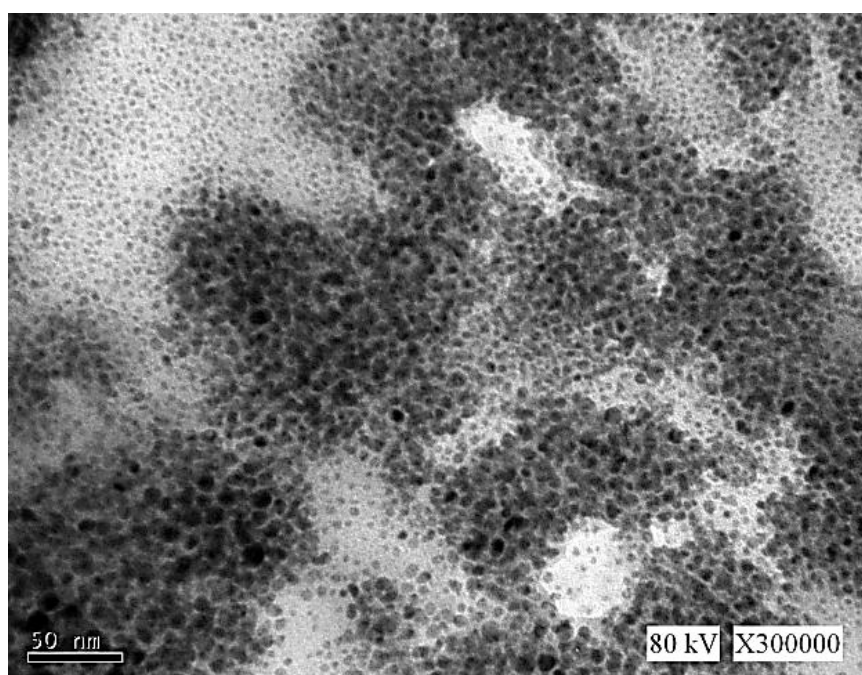


Figure 3.11: TEM image of CDs_{Blue} synthesized from α -cellulose via acid dehydration method.

3.4.2 Thermal Carbonization of α -Cellulose

3.4.2.1 Characterization of CDs

Facile one-step synthesis approach has also been adopted for the synthesis of CDs via simple thermal carbonization of α -cellulose in furnace. α -cellulose is the insoluble fibrous residue that can be commonly found in agricultural waste. This makes a commonly available cheap and green carbon source as starting precursor for the synthesis of CDs. During thermal carbonization, cleavage of glycosidic linkages of α -cellulose will occur. Hence, polymerization degree was reduced and resulting in the formation of carbon dioxide, water and a variety of hydrocarbon derivatives [211]. Fluorescent CDs was most likely to be one of the products formed during this stage of thermal decomposition. Figure 3.12 shows the absorbance, excitation and emission spectra of CDs obtained by carbonizing α -cellulose at 250 °C for 30 minutes.

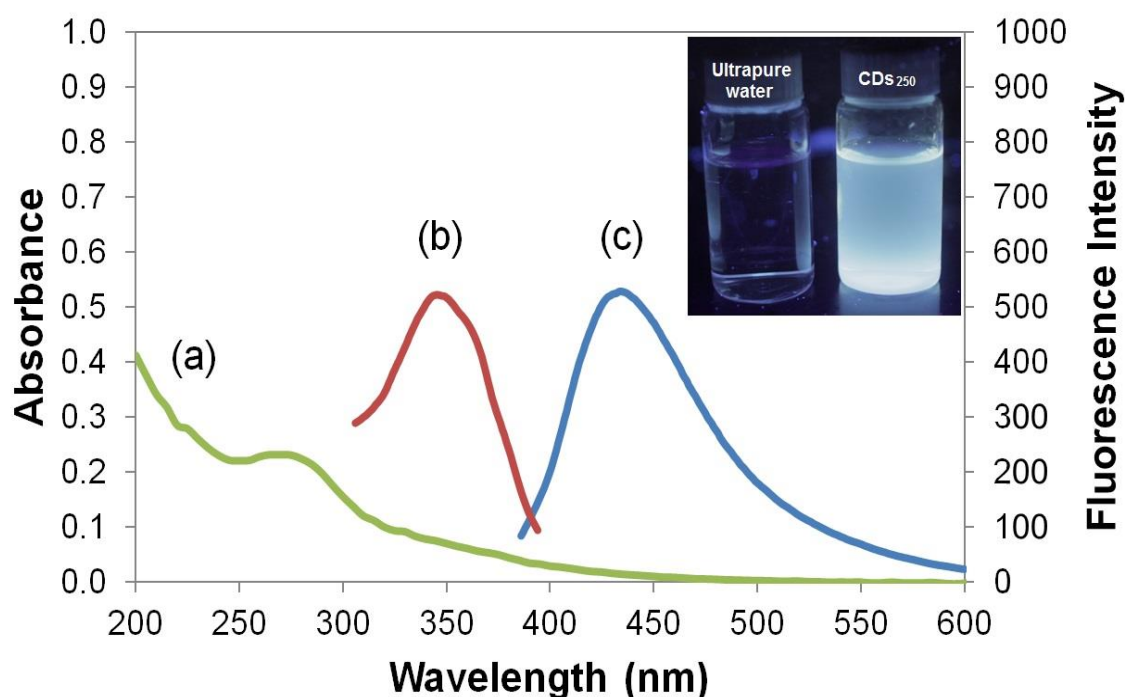


Figure 3.12: The (a) absorbance, (b) excitation and (c) emission spectrum of CDs synthesized from α -cellulose via thermal carbonization. Inset: Photograph of ultrapure water (left) and CDs (right) under exposure of UV light.

From Figure 3.12, the UV-Vis spectrum showed a strong band at around 270 nm that could be attributed to the $\pi \rightarrow \pi^*$ transition of CDs with graphitic structure [4, 212]. The fluorescence spectrum showed that the obtained CDs exhibited optimum fluorescence emission at 435 nm which was in the range of blue emission upon excitation at 346 nm. The inset in Figure 3.12 shows that the CDs exhibited bright blue fluorescence under exposure of ultraviolet (UV) light. The FWHM of the CDs obtained at 250 °C was evaluated to be approximately 83 nm. The relatively narrow FWHM indicated that the CDs produced possess a homogenous size distribution [56].

The organic functional groups on the surface of CDs were identified using FTIR. The FTIR spectra of the untreated α -cellulose and CDs treated at 250 °C were shown in Figure 3.13.

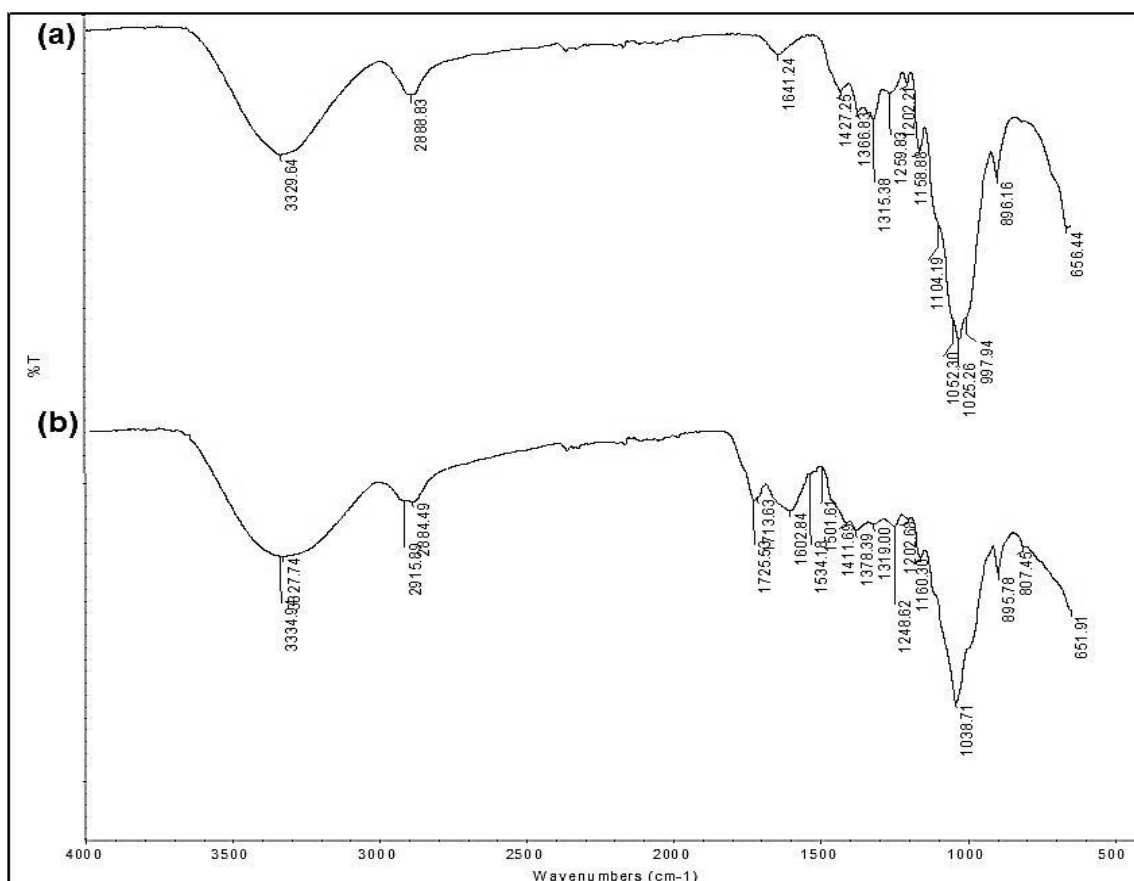


Figure 3.13: FTIR absorption spectrum for (a) untreated α -cellulose and (b) CDs carbonized in furnace at 250 °C for 30 minutes.

The FTIR spectrum (Figure 3.13) of CDs treated at 250 °C showed –OH stretch in the alcohol or phenol group at 3334.94 cm⁻¹, alkane C–H stretch at 2915.89 cm⁻¹, aromatic C=C and C–C stretch at 1602.84 and 1411.69 cm⁻¹ respectively, carboxylic acid C–O stretch at 1000-1320 cm⁻¹, C-O-C in pyranose ring at 1038.71 cm⁻¹ and aromatic C–H stretch at 895.78 cm⁻¹. Besides, it was observed that vibration stretch of carboxylic acid at 1725.53 cm⁻¹ that can be found in CDs treated at 250 °C was not present in the spectrum of untreated α-cellulose. It was also observed that the amide C=O stretch at 1641 cm⁻¹ significantly increased after thermal pyrolysis of α-cellulose. This suggested that oxidation process has occurred after treatment at high temperature hence more carbonyl groups were formed on the surface of the CDs. The FTIR profile indicated that functional groups such as alcohol or phenol, alkane, aromatic groups and carboxylic acid are present and form the surface defects of CDs, which also suggested that the combustion of α-cellulose was incomplete. Due to this reason, CDs synthesized at 250 °C still retaining the functional groups that were initially present in the starting materials.

The CDs obtained by thermal carbonization possessed excellent water solubility. Moreover, the photostability of the CDs as shown in Figure 3.14 were relatively stable with only the decreased of around 3.98% in fluorescence intensity after continuous exposure to UV irradiation for 60 minutes.

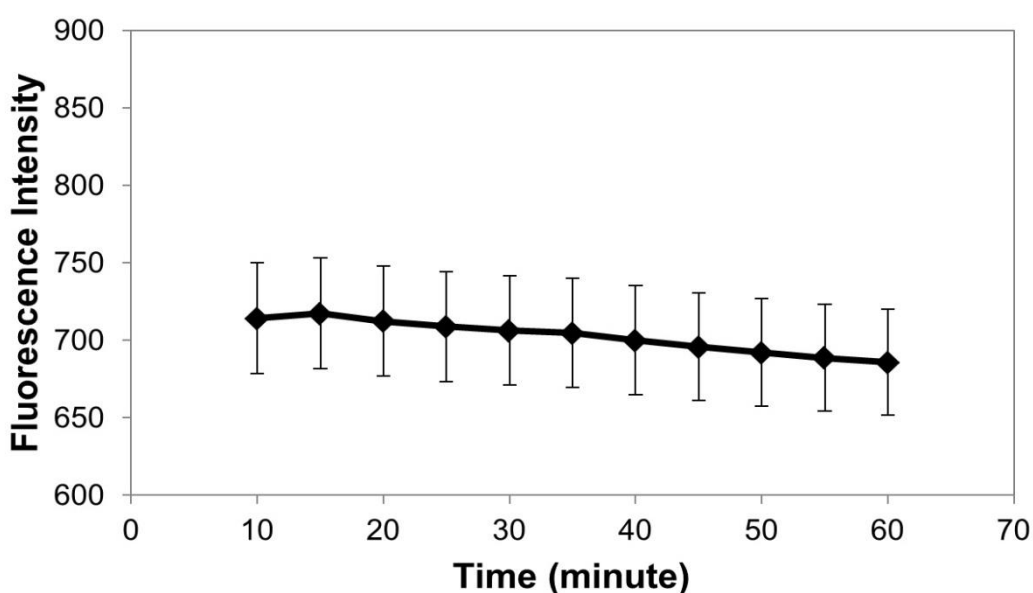


Figure 3.14: Photostability measurement of CDs₂₅₀ monitored at 435 nm upon excitation at 346 nm for 60 minutes.

3.4.2.2 Effect of Pyrolysis Conditions

It is crucial to optimize the synthetic conditions to ensure the CDs portray desired fluorescence properties. Therefore, α -cellulose was treated with different temperatures in a furnace. Physical appearance of the resulting products obtained after 30 minutes of pyrolysis were photographed as shown in Figure 3.15.

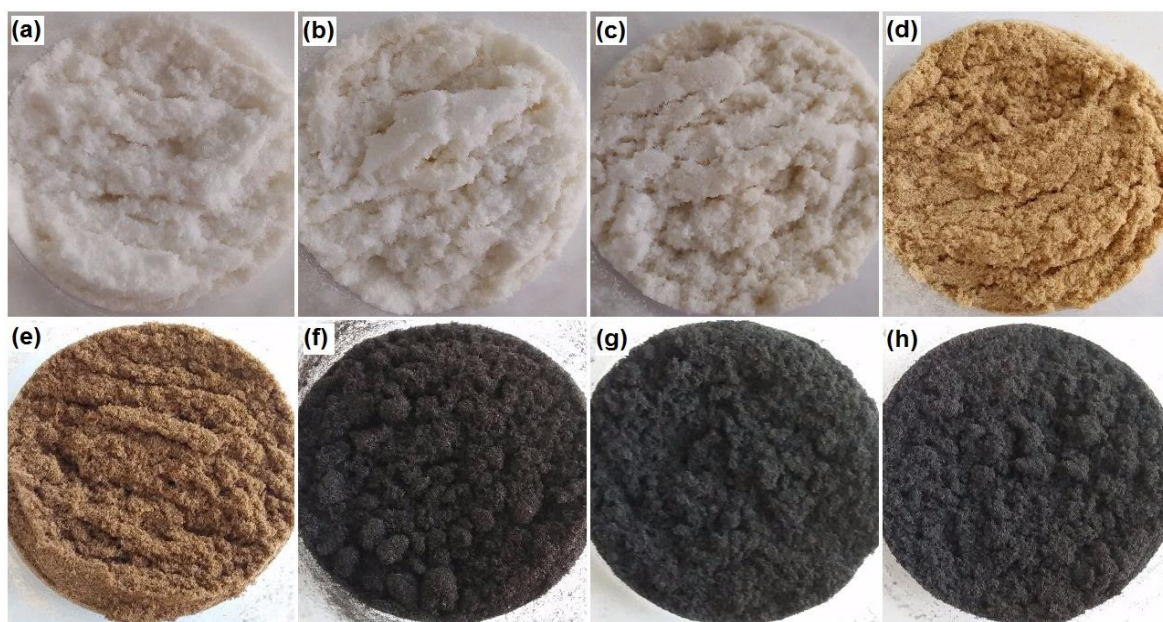


Figure 3.15: Photographs of (a) untreated α -cellulose and the products after thermal pyrolysis at different temperatures of (b) 200 °C, (c) 225 °C, (d) 250 °C, (e) 275 °C, (f) 300 °C, (g) 350 °C and (h) 400 °C.

A clear colour gradient can be observed for the end-products obtained at different temperature. The photograph shows that α -cellulose as starting precursor before pyrolysis was fine white powder. There was no significant change in colour when the α -cellulose was heated at 200 °C for 30 minutes. A very light yellowish powder product was yielded when the starting precursor was heated at 225 °C. Once the carbonization temperature was increased to 250 °C, it was observed that the fine white α -cellulose powder turned into light brown-coloured product. At elevated temperature, dark brown product was produced when the carbonization temperature was increased to 275 °C. Finally, black fine powder was obtained when α -cellulose was treated at temperature

beyond 275 °C. The black fine powder was most probably the chars produced as a result of complete pyrolysis of α -cellulose. Formation of char due to decomposition of α -cellulose was suggested to involve the breakage of 1,4-glucosidic bonds leading to depolymerization. Moreover, ring opening of the α -cellulose structure could be induced by breaking of 1,5-acetal bonds during pyrolysis [213].

After carbonization in furnace, the resulting products were centrifuged and filtered to remove any insoluble large residues in order to isolate the CDs. The fluorescence properties of the isolated samples were then measured using a fluorescence spectrophotometer. The fluorescence emission of the isolated CDs obtained at different pyrolysis temperature was shown in Figure 3.16.

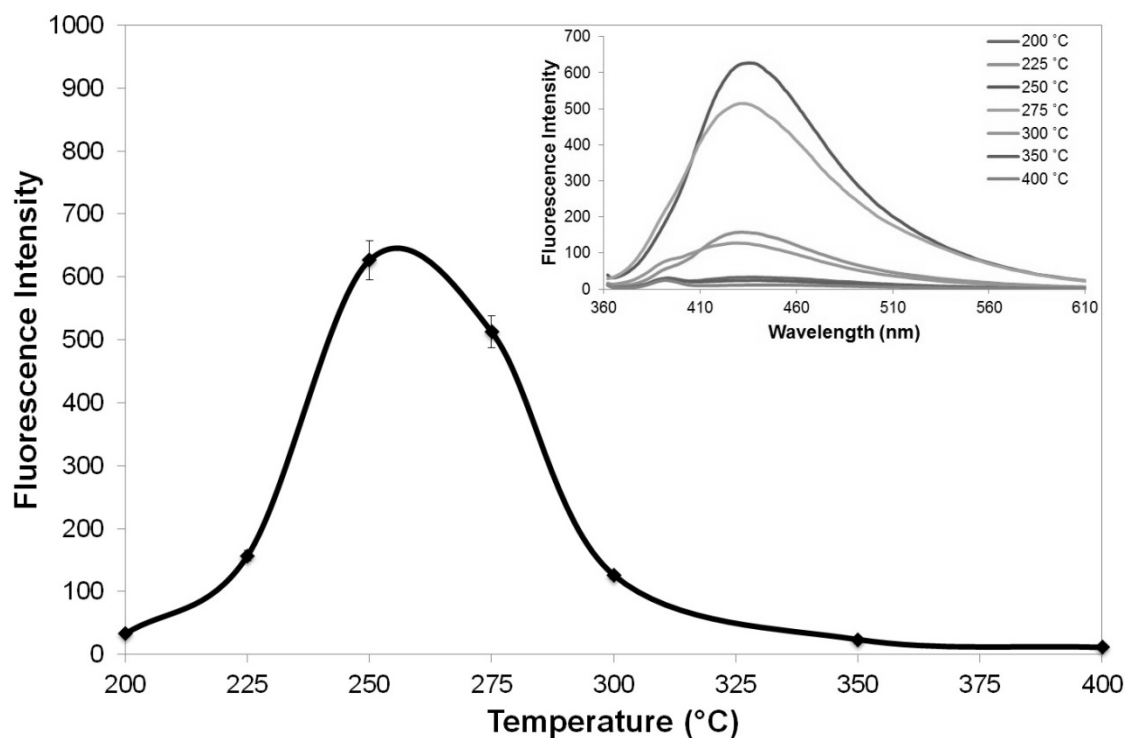


Figure 3.16: Emission of CDs carbonized at different temperatures monitored at 435 nm upon excitation at 346 nm. Inset: Emission spectrum of CDs synthesized at different temperatures.

α -cellulose is fine white fibrous material that is insoluble in water and possess no or low fluorescence property when viewed under UV light. Moreover, no signal could be detected when the solution suspended with α -cellulose was measured using the fluorescence spectrophotometer. Similarly, the CDs isolated from the sample carbonized at 200 °C displayed very slight and insignificant fluorescence. The fluorescence intensity increased with increasing pyrolysis temperature. From Figure 3.16, it was observed that CDs with highest fluorescence intensity can be obtained when α -cellulose was carbonized at 250 °C. Therefore, this has been adopted as the optimum temperature for the synthesis of fluorescence CDs by thermal carbonization of α -cellulose. It was further observed that the fluorescence intensity of CDs obtained at temperature beyond 250 °C have decreased gradually. At 400 °C, significantly low or almost no fluorescence could be detected. Overall, this result implies that temperature below 250 °C was insufficient to decompose and carbonize α -cellulose into highly fluorescence CDs. The temperature to produce brightly fluorescence CDs reached optimum at 250 °C. Pyrolysis at temperature higher than 300 °C will eventually lead to the excessive combustion and severe decomposition of α -cellulose. Hence, loss of fluorescence properties due to the production of chars, tars and gaseous products [214].

The inset of Figure 3.16 shows the full emission spectrum of CDs prepared at different temperature when excited at 346 nm. All CDs samples obtained at different temperatures showed maximum fluorescence emission centred at 435 nm. There was no shift in the fluorescence emission when different pyrolysis temperatures were employed for the pyrolysis of α -cellulose. This in turn indicated that only single species of CDs was present. The FWHM of the fluorescence emission bands of the CDs obtained at different temperatures were all evaluated to be less than 100 nm which are comparable to the value reported in literature [215].

The optimum reaction time for the thermal carbonization of α -cellulose was also investigated. The pyrolysis temperature of 250 °C was fixed since the temperature could produce CDs with highest fluorescence intensity. The effect of time was studied by varying the carbonization time for the pyrolysis process

at 250 °C in high temperature furnace. The fluorescence of CDs synthesized at 250 ° from α -cellulose at different time variation monitored at 435 nm upon excitation at 346 nm as shown in Figure 3.17.

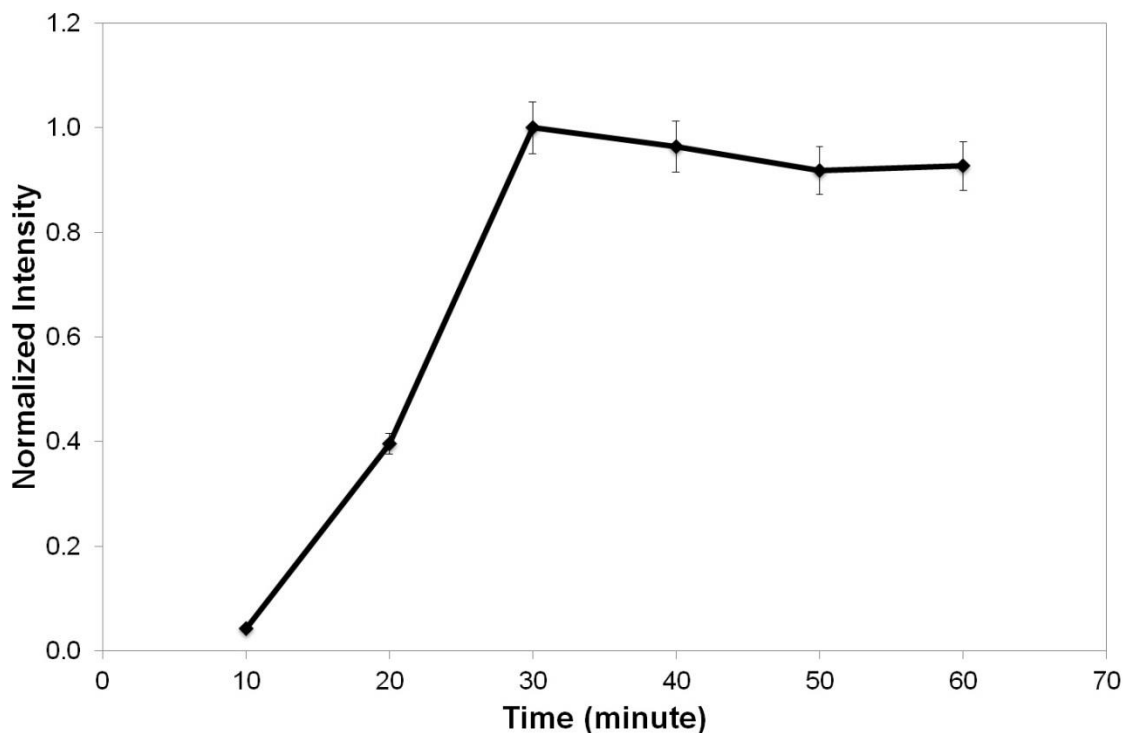


Figure 3.17: Emission of CDs synthesized from α -cellulose treated at 250 °C in furnace at different time variation monitored at 435 nm.

The optimum time required to produce CDs with highest fluorescence intensity was found to be 30 minutes at 250 °C. Shorter carbonization period produced CDs with insignificant fluorescence due to incomplete carbonization as mentioned previously. Carbonization reached optimum at 30 minutes and it was realized that carbonization at a longer time period did not show significant enhancement in terms of the fluorescence of CDs. Hence, CDs synthesized by carbonizing α -cellulose in furnace at 250 °C for 30 minutes was adopted as optimum carbonization conditions for further study. The as-synthesized CDs obtained at the optimum conditions was purified by conventional centrifugation and filtration, which thereafter depicted as CD₂₅₀ was kept at 4 °C until further use. The yield from 1 g of α -cellulose was determined to produce 28 mg of CDs which was about 2.8% of the mass of starting material.

3.4.2.3 Effect of pH

The stability of CDs at different pH conditions is crucial to be investigated in order to maximize the applications of CDs. Hence, the effect of pH on the fluorescence intensity of CDs₂₅₀ in aqueous solutions was investigated. The pH of the CDs solutions were adjusted in the range of pH2 to 12 with sodium hydroxide and sulphuric acid. The fluorescence of CDs suspended in different pH solutions were then monitored at 435 nm when excited at 346 nm as shown in Figure 3.18.

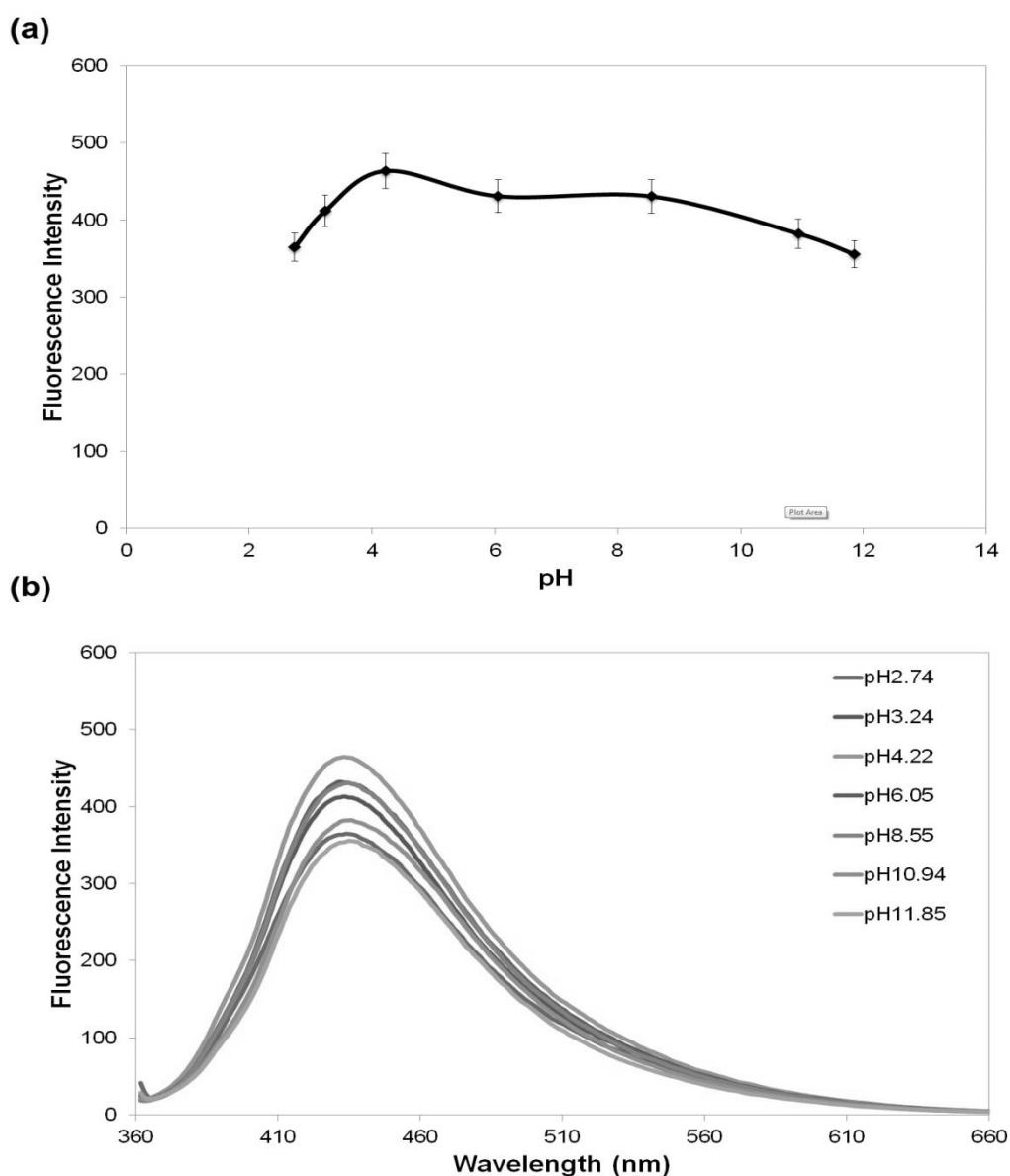


Figure 3.18: (a) Variation of fluorescence intensity and (b) fluorescence emission spectrum of CDs₂₅₀ in aqueous solutions of different pH values.

The fluorescence of CDs₂₅₀ decreased slightly at the low and high pH ranges (Figure 3.18 (a)). However, no significant changes in the fluorescence of CDs₂₅₀ could be observed in aqueous solutions with pH ranging from pH 4 to 8 indicated that CDs₂₅₀ were relatively stable over a wide range of pH. In addition, Figure 3.18 (b) shows that the fluorescence emission spectrum of CDs did not shift in aqueous solutions with different pH values. This result further confirms that CDs₂₅₀ exhibited high stability over a wide pH range. This pH-independent property has broadened the applications of CDs₂₅₀ especially in the field of chemical sensing in the environment where the pH is usually unpredictable due to the presence of a wide range of contaminants.

3.4.3 Thermal Carbonization of L-Glutamic Acid

3.4.3.1 Effect of Pyrolysis Conditions

Beside α -cellulose, L-glutamic acid was also used as carbon source for the synthesis of CDs via thermal carbonization as another comparison study. L-glutamic acid which is also known as (2S)-2-aminopentanedioic acid in IUPAC system is a non-essential amino acid that consists of two carboxyl groups and one amine group with molecular weight of 147.13 g/mol [216]. Figure 3.19 illustrates the schematic diagram of production of CDs from L-glutamic acid by thermal pyrolysis.

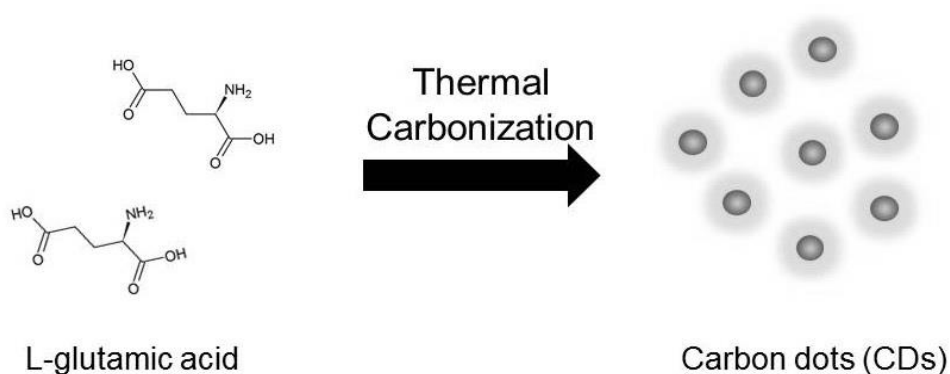


Figure 3.19: Schematic diagram of CDs formation from L-glutamic acid.

In a typical synthesis process, approximately 0.5 g of L-glutamic acid was weighed into a crucible and carbonized in high-temperature furnace. The carbonized product was then cooled to room temperature, resuspended in ultrapure water and filtered through 0.22 μm syringe filter to remove any large undissolved particles. The optimum reaction temperature to carbonize L-glutamic acid to obtain CDs with maximum fluorescence was investigated.

Figure 3.20 shows the photographs of the resultant products of L-glutamic acid carbonized at different temperatures in furnace for 20 minutes under both visible light and UV irradiation. Ultrapure water was included as a non-fluorescence solution for comparison. Under visible light, a clear colour gradient could be observed from clear, light brown, reddish brown, dark brown then yellowish and finally light brown solutions. These solutions with different colour gradients were obtained with increasing carbonization temperature from 200 to 400 $^{\circ}\text{C}$. It was clearly shown that under UV exposure, the product obtained at 200 $^{\circ}\text{C}$ did not show obvious fluorescence. However, solutions obtained beyond 200 $^{\circ}\text{C}$ displayed bright blue fluorescence when viewed under UV light.

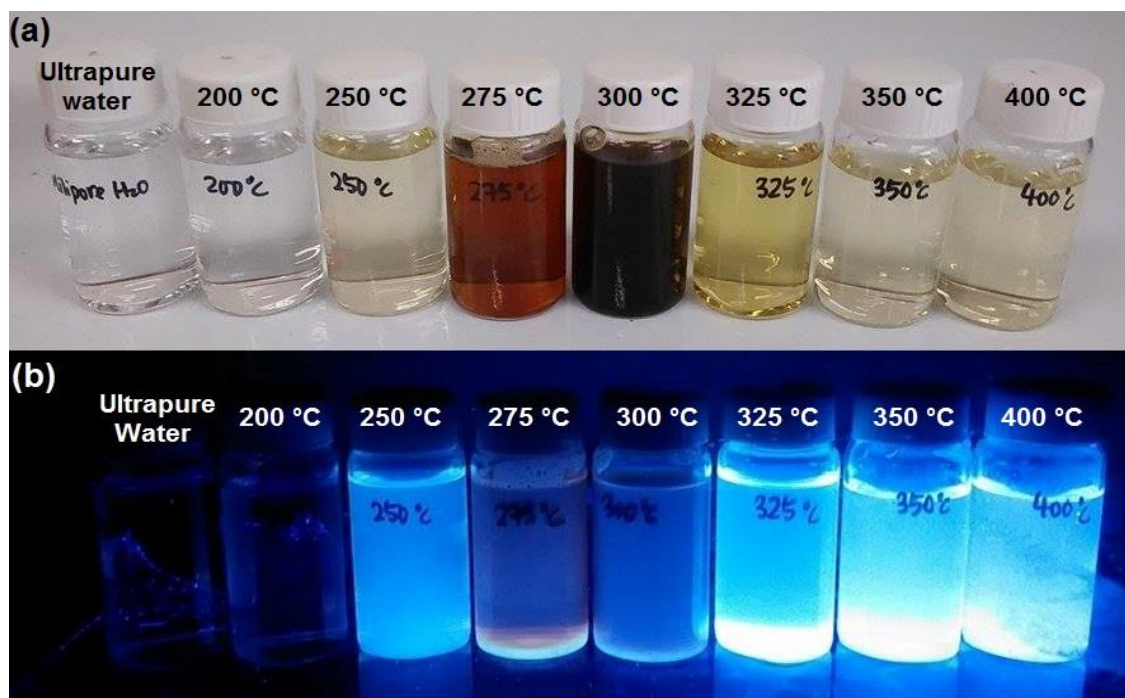


Figure 3.20: Photographs of CDs synthesized by thermal pyrolysis of L-glutamic acid at different temperature under (a) visible light and (b) UV exposure.

In order to further clarify the optimum temperature required for the production of CDs from L-glutamic acid, the fluorescence intensity of the solutions obtained at different temperature were appropriately diluted and measured with fluorescence spectrophotometer as shown in Figure 3.21. After diluting 1 ml of CDs stock solutions with 30 ml of ultrapure water, it was further confirmed that 200 °C was not high enough to carbonize L-glutamic acid into CDs because no fluorescence could be observed or detected. CDs produced at 300 °C displayed highest fluorescence intensity, followed by CDs obtained at 325 °C. However, slight or almost no fluorescence could be detected for CDs obtained at even higher temperatures at the same dilution factor. This indicated that CDs obtained at temperature higher than 300 °C exhibited lower fluorescence intensity that could not be detected at dilution factor of 1:30. Hence, the CDs synthesized from thermal carbonization of L-glutamic acid at optimum condition of 300 °C for 20 minutes was thereafter depicted as CDs_{Glu} and used for further study.

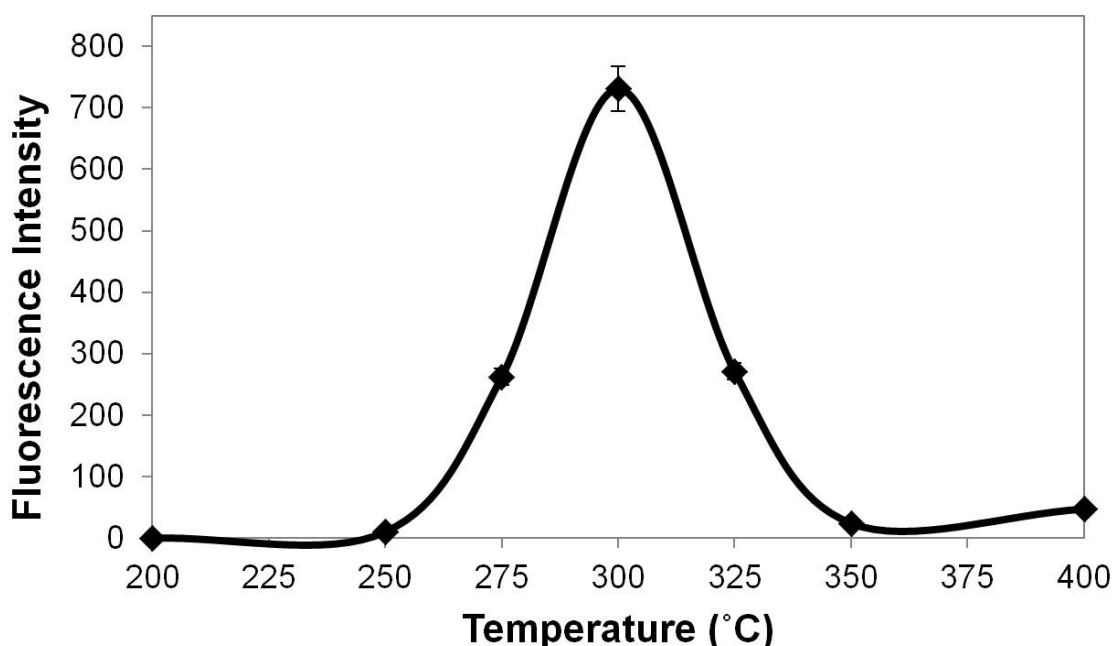


Figure 3.21: Variation of fluorescence intensity monitored at 440 nm when excited at 365 nm for CDs prepared at different temperatures.

3.4.3.2 Characterization of CDs

The absorbance, fluorescence excitation and emission of CDs_{Glu} synthesized by thermal carbonization of L-glutamic acid at 300 °C for 20 minutes were illustrated in Figure 3.22. A broad absorption band centred at around 300 nm with a tail extending to the visible region could be observed in the absorption spectrum. Such absorption band has been typically assigned to the $n \rightarrow \pi^*$ transition [217, 218]. The CDs_{Glu} obtained from L-glutamic acid was found to exhibit bright blue fluorescence when exposed under UV light as mentioned previously. The fluorescence spectrum recorded using fluorescence spectrophotometer further confirmed that the CDs_{Glu} emitted optimally at 440 nm which was in the range of blue PL region upon excitation at 365 nm. The FWHM of the emission spectrum was determined to be approximately 92 nm which was relatively narrow (<100 nm) suggesting that the CDs_{Glu} obtained exhibited homogenous sized distribution [56].

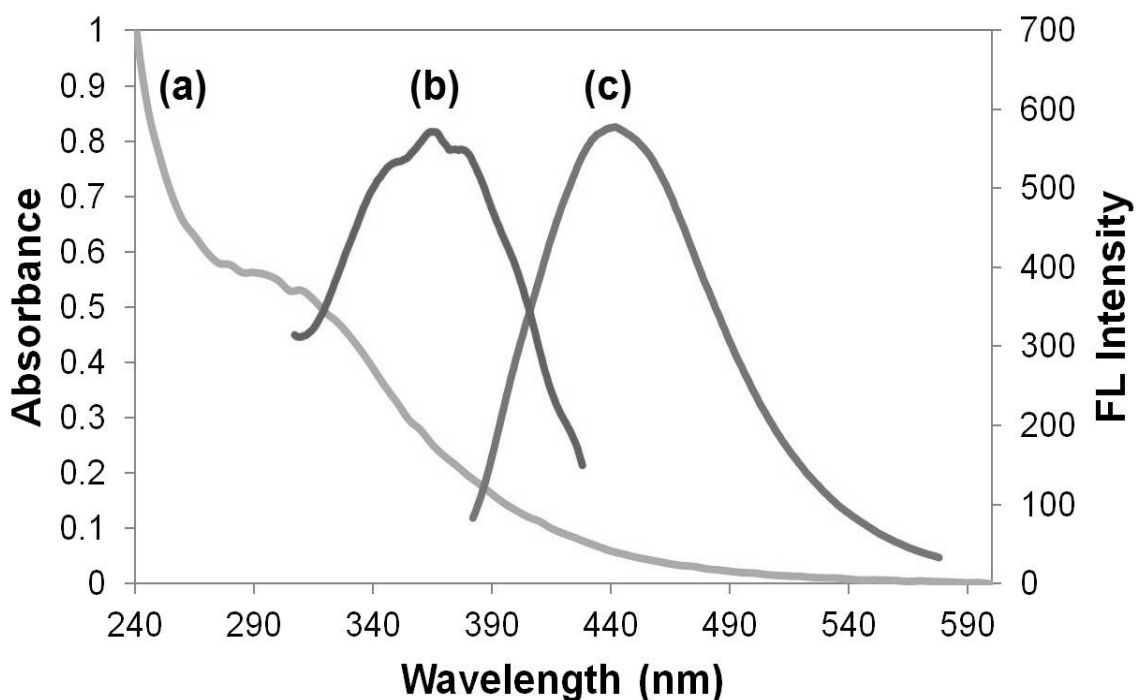


Figure 3.22: The (a) absorbance, (b) excitation and (c) emission spectrum of CDs_{Glu} synthesized by thermal pyrolysis of L-glutamic acid.

Figure 3.23 (a) illustrates the fluorescence emission spectra of CDs_{Glu} monitored over the excitation wavelengths of 330 to 410 nm, while Figure 3.23 (b) displays the contour plot of the corresponding fluorescence spectrum of CDs_{Glu} .

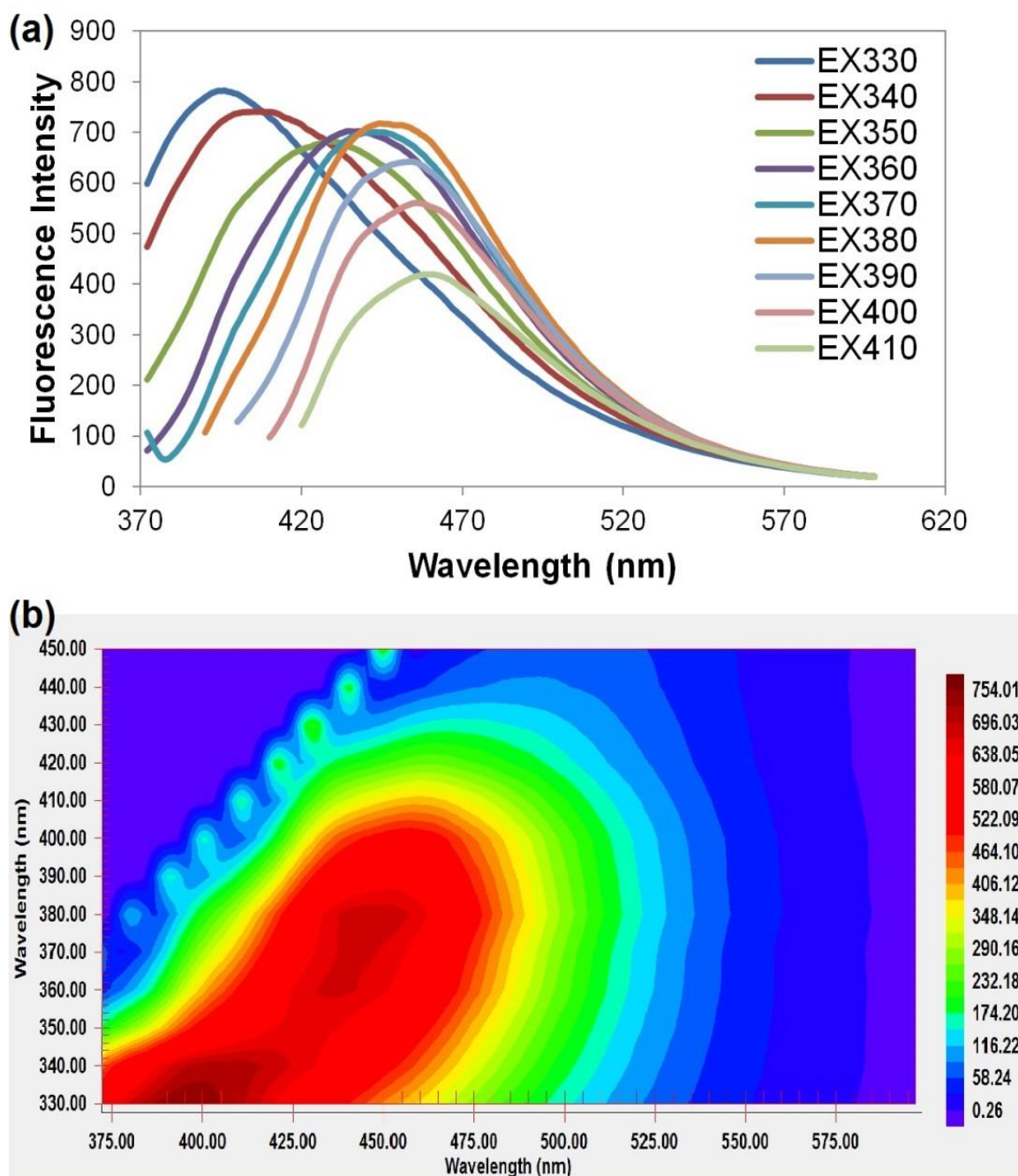


Figure 3.23: (a) Fluorescence emission spectra of CDs_{Glu} excited at increasing excitation wavelength from 330 nm to 410 nm; (b) Contour plot of fluorescence spectrum of CDs_{Glu} .

The CDs_{Glu} obtained from thermal pyrolysis of glutamic acid exhibited excitation-dependent PL properties (Figure 3.23). The emission wavelengths of CDs_{Glu} were relatively broad ranging from 350 to 450 nm when excited in the range of 330 to 410 nm. As the excitation wavelengths increased, the emission spectrum red-shifted to longer wavelengths. The excitation wavelength dependence of the fluorescence emission could be reflected as either the effects due to CDs_{Glu} particles with different sizes or the distribution of the different emissive sites on CDs_{Glu} [202]. Since the relatively narrow FWHM has suggested that the CDs_{Glu} obtained from L-glutamic acid possess homogenous particles size, thus the latter is more likely to cause the shift in the fluorescence emission wavelengths of the CDs_{Glu} . It was reported that the surface oxidation degree on the surface of CDs_{Glu} with homogenous size distribution may contribute to the excitation-dependent properties [219]. Careful analysis of the contour plot revealed that CDs_{Glu} exhibited maximum emission at 440 nm when excited at 365 nm. Although the PL mechanism of CDs_{Glu} is not yet fully understood, several general mechanisms have been suggested. This is related to the surface energy traps or surface states, radiative recombinant, quantum confinement effect and armchair and zigzag edge effects [71].

Other than ultrapure water, the effect of sodium acetate/acetic acid buffer solution on the fluorescence emission of CDs_{Glu} was investigated. Buffer solution of approximately pH 5 was prepared using acetic acid which is a weak acid and its conjugate base of sodium acetate. The isolated CDs_{Glu} were lyophilized and resuspended in different types of solvents, followed by measuring the fluorescence emission spectrum using the fluorescence spectrophotometer. Figure 3.24 shows the fluorescence emission spectrum of CDs_{Glu} suspended in two different solvents. The results clearly indicated that neither significant change in the fluorescence intensity nor shift in the fluorescence emission spectrum of CDs_{Glu} could be observed when suspended in the two solvents. Fluorescence properties of CDs_{Glu} were found stable in both ultrapure water as well as buffer solution. This has widened the range of applications of CDs_{Glu} .

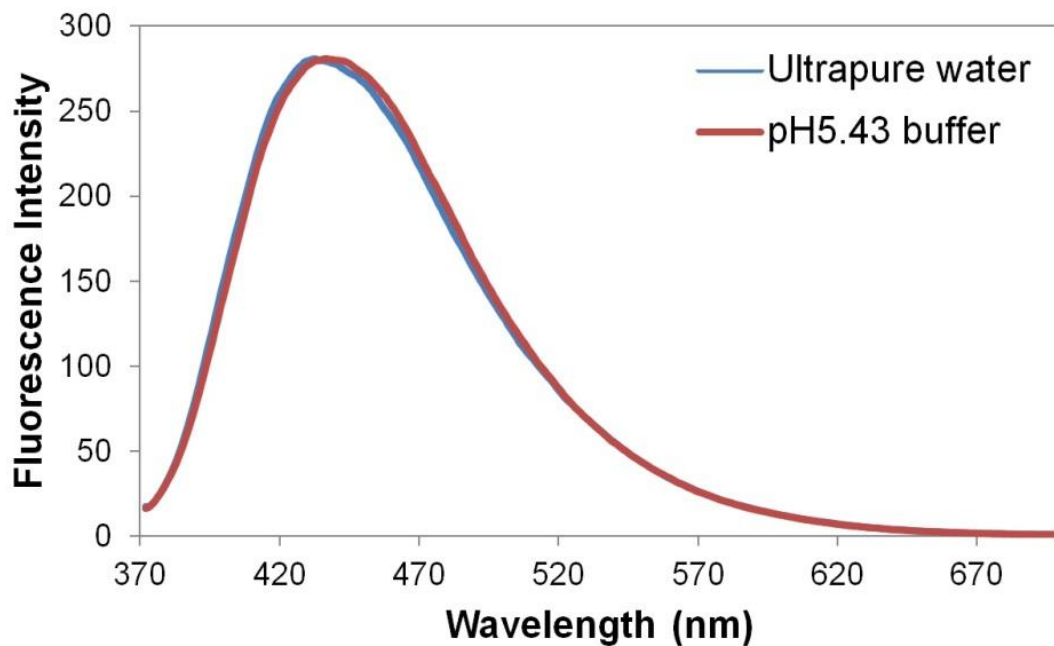


Figure 3.24: Fluorescence emission spectrum of CDs_{Glu} suspended in ultrapure water and sodium acetate/acetic acid buffer with pH5.43.

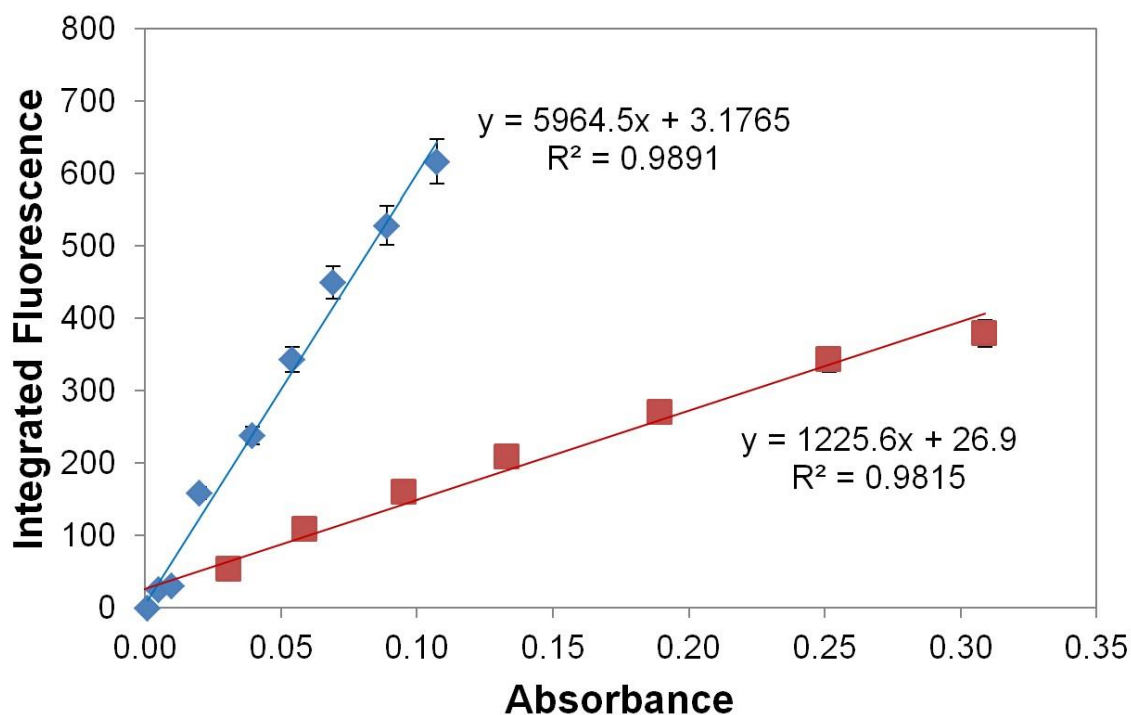


Figure 3.25: Plot of integrated fluorescence intensity versus absorbance for quantum yield determination of CDs_{Glu} (red line) using quinine sulphate (blue line) as standard.

Quinine sulphate was used as standard for the determination of the quantum yield of CDs_{Glu} . Fluorescence emission and absorbance of both the standard and CDs_{Glu} were measured simultaneously. The fitting of integrated fluorescence against absorbance as shown in Figure 3.25 was constructed to calculate the quantum yield. The quantum yield of the CDs_{Glu} was determined to be 11.1% which is comparable to the values reported in literature [79, 98].

CDs are commonly found to exhibit high photostability. In this study, the photostability was determined by exciting the CDs_{Glu} continuously for a period of 60 minutes at 365 nm and the fluorescence intensity at 440 nm was recorded at every 5-minute intervals as shown in Figure 3.26.

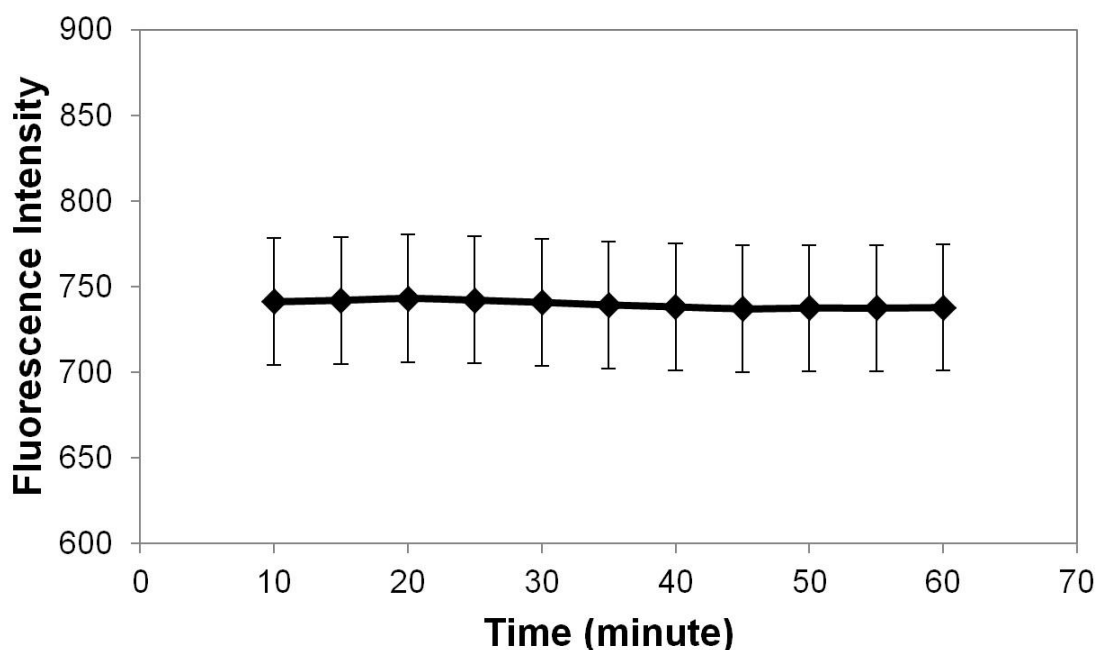


Figure 3.26: Photostability measurement of CDs_{Glu} monitored at 440 nm upon excitation at 365 nm for 60 minutes.

The result reveals that CDs_{Glu} possessed high photostability with a negligible decrease in fluorescence of only 0.45% over the period of 60 minutes. The yield of CDs_{Glu} from thermal pyrolysis of L-glutamic acid was as high as 85.36% w/w. Physiochemical properties of the various types of CDs obtained in this study are summarized in Table 3.1 as follows.

Table 3.1: Summary of the properties of different types of CDs.

	CDs_{Green}	CDs_{Blue}	CDs₂₅₀	CDs_{Glu}
Starting precursor	α -cellulose	α -cellulose	α -cellulose	L-glutamic acid
Method of synthesis	Acid hydrolysis	Acid hydrolysis	Thermal pyrolysis	Thermal pyrolysis
PL colour	Green	Blue	Blue	Blue
Optimum excitation	450 nm	357 nm	346 nm	365 nm
Optimum emission	500 nm	456 nm	435 nm	440 nm
Photostability	Low	High	High	High
pH	Dependent	Dependent	Independent	-
QY	6.4 %	4.0 %	-	11.1 %
Yield	-	29.58 %	2.8 %	85.36 %

3.5 Conclusions

CDs as the recent rising star in the family of carbon nanomaterials have been successfully synthesized in this study. α -cellulose as an environmental friendly organic fiber was used as starting material for the synthesis of CDs via acid hydrolysis and thermal pyrolysis approach. The fluorescence of CDs could be altered by precisely control the synthesis conditions. CDs emitting bright green and blue fluorescence could be produced from α -cellulose using facile acid hydrolysis approach. Milder synthesis condition such as lower temperature promoted the formation of CDs exhibiting bright green fluorescence (CDs_{Green}). In contrast, higher temperature was favorable for the formation of blue emitting CDs (CDs_{Blue}). The CDs_{Green} was found to be much less stable in terms of photostability as compared to CDs_{Blue}. The narrow pH range of CDs_{Green} makes it a challenge to be isolated and used for further study. On the other hand, CDs_{Blue} that are stable over a wider range of pH was successfully isolated by salting out method using acetone as solvent to promote crystallization. The

optimum emission of CDs_{Green} was 500 nm when excited at 450 nm. The optimum excitation and emission of CDs_{Blue} were 357 and 456 nm respectively.

Beside acid hydrolysis, simple thermal pyrolysis was also employed to produce CDs from α -cellulose. Thermal carbonization is a comparatively greener approach because no acids are required. CDs with blue fluorescence were successfully obtained from thermal carbonization of α -cellulose. The blue fluorescence CDs exhibited optimum PL emission at 435 nm upon excitation at 346 nm. The optimum carbonization temperature and time in high temperature furnace for the synthesis of CDs was optimized and found to be 250 °C and 30 minutes respectively. The CDs is thereafter depicted as CDs₂₅₀.

In addition to α -cellulose, L-glutamic acid which is one of the amino acids was also used as carbon source for the synthesis of CDs. L-glutamic acid consists of two carboxyl groups and one amine group could be self-passivated in one-step synthesis by thermal carbonization. The CDs obtained from L-glutamic acid exhibited bright blue fluorescence with optimum excitation at 365 nm and emission at 440 nm. The optimum synthesis conditions were carbonized at 300 °C for 20 minutes in high temperature furnace. The CDs synthesized from L-glutamic acid at optimum synthesis conditions is depicted as CDs_{Glu}. The QY of CDs_{Glu} was calculated to be 11.1 % using quinine sulphate as standard. This QY was the highest among all the CDs produced in this study.

Chapter 4 Interface Study on Carbon Dots and Its Potential as Metal Ions Sensing Receptors

4.1 Executive Summary

CDs have been extensively utilized as fluorescence detection probes for the application of chemical sensing especially in the area of metal ions detection. Surface functionalization which involves encapsulating a thin layer of capping agent on the CDs surface is often employed to enhance the performance of CDs for specific applications.

In this chapter, the analytical potentials of the different types of CDs synthesized previously, namely CDs_{Green}, CDs_{Blue}, CDs_{Glu} and CDs₂₅₀ will be evaluated. The metal ions sensing potentials of both CDs_{Green} and CDs_{Blue} were investigated without further surface passivation or functionalization. On the other hand, surface functionalization of CDs_{Glu} and CDs₂₅₀ with chitosan and Tris(hydroxymethyl)aminomethane respectively will be discussed in detail. The sensing applications of the different types of CDs for metal ions detection by testing against various metal cations are also described.

The different CDs systems are found to exhibit distinct metal ions sensing capabilities. In this chapter, several metal ions detection assays based on the different CDs systems developed will be reported. Detailed discussions on the analytical potentials of the four types of CDs systems are also provided.

4.2 Introduction

Heavy metal contamination in the environment is of great concern worldwide. Exposure to heavy metals can cause toxic effects to plants and human. The adverse health effects of heavy metals have been extensively studied and have been known for a long time. Due to the threatening effects of these heavy metals, rapid detection and subsequently the removal from the environment are always at urge.

Fluorescence CDs are non-toxic and possess unique physiochemical properties and have captivated immense attention to be developed into sensitive probes for detection of heavy metal ions. Post-synthesis steps such as surface passivation and functionalization are often adopted to further improve the optical and chemical properties, where at the same time to tailor specific feature to suit certain application.

Different types of surface passivating agents ranging from simple molecules exhibiting specific chemical functional groups to larger biomolecules that possess bioactivities can be used. Chitosan (CS) is a biopolymer comprising D-glucosamine and N-acetylglucosamine which can be derived from crustacean shells by partial deacetylation of chitin [220]. CS possess good biocompatibility, hydrophilicity, biodegradability, non-toxicity and chemical stability [221]. Most importantly, CS was chosen as a capping agent for surface modification of CDs_{Glu} due to its excellent chelating ability with metal ions [222].

Besides, Tris(hydroxymethyl)aminomethane (TRIS) which is also known as 2-amino-2-(hydroxymethyl)-1,3-propanediol or THAM is also employed as another capping agent for surface functionalization of CDs₂₅₀. TRIS comprises an amino group that is sterically hindered by three hydroxyl methyl groups attached to a tertiary carbon atom [223]. It is commonly used as pH buffers in biochemical studies. Over the past few decades, TRIS was claimed to be a potential ligand for metal ions due to the presence of a basic site, namely the amino group [224]. It is also reported that TRIS is able to form complexes with some metal ions [225]. Due to this reason, TRIS was used as a capping agent for surface functionalization of CDs₂₅₀ produced from α -cellulose.

The metal ions sensing potentials of the different types of CDs synthesized in this study were investigated. Bare CDs_{Green} and CDs_{Blue} synthesized from acid hydrolysis of α -cellulose were evaluated for the metal ions detection capabilities without further surface passivation and functionalization. In addition, two different CDs systems based on CDs_{Glu} and CDs₂₅₀ were developed by surface modification with CS and TRIS respectively. The interface study of the bare CDs and their interactions with respective capping agents towards metal ions detection was also investigated.

4.3 Experimental Design

4.3.1 Materials and Reagents

Metal salts of cadmium chloride (CdCl_2), copper nitrate ($\text{Cu}(\text{NO}_3)_2$), lead nitrate ($\text{Pb}(\text{NO}_3)_2$), aluminium nitrate ($\text{Al}(\text{NO}_3)_3$), nickel nitrate ($\text{Ni}(\text{NO}_3)_2$), cobalt nitrate ($\text{Co}(\text{NO}_3)_2$), magnesium nitrate ($\text{Mg}(\text{NO}_3)_2$), chromium nitrate ($\text{Cr}(\text{NO}_3)_3$) and zinc nitrate ($\text{Zn}(\text{NO}_3)_2$) were purchased from Acros Organics. Sodium arsenite (NaAsO_2) and iron nitrate ($\text{Fe}(\text{NO}_3)_3$) were purchased from Fisher Chemical. Mercuric nitrate ($\text{Hg}(\text{NO}_3)_2$) and mercuric chloride (HgCl_2) were purchased from Sigma Aldrich and Fisher Chemicals, respectively. Chitosan and Tris(hydroxymethyl)aminomethane (TRIS) were used as capping agent in this study. Chitosan ($\geq 75\%$ deacetylation degree) was purchased from Sigma Aldrich whereas TRIS was purchased from 1st Base Chemicals. All chemicals used were of analytical grade and used as received without further purification unless otherwise stated. Ultrapure water obtained from Milipore Mili-Q Advantage-A10 and Milipore Elix-5 water purification system ($\sim 18.2 \text{ M}\Omega\cdot\text{cm}$, 25°C) was used throughout the study.

4.3.2 Instrumentations

Fluorescence measurements were recorded using fluorescence spectrophotometer (Cary Eclipse Varian). Appropriately diluted CDs sample was transferred into a quartz cuvette of 4 clear sides with a path length of 1 cm and the settings of both excitation and emission slits were altered accordingly to obtain optimum fluorescence excitation and emission. UV-Vis absorption spectra were obtained using UV-Visible spectrophotometer (Varian Cary 50) within the range of 200 nm to 800 nm. Ultrapure water was used as reagent blank for the absorbance measurement. Adjustment of pH was done by using a pH meter (Mettler Toledo SevenEasy).

4.3.3 Surface Modification of CDs

The as-prepared CDs_{Green} and CDs_{Blue} obtained from acid hydrolysis of α -cellulose at different reaction conditions were tested against different metal ions without further surface modification. The CDs_{Glu} obtained from thermal pyrolysis of L-glutamic acid in high temperature furnace at 300 °C for 20 minutes were surface modified with chitosan. Whereas, CDs₂₅₀ prepared from thermal pyrolysis of α -cellulose at 250 °C for 30 minutes were isolated and surface functionalized with TRIS.

The interface study of the bare CDs_{Glu} and chitosan towards its potential in metal ions detection was investigated. Sodium acetate/acetic acid buffer solution of pH 5 was used as aqueous medium for the interface study between CDs_{Glu} and chitosan. CDs_{Glu} and chitosan with concentration of 10 mg/ml were first suspended and dissolved in the buffer solution of pH 5 separately. Interface study of CDs_{Glu} and chitosan was investigated by mixing equal volume of chitosan solution to CDs_{Glu}. Changes in fluorescence emission and absorption before and after the addition of chitosan were measured using fluorescence spectrophotometer and UV-Vis spectrophotometer.

On the other hand, surface functionalization was performed by mixing equal volume of 0.5 M TRIS solution to CDs₂₅₀ solution. The mixture was then vortex to mix well and left to stir for 10 minutes at room condition to facilitate chelating balance. The optical properties of the bare and surface functionalized CDs₂₅₀

were recorded using fluorescence spectrophotometer and UV-Vis spectrophotometer. The CDs₂₅₀ were then tested against various metal ions to identify its potential as metal ions sensing receptors.

4.3.4 Metal Ions Sensing Potential

The obtained CDs were suspended in ultrapure water to desired concentration with the highest fluorescence emission. To investigate the potential of the CDs as metal ion sensing probes, a series of stock solutions of metal ions with concentration of 0.1 M was prepared from the respective metal salts in ultrapure water. The different metal ions (Ni(II), Cd(II), As(II), Al(III), Zn(II), Cr(III), Co(II), Cu(II), Fe(III), Mg(II), Pb(II) and Hg(II) ions) from their respective stock solutions were incubated with a prefixed volume of CDs. The fluorescence emission before and after the addition of various metal ions were recorded using a fluorescence spectrophotometer.

4.4 Results and discussion

4.4.1 Potential of CDs_{Green} as Metal Ions Sensing Receptors

4.4.1.1 Assay for $Hg(II)$ Ions Detection

The presence of functional groups on the surface of CDs_{Green} can act as potential sites for heavy metal cations interactions. The potential of CDs_{Green} as analytical assay was evaluated. The final fluorescence intensity recorded was normalized against the initial fluorescence of CDs_{Green} as shown in Figure 4.1. Among all the heavy metal cations tested, the fluorescence emission of CDs was quenched by 55% in the presence of $Hg(II)$ ions whereas no significant change in fluorescence can be observed for other heavy metal cations tested. It was reported that the fluorescence quenching could be attributed to the non-radiative electron transfer from the excited states to the d orbital of $Hg(II)$ ions [226, 227].

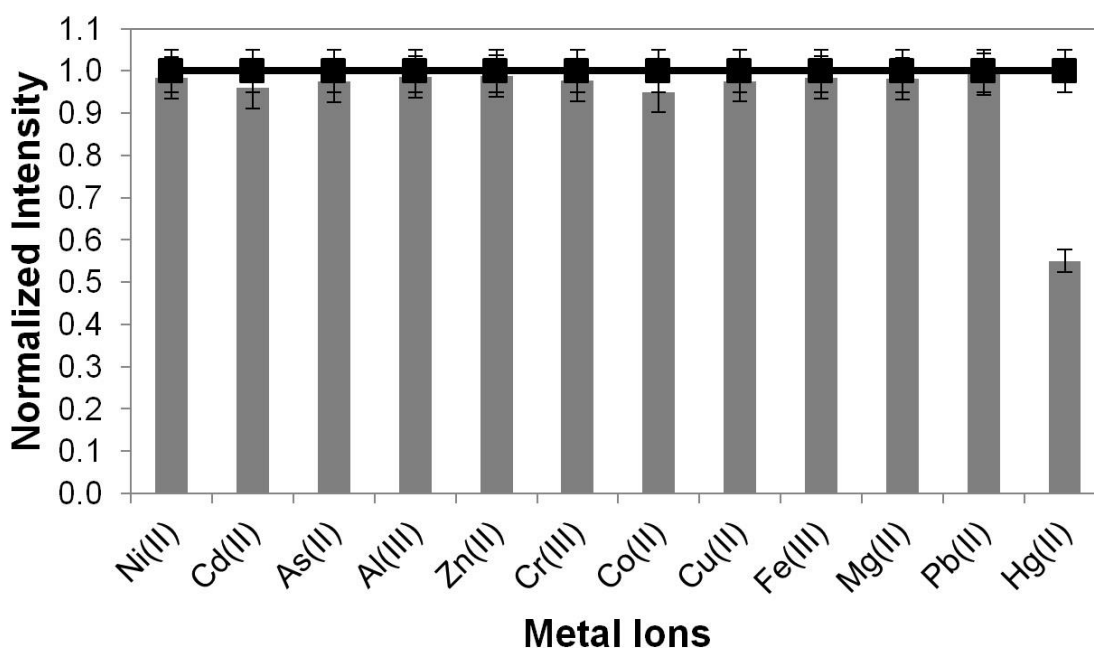


Figure 4.1: The normalized fluorescence intensity of CDs_{Green} recorded at 500 nm in the presence of different metal ions at concentration of 16.08 μM . The line represents the baseline of initial intensity in the absence of metal ions.

The assay was highly specific as it responded only towards Hg(II) ions and there showed low interference from the other heavy metal cations tested. Figure 4.2 illustrates photographs of CDs_{Green} incubated with different heavy metal cations under visible light and UV exposure. The samples incubated with various heavy metal cations appeared as yellowish brown and no distinct difference in colour could be observed under visible light. However, under the exposure of UV, it clearly showed that the fluorescence of CDs_{Green} was effectively quenched by Hg(II) ions. There was no significant change in fluorescence upon addition of other heavy metal cations into the CDs solution. Such result strongly demonstrates that the developed assay has outstanding selectivity towards Hg(II) ions. The high selectivity could be attributed to the strong interactions between the carboxyl groups on CDs_{Green} surface and Hg(II) ions which resulted in fluorescence quenching through electron or energy transfer [228].

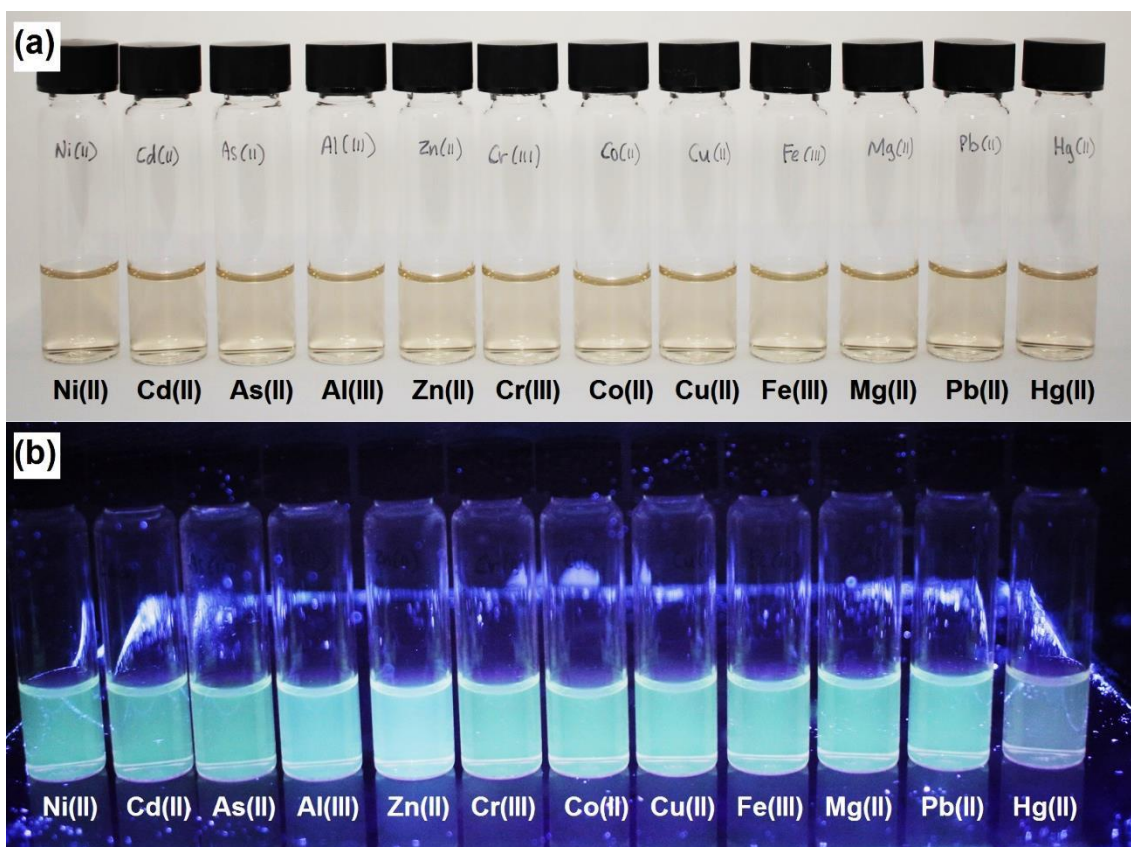


Figure 4.2: Photographs of CDs_{Green} incubated with different metal ions taken under (a) visible light and (b) UV exposure.

4.4.1.2 Detection Assay on Real Water Samples

The high specificity and selectivity of the assay towards Hg(II) ions have suggested that it can be potentially applied for real water samples monitoring for the purpose of pollution control. The analytical characteristic of the assay had been evaluated by construction of the dynamic response range for Hg(II) ions. The change in fluorescence emission of CDs_{Green} in the presence of Hg(II) ions at different concentrations is shown in Figure 4.3. A concentration-dependent trend was observed for the analytical assay. The fluorescence emission of the CDs_{Green} decreased gradually as the concentration of Hg(II) ions was increased up to 160 μ M. The fluorescence of CDs_{Green} was completely quenched at concentration above 160 μ M.

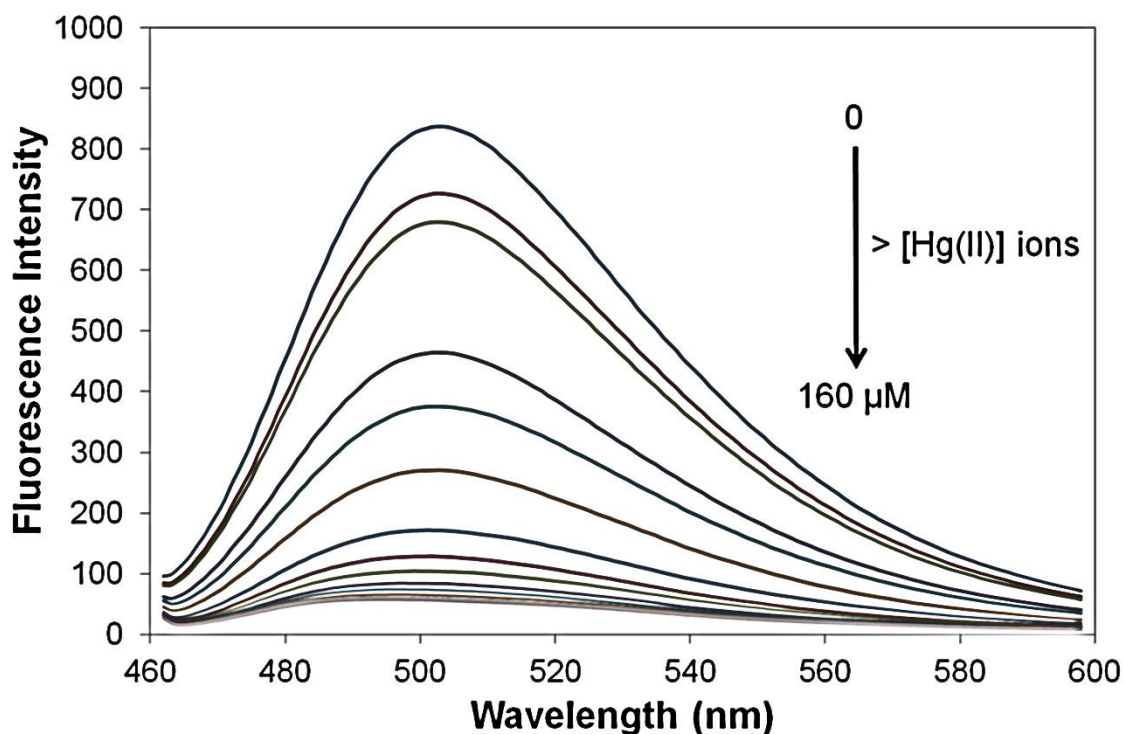


Figure 4.3: The effect of quenching on the fluorescence intensity of CDs_{Green} in the presence of Hg(II) ions at different concentrations monitored at 500 nm.

Standard Stern-Volmer analysis had been adopted to model the quenching profile of the developed analytical assay in the presence of Hg(II) ions. The Stern-Volmer relationship can be defined by the following Equation 4:

$$F_0/F = K_{SV}[C] + 1 \quad \text{(Equation 4)}$$

where F_0 is the initial fluorescence emission of the CDs, F is the fluorescence after addition of analyte, K_{SV} is the Stern-Volmer quenching constant and $[C]$ is the concentration of metal ions.

The Stern-Volmer plot as shown in Figure 4.4 shows a linear quenching profile ($F_0/F = 0.0955 [\text{Hg(II)}] + 0.4493$) of the assay with increasing concentration of Hg(II) ions. In accordance to the linear relationship derived from Stern-Volmer plot, the K_{SV} obtained was $9.55 \times 10^{-2} \mu\text{M}$ with coefficient determination or R^2 value of 0.9955. The limit of detection (LOD) measured in this assay was calculated to be $0.12 \mu\text{M}$. The LOD value determined in this study is comparable to the literature values reported elsewhere [229, 230].

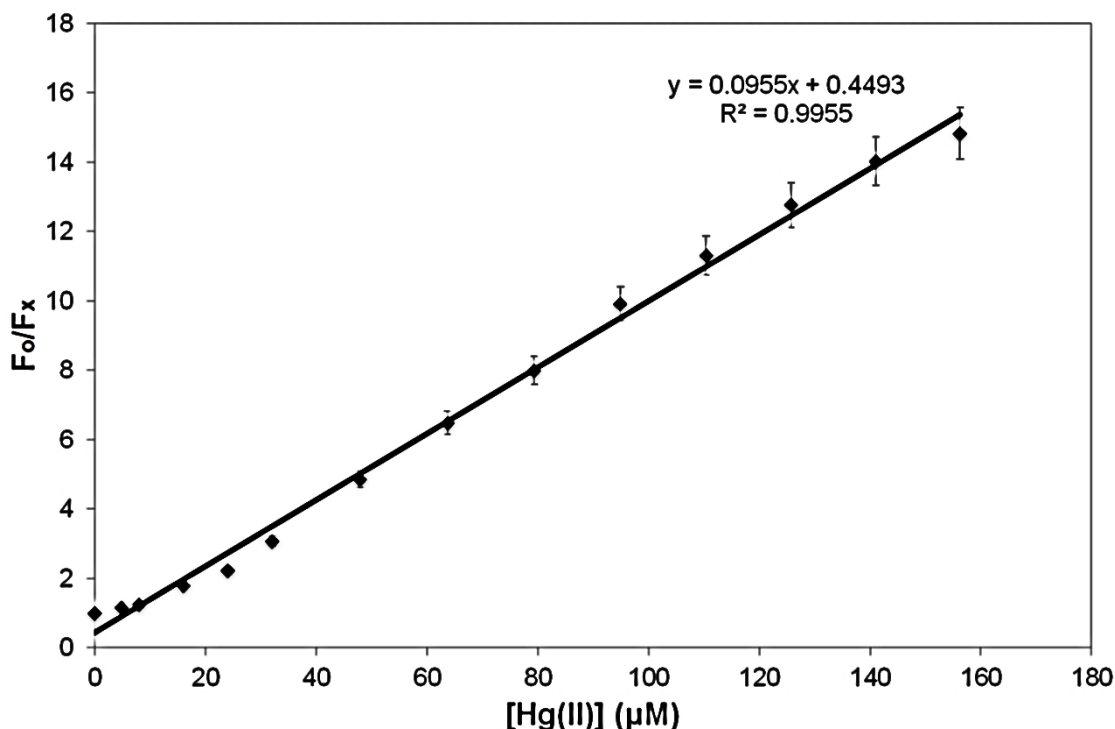


Figure 4.4: Stern-Volmer plot shows the dependence of F_0/F_x on the concentrations of Hg(II) ions within the range of 0 - 160 μM .

Further study had been carried out to evaluate the practical application of the assay for Hg (II) ions detection in tap water samples. Tap water samples were obtained from the lab without any pre-treatment. The tap water samples were then spiked with known concentrations of Hg (II) standard solutions. The sample was then tested with the CDs_{Green} using similar standard procedure and the concentration was derived using the linear range response calibration. In this case, the tap water did not cause any significant change in the CDs_{Green} fluorescence, implying no or low concentration of Hg(II) in the tap water. The spiked samples had shown recovery above 95 % (Table 4.1). This result indicates that the detection assay developed for Hg(II) ions in this study has great potential to be practically utilized for environmental water quality monitoring and alarm system.

Table 4.1: Detection of Hg(II) ions in real water sample spiked with known concentrations of Hg(II) ions.

Amount Spiked (μM)	Amount detected (μM)	Recovery rate (%)
30	28.68	95.60
45	42.90	95.33
60	58.68	97.80

4.4.2 Potential of CDs_{Blue} as Metal Ions Sensing Receptors

4.4.2.1 Detection Assay for Fe(III) Ions

The analytical potential of CDs_{Blue} synthesized by acid hydrolysis of α -cellulose for metal ions sensing was also evaluated. Aqueous solutions of CDs_{Blue} were incubated with a series of different metal ions solutions prepared from their respective metal salts. The changes in fluorescence intensity with and without metal ions solutions were immediately monitored at 456 nm when excited at 357 nm as shown in Figure 4.5. The result reveals that CDs_{Blue} responded specifically towards Fe(III) ions. The fluorescence of CDs_{Blue} was quenched by 61.5% in the presence of Fe(III) at a concentration of 400 μ M. Under the same conditions, no significant change in the fluorescence intensity of CDs_{Blue} could be observed when tested with other metal ions solutions. The result has suggested that CDs_{Blue} is a potential metal ions sensing receptors for specific detection of Fe(III) ions with low interference by other metal ions.

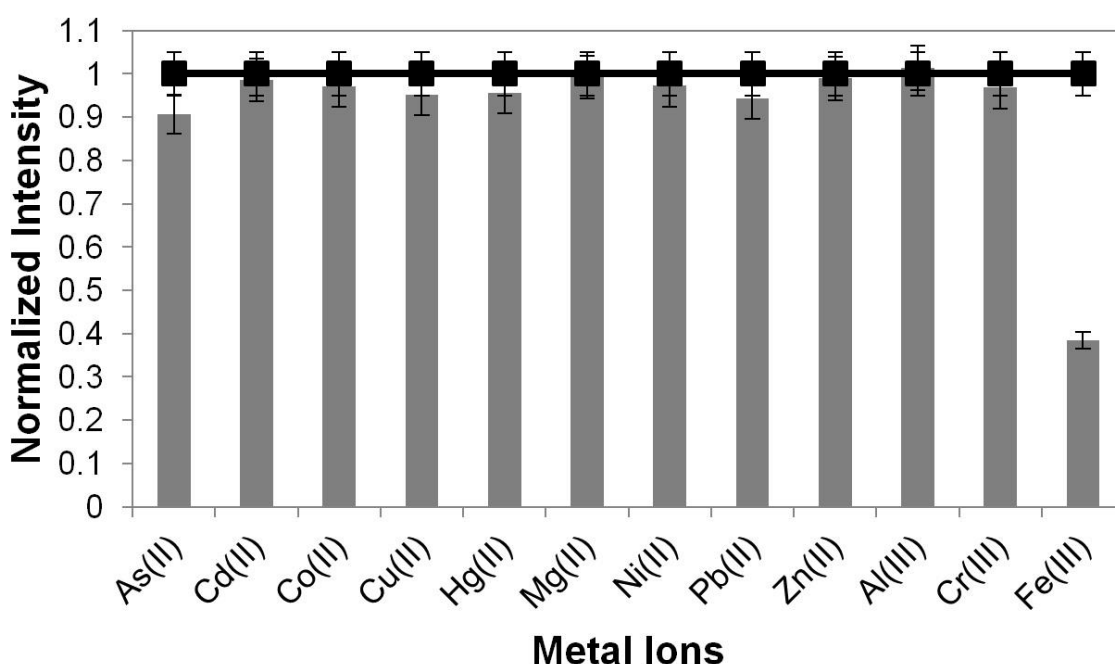


Figure 4.5: Relative intensity of CDs_{Blue} at 500 nm in the presence of different metal ions at concentration of 400 μ M.

The specific interaction between CDs_{Blue} and Fe(III) ions could be explained in terms of the ion selective structures of CDs_{Blue} and the effect of charge transfer [231]. The phenolic hydroxyl groups on the surface of CDs_{Blue} was suggested to possess strong affinity towards Fe(III) ions. Interaction between the hydroxyl groups and Fe(III) ions lead to formation of complexes due to coordination [166, 168]. The electronic structures and distributions of excitons of CDs_{Blue} which induce the acceleration of non-radiative recombination of excitons through energy transfer may be subsequently changed by the complexes formed and resulted in fluorescence quenching [231].

Sensitivity study of Fe(III) ions using CDs_{Blue} as sensing probe was investigated at different concentration of Fe(III) ions in the range of 80-1960 μM . The fluorescence quenching data was plotted as Stern-Volmer plot shown in Figure 4.6. Stern-Volmer plot reveals that the detection assay based on CDs_{Blue} was concentration-dependence. A good linear relationship of fluorescence quenching and Fe(III) ions with K_{SV} value of $3.40 \times 10^{-3} \text{ M}$ was demonstrated. The LOD was determined based on the International Union of Pure and Applied Chemistry (IUPAC) 3σ criterion ($\text{LOD} = 3\sigma/S$ where σ depicted the standard deviation of the intercept and S depicted the slope of the Stern-Volmer plot) [231]. The value of LOD was determined to be $15.66 \mu\text{M}$. The result implies that CDs_{Blue} can be potentially used for highly selective and quantitative detection of Fe(III) ions in aqueous medium.

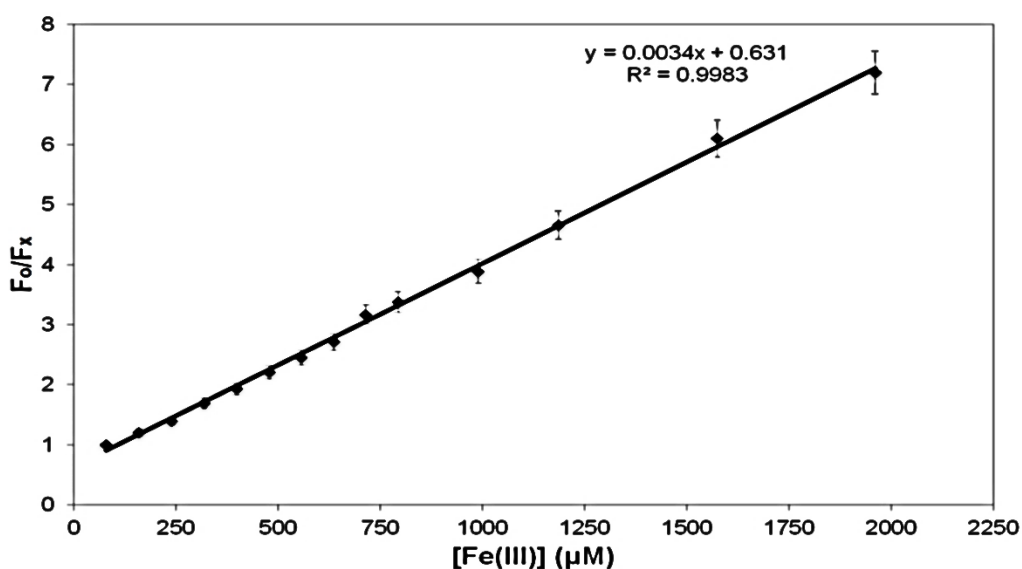


Figure 4.6: Stern-Volmer plot shows the dependence of F_0/F_x on the concentrations of Fe(III) ions within the range of 80-1960 μM .

4.4.3 Interface Study of Bare CDs_{Glu} and Interaction with Chitosan

4.4.3.1 Surface Modification with Chitosan

Chitosan (CS) which is also a poly- β (1 \rightarrow 4)-2-amino-2-deoxy-D-glucose is a natural cationic biopolymer that comprises of one amino group and two hydroxyl groups in a repeating unit of D-glucosamine [232]. Chitosan is only soluble in acidic aqueous solution such as acetic acid. Due to this reason, sodium acetate-acetic acid buffer of pH 5 was used as solution medium in this study. Solubilization of CS in acidic medium is due to the protonation of $-\text{NH}_2$ groups on the repeating unit of D-glucosamine [222]. CS become positively charged upon dissolution in acidic solutions [220]. The effect of sodium acetate-acetic acid buffer solution of pH 5 on the fluorescence of CDs_{Glu} was reported in the previous chapter (Figure 3.24) that neither significant change in fluorescence intensity nor shift in the emission spectrum was observed.

In brief, CS solution was first prepared by dissolving the desired amount of CS flakes in sodium acetate-acetic acid buffer solution of pH 5. Subsequently, surface modification of CDs_{Glu} was carried out by stirring equal volume of isolated CDs_{Glu} and chitosan solution to promote physical adsorption of CS on the surface of CDs_{Glu}. The absorption and fluorescence properties were measured using UV-Vis and fluorescence spectrophotometer and the spectra are shown in Figure 4.7. The absorbance of the broad absorption band centred at around 300 nm with a tail extending to the visible region which may be attributed to the $n \rightarrow \pi^*$ transition and increased slightly after surface modification with CS [217, 218]. As mentioned previously, CDs_{Glu} exhibited optimum fluorescence emission spectrum centred at 440 nm when excited at 365 nm. Both excitation and emission spectrum showed no shift in wavelength and intensity even after surface functionalized with CS.

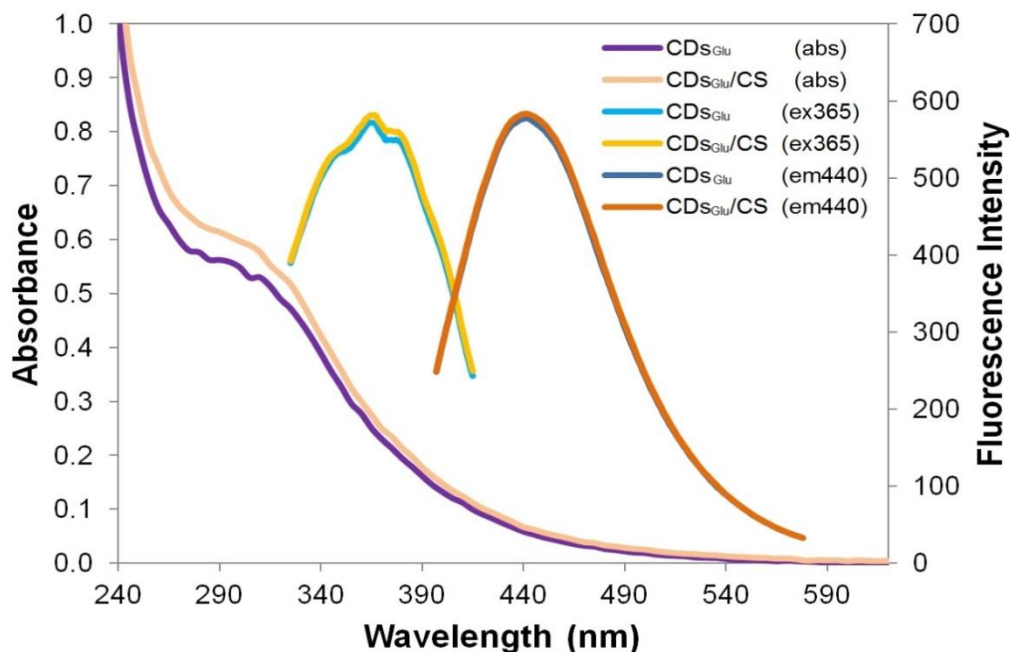


Figure 4.7: Absorption, fluorescence excitation and emission spectrum of bare CDs_{Glu} and CDs_{Glu}/CS.

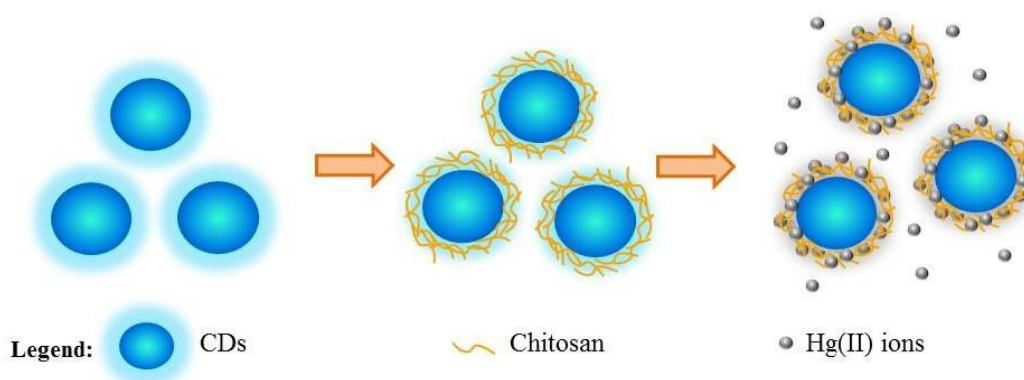


Figure 4.8: Schematic diagram of functionalization of bare CDs_{Glu} with chitosan for Hg(II) ions detection.

The CS-modified CDs_{Glu} which is thereafter denoted as CDs_{Glu}/CS nanoparticles were found to enhance the sensitivity in Hg(II) ions detection. Schematic diagram of surface modification of bare CDs_{Glu} with chitosan for enhanced sensitive detection of Hg(II) ions is illustrated in Figure 4.8. CS was incorporated onto the surface of CDs_{Glu} by stirring to facilitate chelating balance. Eventually, the CS particles would physically adsorb on the CDs_{Glu} surfaces without the need of any coupling agents. Physical adsorption is also known as physisorption. Forces such as Van der Waals interaction, London dispersion forces and intermolecular repulsion are often involved in physisorption [233].

Sensitivity study was investigated by measuring the fluorescence emissions of both bare CDs_{Glu} and CDs_{Glu}/CS in the presence of different concentrations of $Hg(II)$ ions when excited at 365 nm. The fluorescence emission spectra of bare CDs_{Glu} and CDs_{Glu}/CS in the presence of different concentration of $Hg(II)$ ions were shown in Figure 4.9. The fluorescence of both CDs_{Glu} and CDs_{Glu}/CS decreased gradually with increasing concentration of $Hg(II)$ ions which suggested that the bare and surface modified CDs_{Glu} were sensitive to $Hg(II)$ concentration.

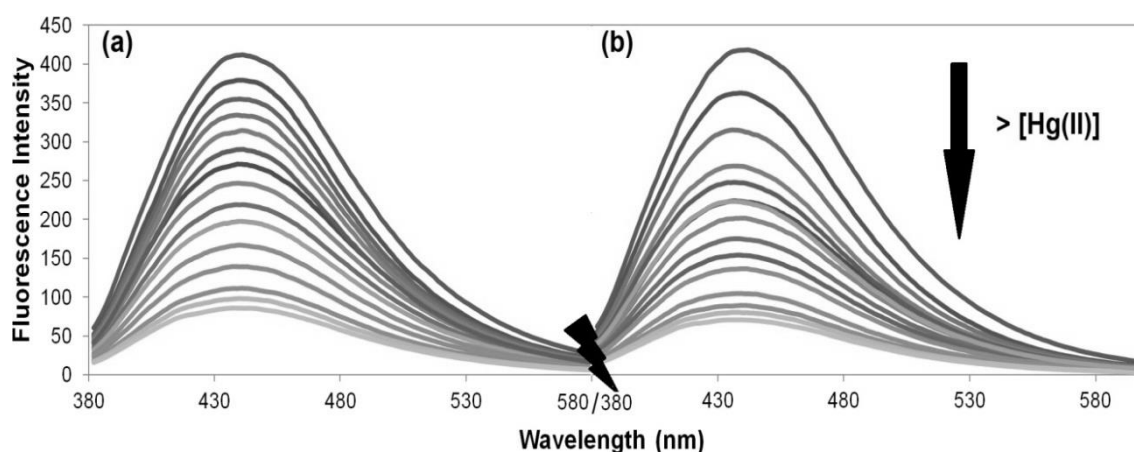


Figure 4.9: Fluorescence emission spectra of (a) bare CDs_{Glu} and (b) CDs_{Glu}/CS in the presence of different concentration of $Hg(II)$ ions.

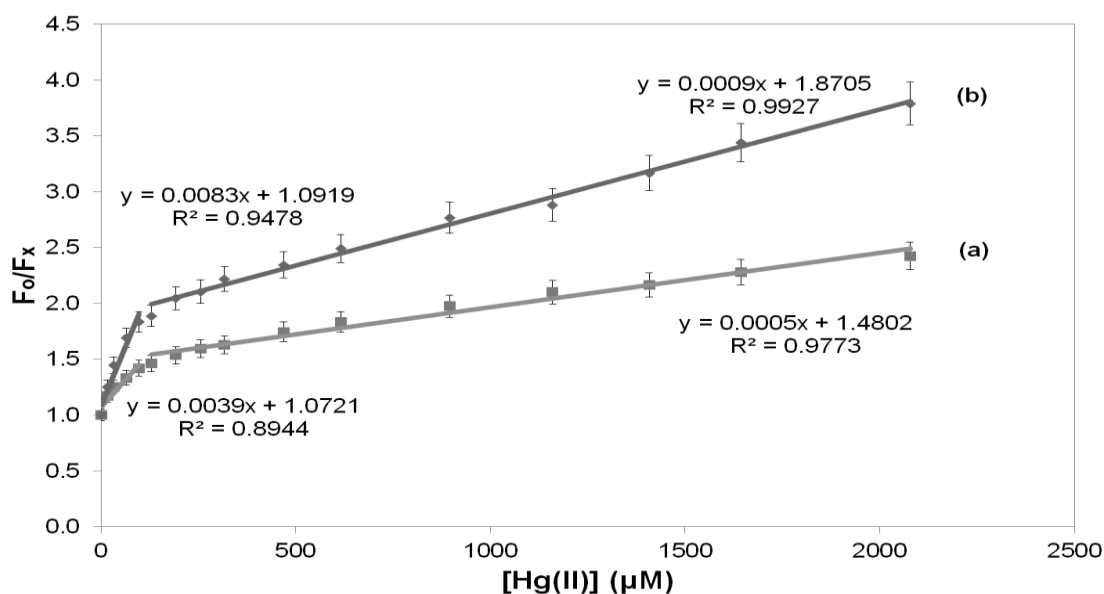


Figure 4.10: Stern-Volmer plot of (a) bare CDs_{Glu} and (b) CDs_{Glu}/CS at different concentrations of $Hg(II)$ ions in the range of 20-2080 μM .

Stern-Volmer plot as shown in Figure 4.10 was generated from the fluorescence quenching data. The result revealed that two linear equations could be generated for both bare CDs_{Glu} and CDs_{Glu}/CS in the concentration range of 20–100 μM and 130–2080 μM .

The detailed analytical performance for the detection of Hg(II) ions for the two types of carbon nanoparticles is presented in Table 4.2. The LOD for bare CDs_{Glu} in the concentration range of 20–100 μM and 130–2080 μM were 0.54 μM and 4.27 μM , respectively. On the other hand, the LOD for CDs_{Glu}/CS in the range of 20–100 μM was 0.18 μM , whereas it was 1.63 μM in the range of 130–2080 μM . This result shows that surface modification of CDs_{Glu} with CS could improve the sensitivity of Hg(II) ions detection and enhance the LOD by at least 60%. The enhancement in LOD was calculated by $[(Final\ LOD - Initial\ LOD)/Final\ LOD] \times 100\%$. The LOD values determined in this study are comparable to the values reported in literature [172, 176].

Table 4.2: Analytical performance of CDs_{Glu} and CDs_{Glu}/CS for Hg(II) ions detection.

Carbon Nanoparticles	Concentration Range (μM)	LOD (μM)	Regression Equation	Determination Coefficient (R^2)
CDs_{Glu}	20-100	0.54	$y = 0.0039x + 1.0721$	0.8944
	130-2080	4.27	$y = 0.0005x + 1.4802$	0.9773
CDs_{Glu}/CS	20-100	0.18	$y = 0.0083x + 1.0919$	0.9478
	130-2080	1.63	$y = 0.0009x + 1.8705$	0.9927

4.4.3.2 Interference Study

The selectivity of the sensing system was evaluated in the presence of other possible interfering metal ions such as Ni(II), Cd(II), As(II), Al(III), Zn(II), Cr(III), Co(II), Cu(II), Fe(III), Mg(II) and Pb(II) ions. The fluorescence intensity in the absence and presence of the possible interfering ions were recorded at 440 nm upon excitation at 365 nm. The relative fluorescence intensities were normalized against the initial fluorescence and presented in Figure 4.11.

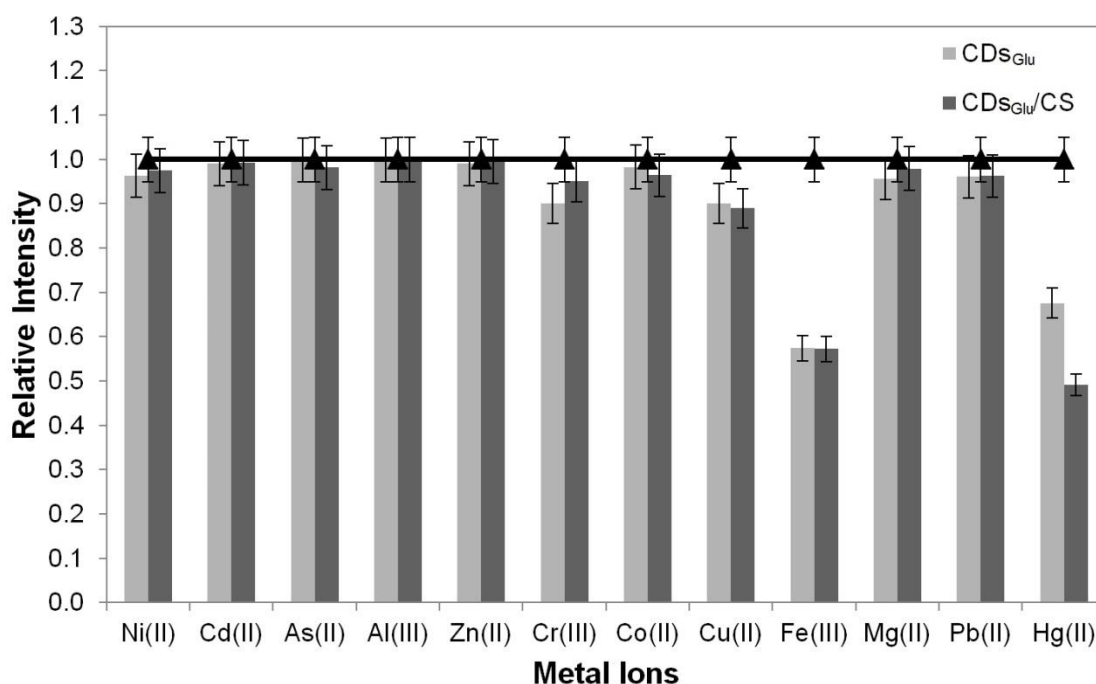


Figure 4.11: Relative intensity of bare CDs_{Glu} and CDs_{Glu}/CS in the presence of different metal ions at concentration of 330 μ M.

Under the same reaction conditions, most of the tested metal cations did not significantly affect the fluorescence of both CDs_{Glu} and CDs_{Glu}/CS. However, it was observed that Fe(III) ions could be a potential interfering ions that would also quench the fluorescence of both CDs_{Glu} and CDs_{Glu}/CS. It was observed that the fluorescence of both bare CDs_{Glu} and CDs_{Glu}/CS were quenched by Fe(III) ions up to approximately 40%. This result implies that the quenching of Fe(III) ions was barely due to the interaction between CDs_{Glu} and Fe(III) ions. The CS present on the surface of CDs_{Glu}/CS would not interact with the Fe(III) ions. This in turn indicated that CS adsorbed on the surface of CDs_{Glu}/CS would only enhance the sensitivity for Hg(III) detection but remained inert towards Fe(III) ions.

Figure 4.12 shows the photographs of bare CDs_{Glu} and $\text{CDs}_{\text{Glu}}/\text{CS}$ in the presence of possible interfering metal cations under UV exposure. The photographs also indicated that Fe(III) ions was a potentials interfering metal cations that would also quench the fluorescence of both bare CDs_{Glu} and $\text{CDs}_{\text{Glu}}/\text{CS}$.

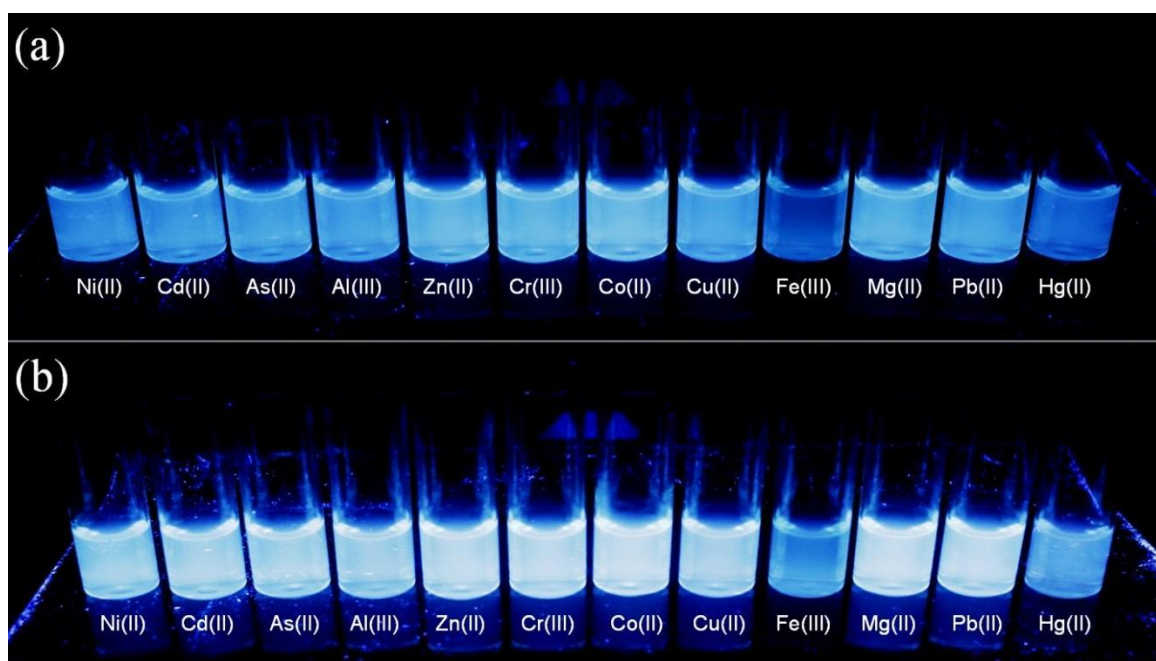


Figure 4.12: Photograph of (a) bare CDs_{Glu} and (b) $\text{CDs}_{\text{Glu}}/\text{CS}$ incubated with various interfering metal ions under UV exposure.

4.4.4 Surface Functionalization of CDs_{250} with TRIS

4.4.4.1 Interaction between CDs_{250} and TRIS

CDs_{250} obtained by thermal carbonization of α -cellulose without involved any acid solutions were further studied. The CDs_{250} were surface modified with TRIS solution. UV-Vis spectrophotometry was adopted to study the binding interaction of CDs_{250} and TRIS. The change in UV-Vis spectra of CDs_{250} in ultrapure water at different concentrations of TRIS was monitored. The UV-Vis spectrum is shown in Figure 4.13.

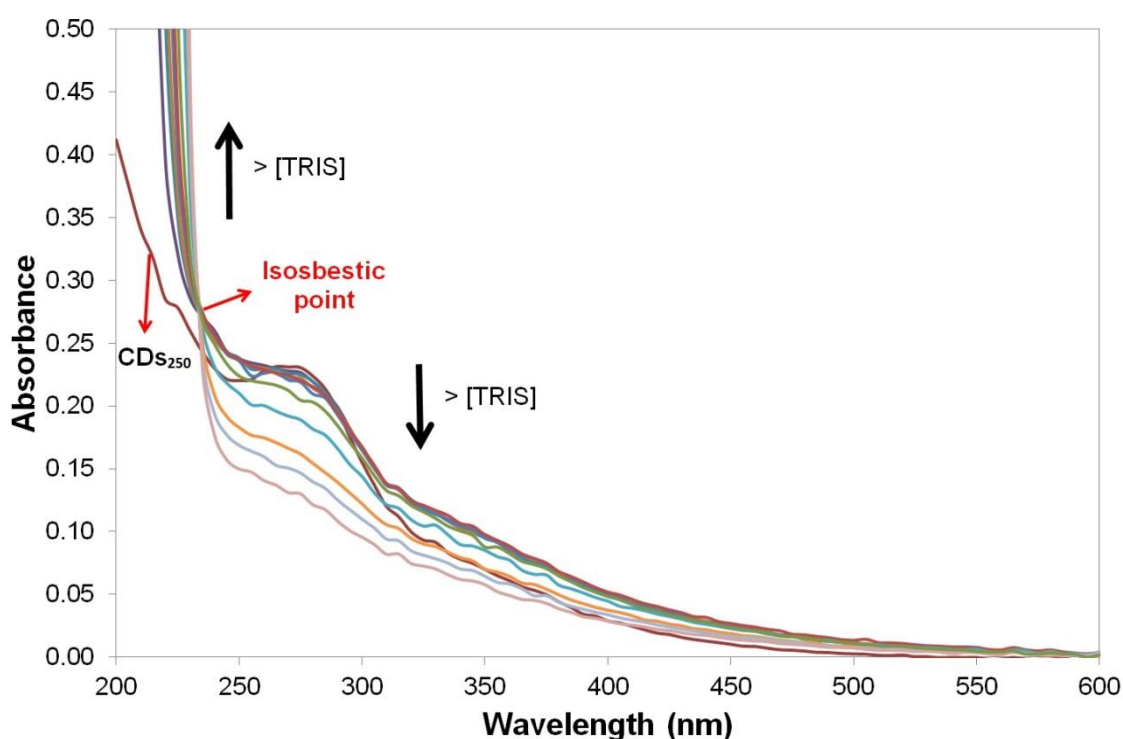


Figure 4.13: Absorption spectra of CDs_{250} in the presence of different concentration of TRIS solution.

Bare CDs_{250} dissolved in ultrapure water exhibited a strong absorption band at 270 nm with a tail extending to the visible region. The absorption peak at 270 nm decreased with increasing concentrations of TRIS solution. An isosbestic point centered at 230 nm was eventually observed. Isosbestic point can be referred to a set of absorption spectra where the sum of concentrations of two principal absorbing components is constant, when plotted on a same graph for a set of solutions [234]. Isosbestic point commonly appeared when electronic spectra are determined on a solution in which a chemical reaction such as

formation of product from reactant is in progress or on a solution in which two absorbing components are in equilibrium [234]. The clear isosbestic point as shown in Figure 4.13 indicated the formation of complexes as a result of interaction between TRIS and CDs₂₅₀. Hence, it is most likely that the CDs₂₅₀ nanoparticles were successfully modified with TRIS due to the formation of complexes.

4.4.4.2 Potential in Metal Ions Sensing

The metal ions sensing potential of both bare CDs₂₅₀ and TRIS-functionalized CDs₂₅₀ (CDs₂₅₀/TRIS) were investigated by testing against various metal ions. The fluorescence intensity ratio of $(F_o - F_x)/F_o$ in the presence of different metal ions for both CDs₂₅₀ and CDs₂₅₀/TRIS solutions are shown in Figure 4.14.

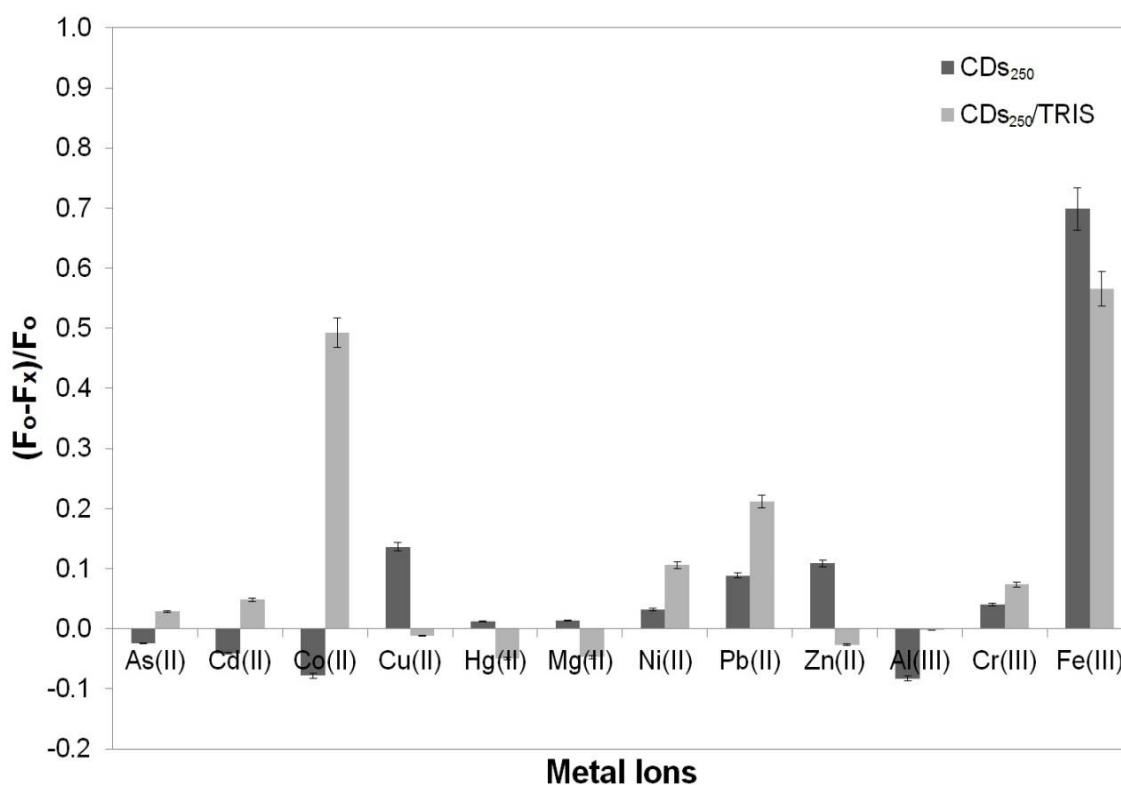


Figure 4.14: Various fluorescence intensity ratio $(F_o - F_x)/F_o$ of the solutions of CDs₂₅₀ and CDs₂₅₀/TRIS in the presence of different metal ions.

From the figure, no significant changes in the fluorescence intensity of CDs₂₅₀ and CDs₂₅₀/TRIS could be observed for most of the metal cations tested. However, the fluorescence of both bare CDs₂₅₀ and CDs₂₅₀/TRIS were

quenched in the presence of Fe(III) ions. The quenching of fluorescence in the presence of Fe(III) ions is most likely attributed to the complex formation between phenolic hydroxyl groups that were found present on the surface of bare CDs₂₅₀ and Fe(III) ions. The fluorescent turn-off mechanism may be ascribed to the charge transfer occurred between the excited CDs₂₅₀ and Fe(III) ions as well as due to the restrained exciton recombination [166]. This result is in agreement with the fluorescent turn-off mechanism for detection of Fe(III) ions as reported elsewhere [235-237].

Interestingly, it was realized that the CDs₂₅₀ that were initially inert to Co(II) ions were found responsive towards Co(II) ions after functionalized with TRIS. The fluorescence of CDs₂₅₀/TRIS was quenched up to 50% in the presence of Co(II) ions. The fluorescence quenching in the presence of Co(II) ions is possibly due to the energy and charge transfer between CDs₂₅₀/TRIS and the complex formed during aggregation [238-240]. Li *et al.* have proved that interaction between CDs and Co(II) ions would lead to complex formation and ultimately quenching in fluorescence as a result of complex aggregations [241]. A typical Stern-Volmer plot was constructed as shown in Figure 4.15 to determine the effect of the concentrations of Co(II) ions on fluorescence quenching.

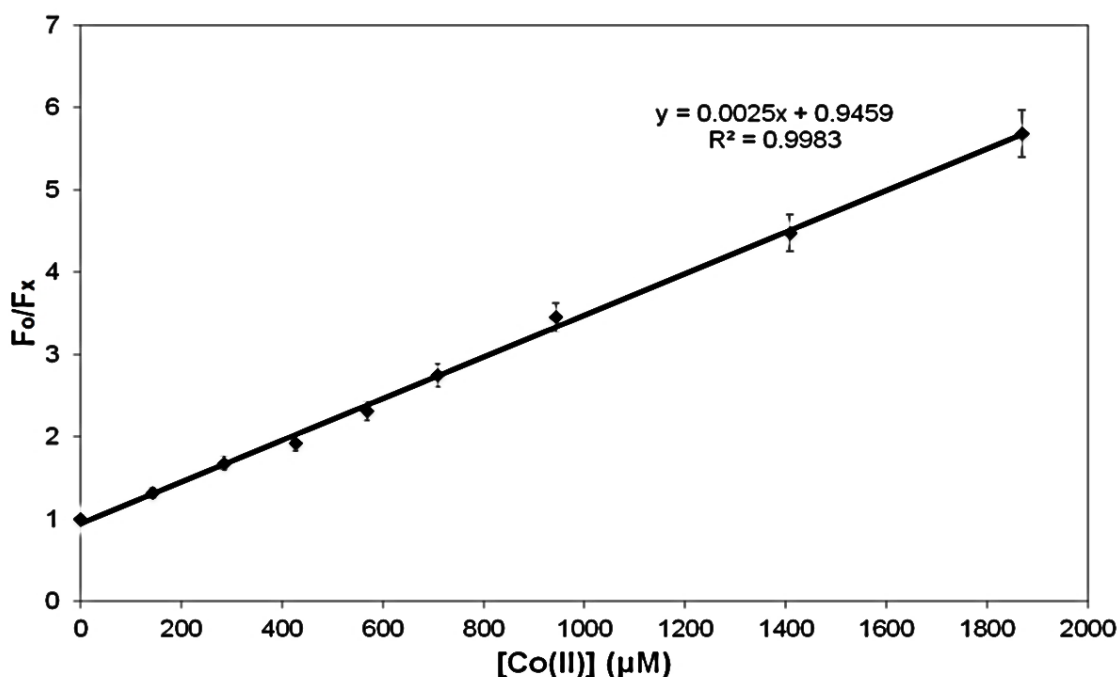


Figure 4.15: Stern-Volmer plot shows the dependence of F_0/F_x on the concentrations of Co(II) ions within the range of 0-1870 μM .

The Stern-Volmer plot shows a good linear relationship in the linear range up to 1870 μM with LOD of 16.84 μM . The result implies that the $\text{CDs}_{250}/\text{TRIS}$ system could be potentially used as sensitive fluorescence turn-off probe for Co(II) sensing upon further development. A summary of the analytical potentials of the different CDs sensing assays developed is shown in Table 4.3 as follows.

Table 4.3: Summary of the analytical potentials of the different CDs sensing systems.

	$\text{CDs}_{\text{Green}}$	CDs_{Blue}	$^*\text{CDs}_{\text{Glu}}/\text{CS}$		$\text{CDs}_{250}/\text{TRIS}$
Analyte	Hg(II)	Fe(III)	Hg(II)		Co(II)
Read Out	Turn off	Turn off	Turn off		Turn off
Linear Range (μM)	0-160	80-1960	20-100	130-2080	0-1870
LOD (μM)	0.12	15.66	0.18	1.63	16.84
K_{SV}	9.55×10^{-2}	3.40×10^{-3}	8.30×10^{-3}	9.00×10^{-4}	2.50×10^{-3}
R^2	0.9955	0.9983	0.9478	0.9927	0.9983
Interfering Ions	-	-	Fe(III)		Fe(III)
Real Sample	Tap Water	-	-		-

* The $\text{CDs}_{\text{Glu}}/\text{CS}$ sensing system was reported to exhibit two linear ranges.

4.5 Conclusions

Different metal ions detection assays have been developed in this study. CDs_{Green} and CDs_{Blue} synthesized by acid hydrolysis of α -cellulose under properly controlled synthesis conditions have found applications as fluorescence turn off sensing probes for detection of Hg(II) and Fe(III) ions, respectively. Practical application of CDs_{Green} in real water samples has also been demonstrated in spiked tap water samples with high recovery rates of above 95%.

Besides, CDs_{Glu} obtained from thermal pyrolysis of L-glutamic acid have been successfully surface functionalized with CS and applied for Hg(II) ions sensing. The functionalized CDs_{Glu}/CS nanoparticles have found to enhance the sensitivity for Hg(II) ions detection. In addition, present study has also successfully demonstrated that TRIS can be employed as a capping agent to surface functionalize CDs₂₅₀ for sensitive detection of Co(II) ions.

However, the results have shown that Fe(III) ions are potential interfering ions that might interfere with the sensing potential of both CDs_{Glu}/CS and CDs₂₅₀/TRIS. Therefore, further study on overcoming the effect of interfering ions is required to further develop the systems into highly specific analytical sensing probes for rapid and sensitive detection of metal ions.

Chapter 5 Binding Isotherms of Carbon Dots

5.1 Executive Summary

Surface passivation or functionalization of CDs is typically constructed to tailor the applications of CDs in various fields. Although immense studies had been carried out to surface functionalize CDs with diverse capping agents, reports on binding isotherms are relatively scarce.

In this chapter, binding isotherms study using spectroscopic technique has been employed to the system of CDs₂₅₀/TRIS as a study model. The presence of Co(II) ions was found to sensitively quench the fluorescence of the CDs₂₅₀/TRIS system. Hence, Co(II) ions was used as the targeted analytes for the system. Ni(II) ions that is inert to the CDs₂₅₀/TRIS system was also included as a reference model. Standard binding analysis methods such as mole ratio method, Stern-Volmer analysis, double log regression and modified Scatchard methods were employed to study the binding isotherms of the CDs₂₅₀/TRIS system. The binding isotherms that describe the relationship between binding affinity of the system towards its targeted analyte and the change in optical properties were established.

Besides, immobilization of CDs₂₅₀ in solid matrix that could be potentially applied for optical fibers was also studied. Sodium alginate that exhibit great capability of forming gel beads in the presence of divalent metal cations was used as a solid support for entrapment of CDs₂₅₀. CDs encapsulated alginate beads were produced successfully in this study.

5.2 Introduction

CDs have emerged as superior carbon nanoparticles that have been extensively studied for various applications in different fields. Post-synthesis strategies are often carried out to enhance the sensitivity and specificity of CDs for desired applications. In the area of chemical sensing, surface functionalization of CDs is always performed to impart CDs as sensitive probes for specific detection of one type of targeted analytes. For instance, Campos *et al.* have fabricated PAMAM-NH₂ functionalized CDs for specific detection of 4-chloro-2,6-dinitroaniline which is an explosive nitrocompound [242]. β -amino alcohol functionalized CDs were also prepared by Wang *et al.* for selective detection of Cu(II) ions under basic conditions [170].

Although considerable studies on surface functionalization of CDs as specific fluorescence nano-sensors have been reported, there are still limited studies on the binding isotherms of CDs. In this study, binding parameters of the interaction between surface-modified CDs and targeted metal ions were extracted using spectroscopic analysis. The binding isotherm that correlates the binding affinity and optical properties of surface functionalized CDs bound with targeted metal ions were investigated and established by employing standard mathematical models.

Practical applications of CDs in optical fibers have triggered research into immobilization of CDs in matrices. One of the challenges in the immobilization is to retain the properties of CDs in the immobilized form. Moreover, leaching of CDs from the matrix should be prevented and at the same time, the matrix must be permeable to the solvent used and the analytes [243]. Several common immobilization approaches on optical fibers include covalent attachment [244], sol-gel immobilization [245] and immobilization on solid support [246].

Encapsulation made in an ionic polysaccharide solution added dropwise into a divalent cation solution to form insoluble gel beads is a simpler technique of immobilization [247]. Alginate is a naturally occurring carbohydrate polymer is typically used in conjunction with calcium ions as crosslinker to form alginate beads [248]. Alginic acid is a biopolymer derived from brown algae and it

contains carboxyl groups that can form complexes with metal ions [249]. In this study, attempt in immobilization of CDs by encapsulation in alginate beads was explored and discussed.

5.3 Experimental Design

5.3.1 Materials and Reagents

Alginic acid sodium salt which is also known as sodium alginate was purchased from Sigma Aldrich. Calcium chloride was purchased from Bendosen. Metal salts of $\text{Ni}(\text{NO}_3)_2$ and $\text{Co}(\text{NO}_3)_2$ were purchased from Acros Organics. TRIS was purchased from 1st Base Chemicals whereas α -cellulose for the synthesis of CDs_{250} was purchased from Sigma Aldrich. All chemicals used were of analytical grade and used as received without further purification unless otherwise stated. Ultrapure water obtained from Milipore Mili-Q Advantage-A10 and Milipore Elix-5 water purification system ($\sim 18.2 \text{ M}\Omega\cdot\text{cm}$, 25°C) was used throughout the study.

5.3.2 Spectroscopic Determination of Binding Isotherms

Fluorescence measurements were recorded using fluorescence spectrophotometer (Cary Eclipse Varian). Appropriately diluted aqueous solution of CDs sample was transferred into a quartz cuvette of 4 clear sides with a path length of 1 cm. The settings of excitation and emission slits were both fixed at 10 nm. UV-Vis absorption spectra were obtained using UV-Visible spectrophotometer (Varian Cary 50) within the range of 200 nm to 800 nm. Ultrapure water was used as blank for the absorbance measurement.

5.3.3 Encapsulation of CDs

CDs were immobilized in sodium alginate beads in present study. In a typical attempt, initial solution of sodium alginate was prepared by accurately weighed 0.1 g of sodium alginate powder and added with 5 ml of ultrapure water. The mixture was then heated on a hotplate with constant stirring to fully dissolve the sodium alginate and to form homogenous solution. The sodium alginate solution was cooled to approximately $35\text{-}40^\circ\text{C}$ before added with the CDs_{250} suspended in 5 ml of ultrapure water. The final concentration of the sodium alginate

solution containing CDs₂₅₀ was now approximately 1% w/v. The solution was then dripped dropwise using a syringe needle into a beaker containing 150 ml 0.1 M calcium chloride solution under constant stirring. The alginate beads formed were then strained and wash several times with ultrapure water and air dried at room temperature.

5.4 Results and discussion

5.4.1 Binding Isotherms Analysis

5.4.1.1 Absorption and Stoichiometry of Co(II)-CDs₂₅₀/TRIS Complex

The analytical potential of CDs₂₅₀/TRIS in the presence of various metal cations was identified in the previous chapter. The intriguing result (Figure 4.14) revealed that surface functionalization has caused the fluorescence intensity of CDs₂₅₀/TRIS to be quenched up to 50% in the presence of Co(II) ions while no significant difference could be observed for the other metal cations. Due to this reason, this system was adopted for further study in terms of binding isotherms. Ni(II) ions that was found inert towards the CDs₂₅₀/TRIS system was used as a negative control. Spectroscopic techniques employing both UV-Vis and fluorescence spectroscopy were used to study the binding isotherms of the system. The absorption spectra of CDs₂₅₀/TRIS in the presence of different concentrations of Ni(II) and Co(II) ions were shown in Figure 5.1 and Figure 5.2 respectively.

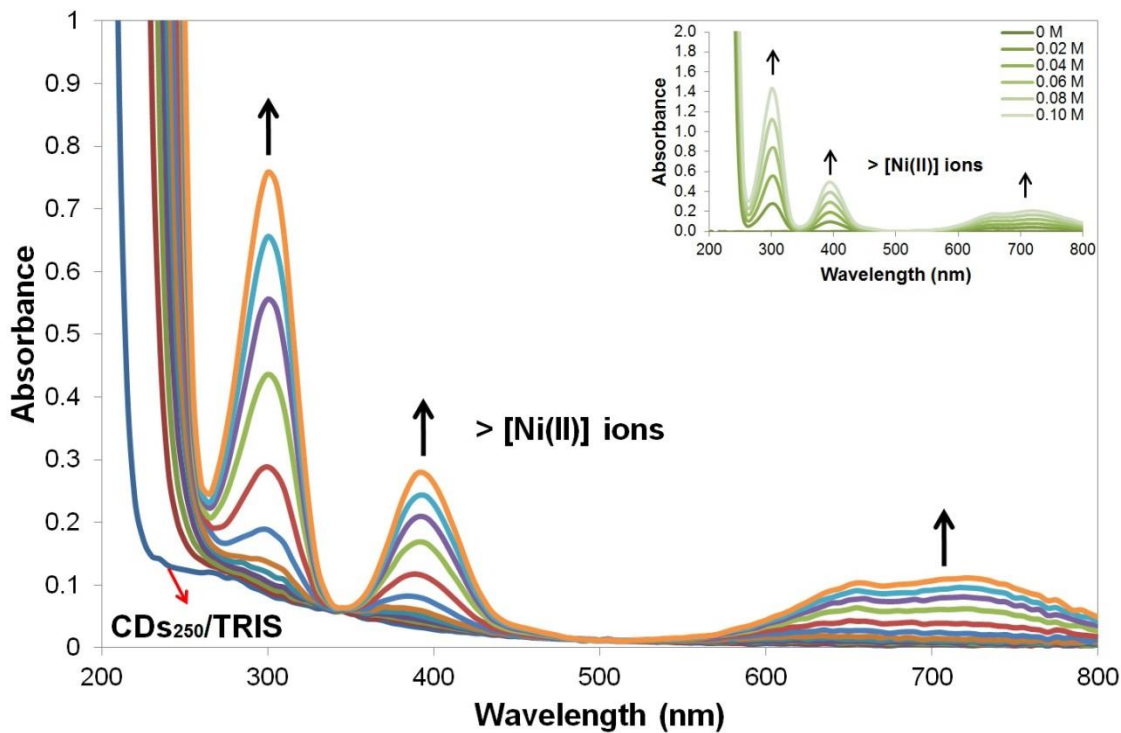


Figure 5.1: Absorption spectra of CDs₂₅₀/TRIS in the presence of Ni(II) ions at different concentrations. Inset: Absorption spectra of different concentrations of Ni(II) ions.

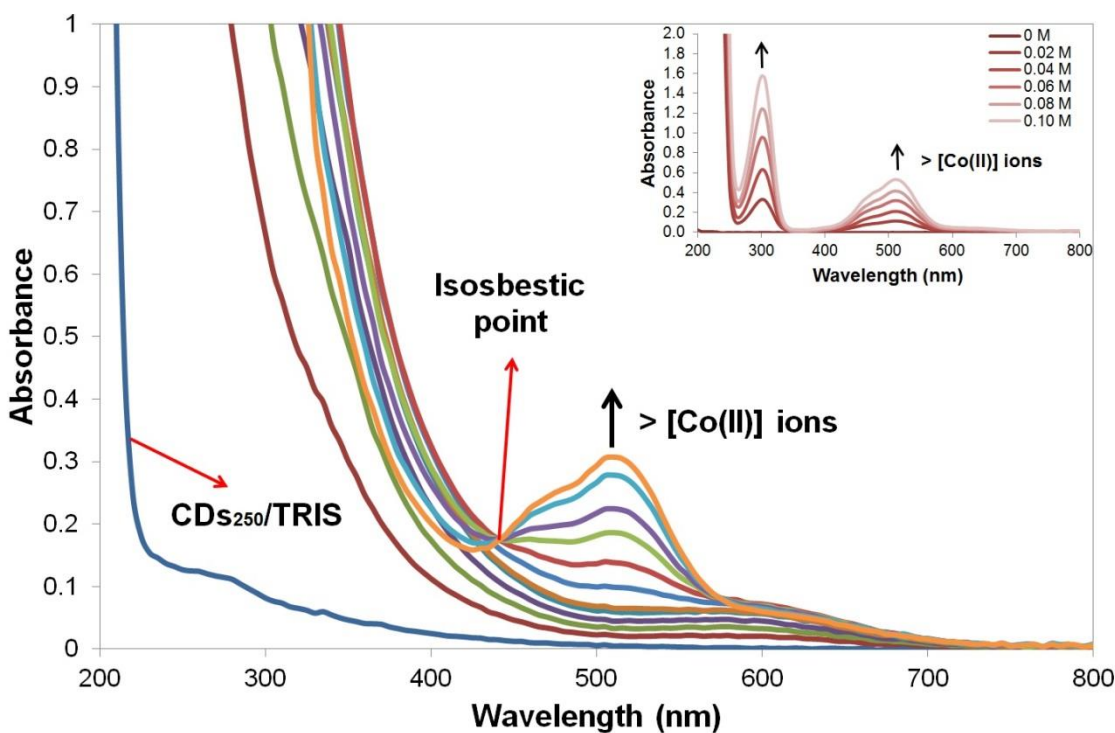


Figure 5.2: Absorption spectra of CDs₂₅₀/TRIS in the presence of different concentrations of Co(II) ions. Inset: Absorption spectra of different concentrations of Co(II) ions.

Presence of isosbestic point in electronic absorption spectra is often used as an indication of formation of complexes or products from reactants [250, 251]. In the presence of Ni(II) ions, there was no obvious isosbestic point could be observed from the absorption spectra of CDs₂₅₀/TRIS as shown in Figure 5.1. The absorption bands centred at 300 nm, 400 nm and 700 nm were found to increase as the amount of Ni(II) ions titrated into the system increased. Similar trend was also observed in the absorption spectra of Ni(II) ions as shown in the inset of Figure 5.1. Hence, the three absorption bands were suggested to be attributed to the absorption by Ni(II) ions. The gradual increase in the absorbance of the CDs₂₅₀/TRIS were purely due to the increasing amount of Ni(II) ions in the system.

On the other hand, a clear isosbestic point at 440 nm was observed in the absorption spectra of CDs₂₅₀/TRIS in the presence of Co(II) ions as shown in Figure 5.2. This indicates that the presence of two species in equilibrium due to formation of complexes as a result of interaction between CDs₂₅₀/TRIS and Co(II) ions [252]. The inset of Figure 5.2 shows the absorption spectra of Co(II) ions at different concentrations. A broad absorption band centred at 510 nm was found to increase with increasing concentrations of Co(II) ions. Therefore, it is most likely that the absorption band centred at 510 nm of the absorption spectra of CDs₂₅₀/TRIS system (Figure 5.2) was attributed to the increasing amount of Co(II) ions in the system.

Mole ratio plot is commonly employed to determine the stoichiometry of complex where the absorbance values are plotted against the corresponding mole ratio [253, 254]. The variation of absorbance at 400 and 440 nm of the CDs₂₅₀/TRIS system in the presence of Co(II) ions at different concentrations are illustrated in Figure 5.3 as mole ratio plots.

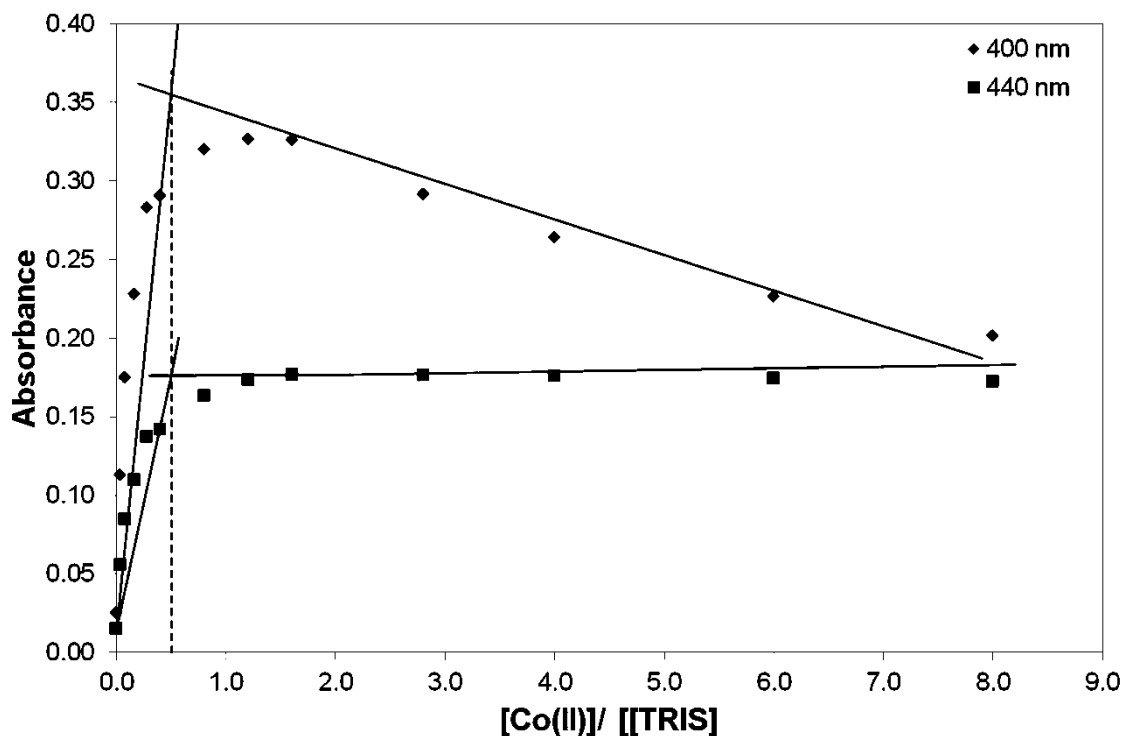


Figure 5.3: Mole ratio plot for the interaction of Co(II) ions with TRIS.

From the figure, it was observed that the absorbance monitored at 400 nm was first increased up to mole ratio of 1 then decreased. Concurrently, the absorbance monitored at 440 nm which was also the isosbestic point increased as the value of mole ratio increased up to mole ratio of 1. Beyond that point, the absorbance values were kept constant at higher mole ratio of [Co(II)] to [TRIS]. It was suggested that these trends could be implied that the formation of complexes as a result of interaction between Co(II) ions and TRIS had reached equilibrium. TRIS molecules present in the system were being used up as reflected by the decrease in the absorbance values at 400 nm beyond mole ratio of 1. Therefore, the amount of complexes formed from the reaction was limited as indicated by the constant absorbance values monitored at 440 nm because TRIS molecules had become a limiting factor in the system although Co(II) ions were present in excess. The stoichiometry of the interaction between Co(II) ions and TRIS was found to be 1:2 ([Co(II)]:[TRIS]) from the mole ratio plots.

5.4.1.2 Stern-Volmer Analysis

Standard Stern-Volmer method was also employed to analyse the fluorescence quenching data. The Stern-Volmer plots based on the fluorescence quenching of CDs₂₅₀/TRIS in the presence of Co(II) and Ni(II) ions were illustrated in Figure 5.4. Ultrapure water was used as baseline to normalize the effect of dilution due to the increasing volume.

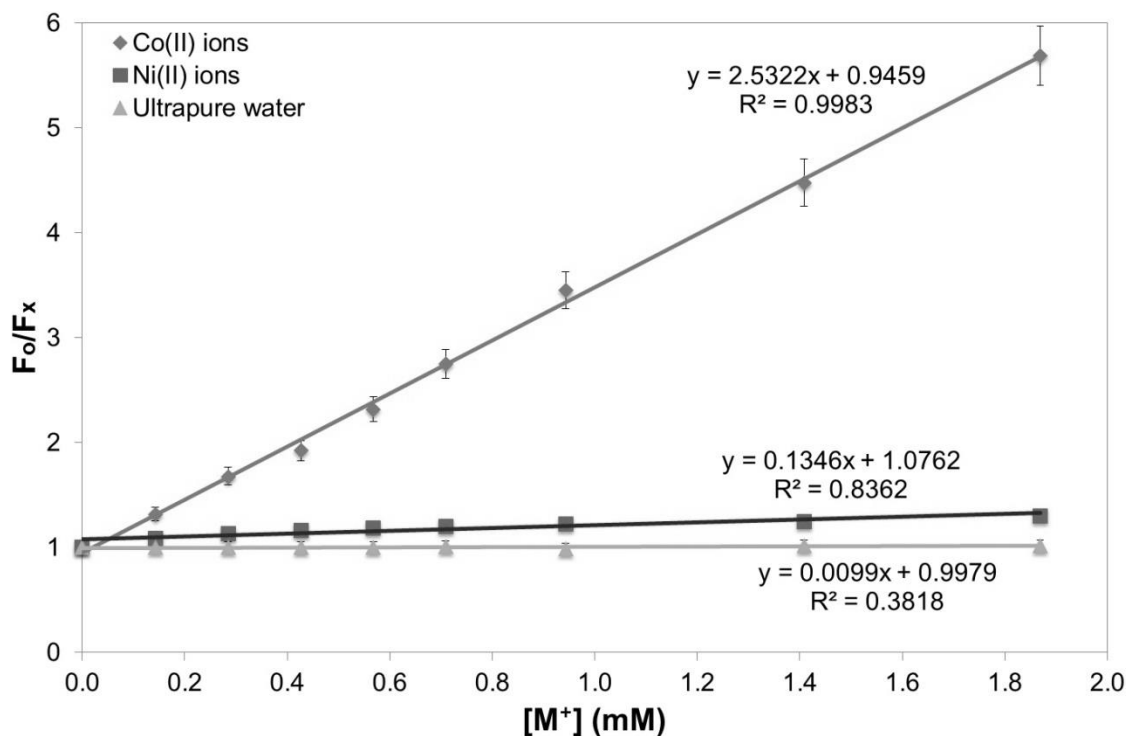


Figure 5.4: Stern-Volmer plot for binding of CDs₂₅₀/TRIS to Co(II), Ni(II) ions and ultrapure at different concentrations.

Fluorescence quenching of CDs₂₅₀/TRIS by Co(II) ions was found to be concentration-dependent with good linear relationship. Significant quenching could be observed for Co(II) ions with linear profile of $F_0/F_x = 2.5322 [\text{Co(II)}] + 0.9459$ with R^2 value of 0.9983, where 2.5322 mM is the K_{SV} value. TRIS could interact with metal cations by formation of different types of bonding, namely the purely coordinate metal-oxygen bond, metal-nitrogen bond and coordinate-covalent bond with alkoxy oxygen as shown in Figure 5.5 a, b and c respectively [255].

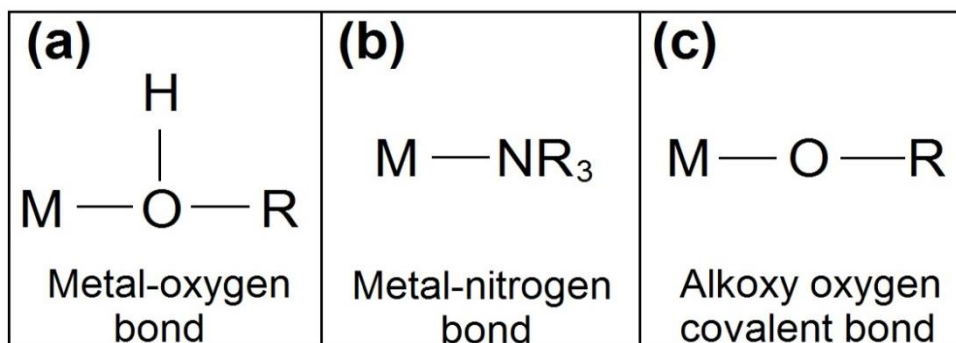


Figure 5.5: Different types of bonding formed between TRIS and Co(II) ions [254].

The interaction between TRIS and Co(II) ions involved 3 stepwise complex formation, in which the different species formed were $[\text{Co}(\text{TRIS})]^{2+}$, $[\text{Co}(\text{TRIS})_2]^{2+}$ and $[\text{Co}(\text{TRIS})_3]^{2+}$ [256]. Hence, the fluorescence quenching of $\text{CDs}_{250}/\text{TRIS}$ by Co(II) ions could be due to the interruption of the photoinduced charge separation and radiative recombination of CDs upon deposition of the complexes on the surfaces of $\text{CDs}_{250}/\text{TRIS}$ [239].

The Stern-Volmer plot of Ni(II) ions (Figure 5.4) shows a slightly elevated gradient ($K_{\text{SV}} = 0.1346 \text{ mM}$) when compared to the baseline of ultrapure water ($K_{\text{SV}} = 0.0099 \text{ mM}$). Although no clear isosbestic point could be observed in the absorption spectra of $\text{CDs}_{250}/\text{TRIS}$ in the presence of Ni(II) ions as mentioned previously (Figure 5.1), it was reported that Ni(II) ions would interact with TRIS and form complexes such as $[\text{Ni}(\text{TRIS})]^{2+}$, $[\text{Ni}(\text{TRIS})_2]^{2+}$ and $[\text{Ni}(\text{C}_3\text{H}_4\text{N}_2)]^+$ [257]. However, the reaction between Ni(II) ions and TRIS was claimed to be extremely slow. Bologni *et al.* realized that reaction performed by ordinary titration may last several days, even then equilibrium may not be reached at all points [258]. Hence, it was suggested that the slight elevation could be attributed to the slight interaction between Ni(II) ions and TRIS.

5.4.1.3 Double Log Regression Model

Static fluorescence quenching involves the formation of non-fluorescent complex as a result of interactions between reactants [259]. The number of binding sites (n) and binding constant (K_A) of a static quenching process can be obtained from a regression curve deduced based on the quenching reaction as Equation 5 [260, 261].



Based on the quenching reaction, the binding/ association constant, K_A can be obtained as Equation 6.

$$K_A = \frac{[Q_nB]}{[Q]^n[B]} \quad \text{(Equation 6)}$$

where $[Q]$ depicted concentration of quencher which is the metal ions in this case, $[B]$ depicted concentration of the ligand of CDs₂₅₀/TRIS and $[Q_nB]$ depicted the concentration of non-fluorescent complex formed as a result of the reaction. The total concentration of ligand, $[B_o]$ can be expressed as Equation 7, where $[B]$ is the concentration of unbound molecules.

$$[B_o] = [Q_nB] + [B] \quad \text{(Equation 7)}$$

The fluorescence intensity is proportional to the concentration of the ligand which can be written as shown in Equation 8.

$$\frac{F_o}{F} = \frac{B_o}{B} \quad \text{(Equation 8)}$$

From the above equations, the equilibrium between free and bound molecules can be describes as Equation 9.

$$\log \frac{F_o - F}{F} = \log K_A + n \log [Q] \quad \text{(Equation 9)}$$

Where K_A and n can be derived from a plot of $\log(F_o - F)/ F$ versus $\log[Q]$ as shown in Figure 5.6.

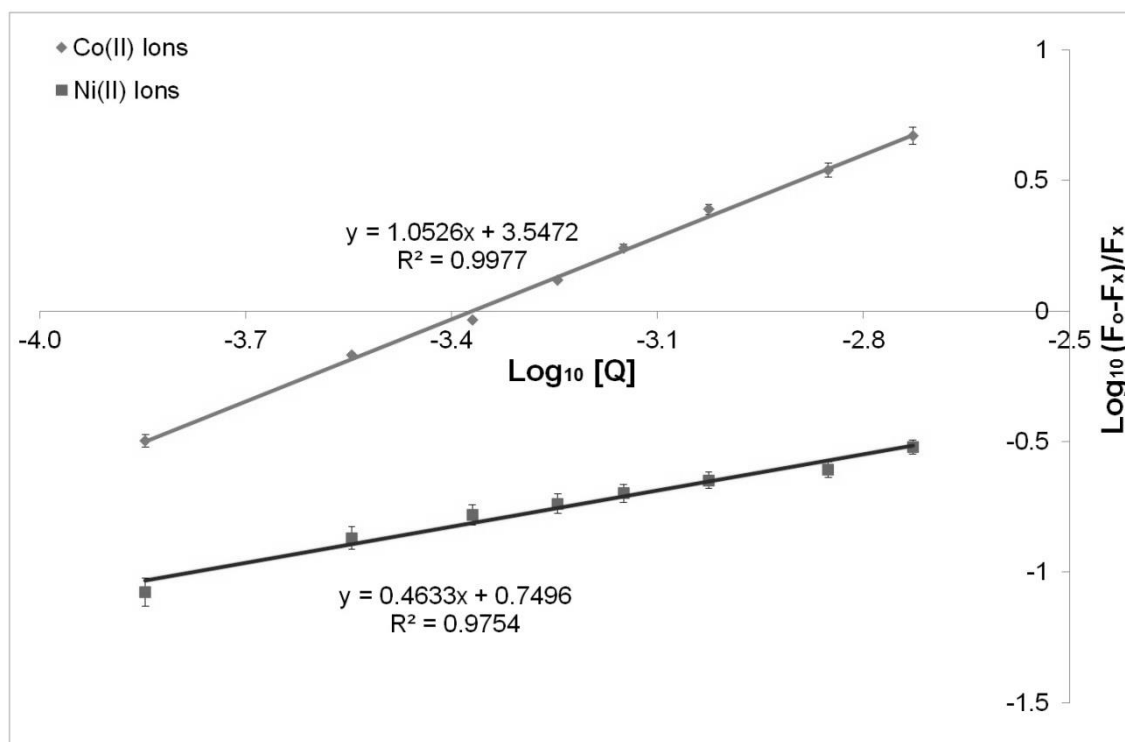


Figure 5.6: Plot of $\log_{10} (F_o - F_x) / F_x$ against $\log_{10} [Q]$.

The value of n for Co(II) ions was determined to be 1.0526 which is approximately equals to 1 indicated that there was only one kind of binding site present on the CDs₂₅₀/TRIS nanoparticles for the binding of Co(II) ions [262]. The K_A value for binding of Co(II) ions was calculated to be 3525.3 L/mol which was greater than that of Ni(II) ions which was found to be 2.9 L/mol. The binding affinity of CDs₂₅₀/TRIS to Co(II) ions was found to be much more stronger when compared to that of Ni(II) ions. Hence, the result evidenced that higher fluorescence quenching could be induced by stronger binding affinity between CDs₂₅₀/TRIS and Co(II) ions.

5.4.1.4 Modified Scatchard Method

Modified Scatchard method as described by Levine was also adopted to model the binding data in order to determine the K_A and n for the interaction of Co(II) and Ni(II) ions with CDs₂₅₀/TRIS system [263]. For the first binding site where $R = 1.0$, the maximal quenching of fluorescence, m_1 can be expressed as Equation 10 as follows.

$$m_1 = F_0 - F_1 \quad \text{(Equation 10)}$$

where F_0 is the initial fluorescence of metal ions in the absence of ligand and F_1 is the fluorescence intensity at metal ions/ ligand ratio of 1.0. Therefore, fractional quench, Q for an observed fluorescence, F can be written as Equation 11.

$$Q = \frac{F_0 - F}{m_1} = \frac{F_0 - F}{F_0 - F_1} \quad \text{(Equation 11)}$$

Since quenching is linearly related to binding, hence, Equation 12 is given as follows.

$$Q = \frac{[M^+]_B}{[L]_T} \quad \text{(Equation 12)}$$

where $[M^+]_B$ represents the concentration of metal ions bound by ligand and $[L]_T$ is the total ligand concentration. Following that, the concentration of free/unbound metal ions, $[M^+]_F$ can be expressed as Equation 13.

$$[M^+]_F = [M^+]_T - [M^+]_B = [M^+]_T - Q[L]_T \quad \text{(Equation 13)}$$

The concentration of free/ unbound ligand is written as Equation 14.

$$[L]_F = [L]_T - [M^+]_B = (1 - Q) [L]_T \quad \text{(Equation 14)}$$

By substituting Equation 12 – 14 into the association constant equation as described in Equation 6, the following Equation 15 and 16 could be obtained.

$$K_A = \frac{Q[L]_T}{(1 - Q)[L]_T([M^+]_T - Q[L]_T)} \quad \text{(Equation 15)}$$

$$K_A = \frac{Q}{(1-Q)([M^+]_T/L_T - Q)L_T} \quad \text{(Equation 16)}$$

Since the ratio, R can be written as Equation 17 as follows:

$$R = \frac{[M^+]_T}{L_T} \quad \text{(Equation 17)}$$

Thus, K_A can be re-expressed as Equation 18 as shown below.

$$K_A = \frac{Q}{(1-Q)(R-Q)L_T} \quad \text{(Equation 18)}$$

The above equation can then be transformed into Scatchard equation as described in Equation 19 below.

$$nK_A - K_A Q = \frac{Q}{[M^+]_F} = \frac{Q}{(R-Q)L_T} \quad \text{(Equation 19)}$$

The value of K_A and n can then be determined from a least square modified Scatchard plot of $Q/[M^+]_F$ versus Q . The slope of the modified Scatchard plot is equivalent to $-K_A$ while the X-intercept gives the value of n . The modified Scatchard plot obtained from the fluorescence quenching data of the $CDs_{250}/TRIS$ system in the presence of Co(II) and Ni(II) ions was shown in Figure 5.7.

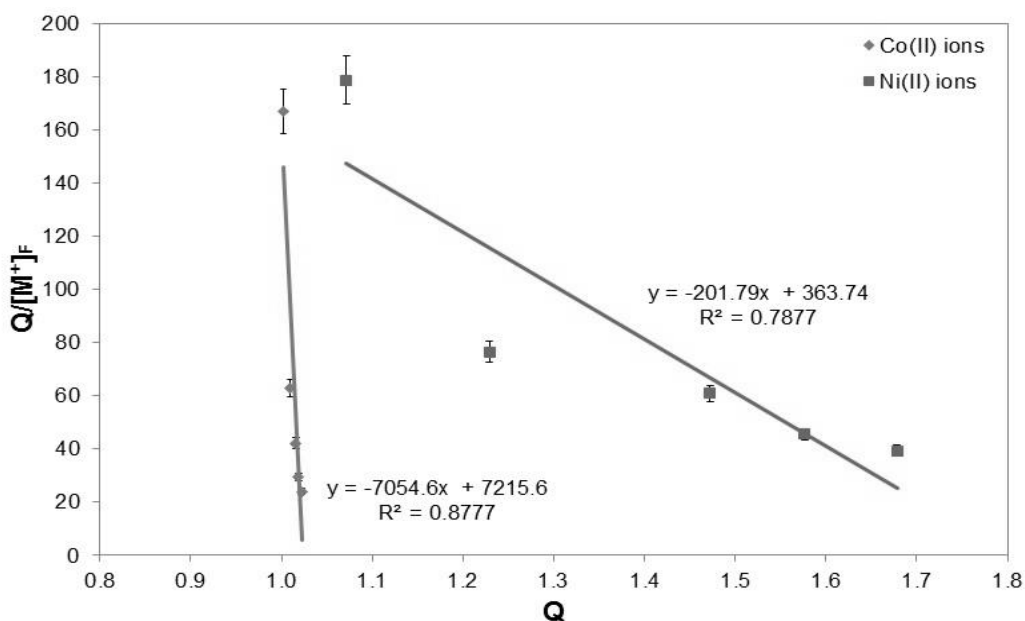


Figure 5.7: Modified Scatchard plot for the interaction of Co(II) and Ni(II) ions with $CDs_{250}/TRIS$ system.

The value of K_A for the interaction between $CDs_{250}/TRIS$ with $Co(II)$ ions determined from the slope of modified Scatchard plot as shown in Figure 5.7 was found to be 7054.6 L/mol whereas for that of $Ni(II)$ ions was determined to be 201.8 L/mol. This result further confirmed that at the same reaction conditions, the binding affinity of $CDs_{250}/TRIS$ to $Co(II)$ ions was stronger when compared to the interaction with $Ni(II)$ ions. The values of n for the binding of $CDs_{250}/TRIS$ to $Co(II)$ and $Ni(II)$ ions were found to be 1.0228 and 1.8026 respectively. The binding parameters determined using standard Stern-Volmer analysis, double log regression model and modified Scatchard method were summarized in Table 5.1.

Table 5.1: Quenching parameters for binding interaction between $CDs_{250}/TRIS$ with $Co(II)$ and $Ni(II)$ ions.

Analysis Model	Binding Parameters	Analyte	
		$Co(II)$ ions	$Ni(II)$ ions
Stern-Volmer	K_{SV} (mM)	2.5322	0.1346
	R^2	0.9983	0.8362
Double Log Regression	K_A ($\times 10^3$ L/mol)	3.5253	0.0029
	n	1.0526	0.4633
	R^2	0.9977	0.9754
Modified Scatchard	K_A ($\times 10^3$ L/mol)	7.0546	0.2018
	n	1.0228	1.8026
	R^2	0.8777	0.7877

From Table 5.1, the values of binding constant (K_A) for interaction of $CDs_{250}/TRIS$ with $Co(II)$ ions and $Ni(II)$ ions determined from the two different models, namely double log regression and modified Scatchard analysis were in good agreement. Both binding models shows that $CDs_{250}/TRIS$ exhibited stronger binding affinity towards $Co(II)$ ions when compared to $Ni(II)$ ions. Besides, the number of binding site (n) for $Co(II)$ ions determined from both double log regression and Scatchard method showed that n equals to approximately 1 indicated that there was only one binding site for $Co(II)$ ions in the $CDs_{250}/TRIS$ system. However, the n value for $Ni(II)$ ions determined from double log regression was found to be 0.4633 whereas the result obtained from

modified Scatchard showed that $n = 1.8026$. Coefficient of determination (R^2) can be defined as the percentage of variability in the dependent variable, which is commonly employed to analyse the fitting degree in linear regression analysis [264, 265]. Value of R^2 is usually ranging from 0 to 1 where high R^2 value corresponds to best fit in linear regression analysis [266]. Therefore, it was suggested that double log regression model could provide results with higher accuracy because the R^2 values for both Co(II) and Ni(II) ions were relatively high when compared to that of modified Scatchard analysis.

5.4.2 CDs Immobilization on Alginate Beads

Alginate is a biodegradable linear copolymer derived from marine algae. It is composed of D-mannuronic acid (M) and L-guluronic acid (G) [267]. The structures of D-mannuronic acid and L-guluronic acid are illustrated in Figure 5.8.

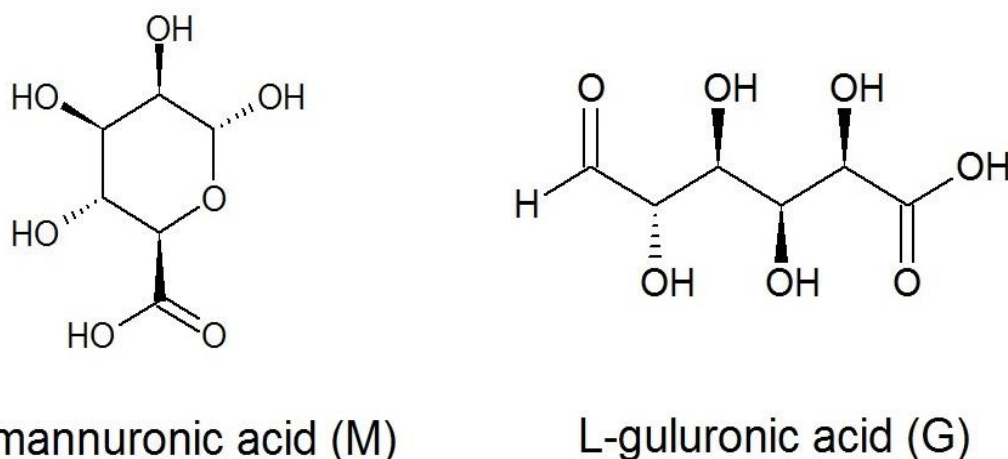


Figure 5.8: Chemical structures of D-mannuronic acid and L-guluronic acid.

Alginate is commonly used for entrapment of drugs and biological molecules due to its capability to crosslink in the presence of bivalent cations by ionotropic gelation [268]. In this study, attempt to encapsulate CDs₂₅₀ in alginate beads was carried out using calcium chloride as crosslinking solution. The steps of immobilization CDs₂₅₀ in alginate beads was illustrated in Figure 5.9.

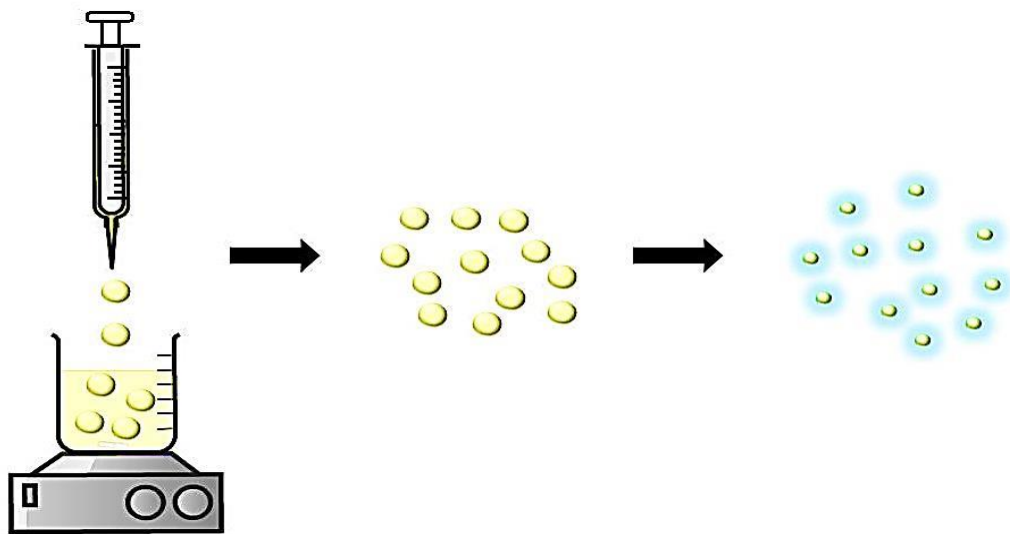


Figure 5.9: Schematic presentation of preparation of CDs₂₅₀ encapsulated alginate beads.

In a typical process, sodium alginate solution was heated to completely dissolve the sodium alginate powder. The sodium alginate suspension was left cool prior to the addition of CDs₂₅₀ solution to avoid excess heating that could possibly alter the properties of CDs₂₅₀. The CDs₂₅₀/sodium alginate solution was then dripped dropwise into the calcium chloride solution using a syringe needle. It was observed that alginate beads were formed immediately once the CDs₂₅₀/sodium alginate solution was dripped into the solution of calcium chloride. The alginate beads formed would initially stay on top of the solution and eventually sink as a result of increase in density, where this process is known as the maturation step [269]. The elasticity of alginate beads could be adjusted by constant stirring in the calcium chloride solution [270].

It was reported that crosslinking in the poly-G segments involved carboxyl and hydroxyl groups by primary valences and secondary valences, respectively [271]. The alginate beads formed were then collected and washed several times with ultrapure water and air dried. The size of the alginate beads were reduced after air dry in room conditions for few days. In order for comparison, plain alginate beads without the addition of CDs₂₅₀ were also produced using the same protocol by substituting the CDs₂₅₀ solution with ultrapure water. The photographs of air-dried plain alginate beads and CDs₂₅₀ encapsulated alginate beads were shown in Figure 5.10.

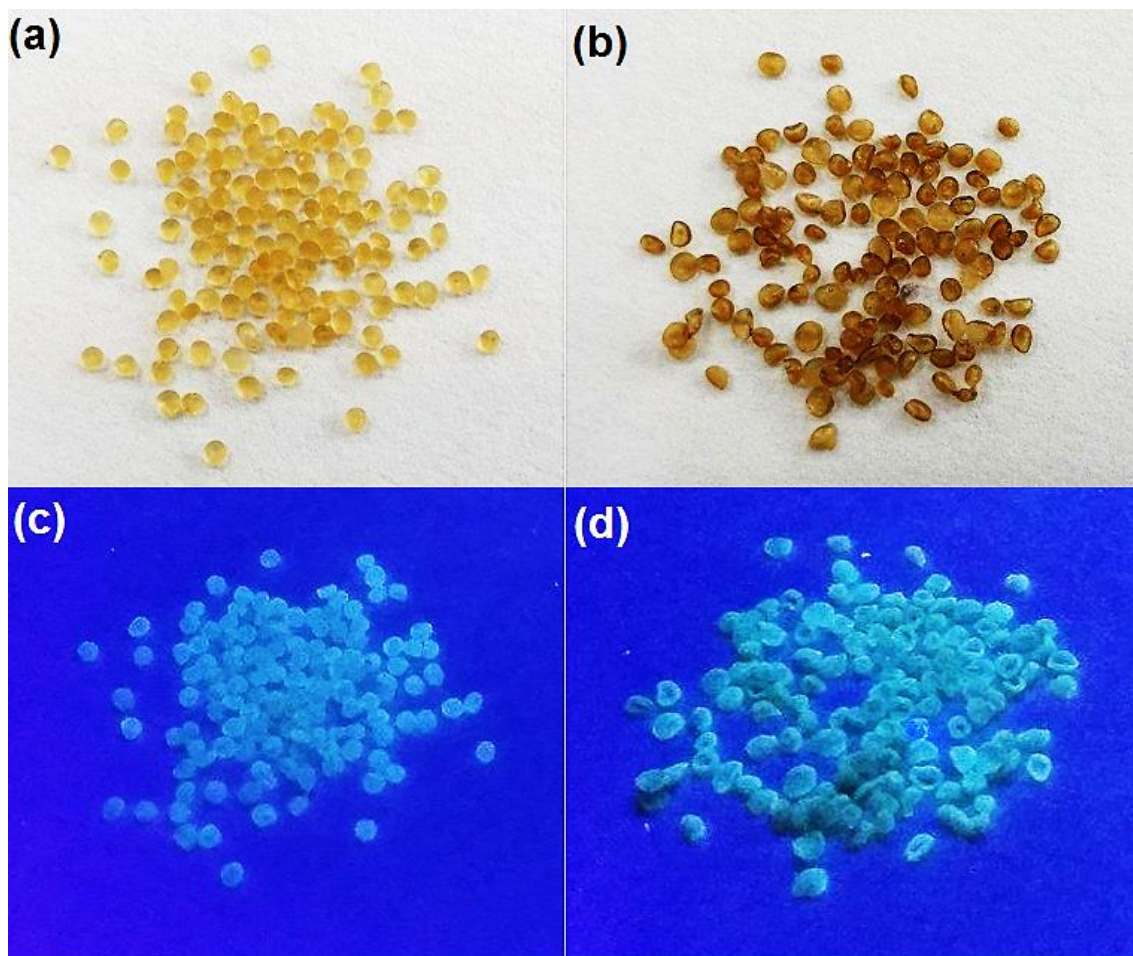


Figure 5.10: Photographs of air-dried (a) plain alginate beads and (b) CDs₂₅₀ encapsulated alginate beads under visible light; (c) plain alginate beads and (d) CDs₂₅₀ encapsulated alginate beads under UV exposure.

It was observed that under visible light, both plain and CDs₂₅₀ encapsulated alginate beads showed similar physical appearance with similar sizes and shapes. When exposed under UV, it was clearly seen that only CDs₂₅₀ encapsulated alginate beads displayed bright blue fluorescence but no fluorescence was observed for the plain alginate beads. The result shows that encapsulation of CDs₂₅₀ in alginate beads was successfully demonstrated and brings a step closer to the practical applications of CDs as fluorescence sensors.

5.5 Conclusions

CDs₂₅₀/TRIS was employed as study model to develop the binding isotherms with Co(II) ions using spectroscopic technique. Ni(II) ions was also introduced as a reference metal cations due to its inert response towards the CDs₂₅₀/TRIS system. Spectroscopic technique was employed to study the binding isotherms of the binding of CDs₂₅₀/TRIS to Co(II) and Ni(II) ions. The presence of isosbestic point in the absorption spectra indicated the formation of complexes as a result of interaction between CDs₂₅₀/TRIS with Co(II) ions. Mole ratio plot and Stern-Volmer plots that illustrated the quenching relationship were also included. In order to determine the binding parameters such as the binding constant and number of binding sites for the interaction between CDs₂₅₀/TRIS with Co(II) and Ni(II) ions, two models namely double log regression analysis and modified Scatchard method were employed. The binding constants for Co(II) ions obtained from both models were in good agreement. It was also realized that the double log regression had better linear fitting based on the R² value, hence it could serve as a better analysis method to model the binding isotherms in this study. The result evidenced that stronger binding affinity would induce greater change in signal in terms of fluorescence quenching. The binding isotherm that correlates the relationship between binding affinity and the change in optical signals of the CDs₂₅₀/TRIS system in the presence of Co(II) ions was established. Attempt in immobilization of CDs₂₅₀ in alginate beads was also demonstrated to be successful.

Chapter 6 Further Works and Conclusions

6.1 Executive Summary

The last chapter of the thesis provided a project summary to sum up the overall findings of the study. This chapter has also outlined several project limitations realized throughout the study. Suggestions on additional works that can be pursued further in order to address the project limitations are also identified.

6.2 Project Summary

In this study, different types of CDs with distinct physiochemical and optical properties namely, CDs_{Green} , CDs_{Blue} , CDs_{Glu} and CDs_{250} have been successfully synthesized from sustainable carbon sources. CDs_{Green} and CDs_{Blue} have been prepared from simple acid hydrolysis of α -cellulose; CDs_{Glu} have been obtained by thermal pyrolysis of L-glutamic acid whereas CDs_{250} have been synthesized from thermal pyrolysis of α -cellulose. Optimization of the synthesis conditions, characterizations and analytical potentials of the different types of CDs were investigated. The formation of both CDs_{Green} and CDs_{Blue} could be precisely altered by adjusting the synthesis conditions such as hydrolysis temperature and time. CDs_{Green} and CDs_{Blue} have also found applications for sensitive and selective sensing of Hg(II) and Fe(III), respectively.

Surface modification and interface study of the bare and functionalized CDs as well as their potential as metal ions sensing probes were identified. CDs_{Glu} have been isolated and surface modified with chitosan through physical adsorption. The chitosan-functionalized CDs_{Glu} (CDs_{Glu}/CS) have found to markedly enhance the sensitivity for Hg(III) detection when compared to the bare CDs_{Glu} . Besides, CDs_{250} functionalized with TRIS ($CDs_{250}/TRIS$) have found to be a potential sensing receptors where the fluorescence could be specifically quenched by Co(II) ions. This interesting result has encouraged further research into binding isotherms study that correlates the relationship between binding affinity and the change in optical signals. The binding isotherms correlation is successfully established using spectroscopic techniques adopting several standard binding models.

6.3 Project Limitations

Throughout the studies, several project limitations due to time constraints have been identified. At present, it still remains a challenge to isolate $\text{CDs}_{\text{Green}}$ synthesized via acid hydrolysis of α -cellulose. $\text{CDs}_{\text{Green}}$ was found to be highly sensitivity towards the change in surrounding pH. It was realized that the green fluorescence of $\text{CDs}_{\text{Green}}$ was quenched immediately after the surrounding pH that the CDs suspended in was adjusted to slightly higher pH (pH > 3). The property of $\text{CDs}_{\text{Green}}$ that was extremely sensitive towards change in pH was suggested to be attributed to the surface functional groups. Further studies are required in order to fully understand the properties of $\text{CDs}_{\text{Green}}$, then isolation of $\text{CDs}_{\text{Green}}$.

Besides, the analytical potentials of some of the assays developed based on CDs in this project were interrupted in the presence of interfering metal cations. For instance, $\text{CDs}_{\text{Glu}}/\text{CS}$ system was sensitive towards both Fe(III) and Hg(II) ions while the fluorescence of $\text{CDs}_{250}/\text{TRIS}$ system for Co(II) detection would also be quenched in the presence of Fe(III) ions. The specificity of the developed systems can be further improved so that more robust assays for rapid and sensitive detection of metal cations present in the environment can be developed.

In addition, immobilization of CDs is particularly important for development of devices such as fiber optics by utilizing CDs as sensing receptors. Although immobilization of CDs on solid support have been proposed and performed on alginate beads, detailed studies on the immobilization of CDs in alginate beads are not explored in this project due to time constraint. Therefore, it would be of great advantage to further explore on the aspect of CDs immobilization in order to actualize the utilization of CDs as sensitive sensing probes.

6.4 Further Works

In order to address the project limitations, some additional works that can be further performed are identified. Further characterization of CDs_{Green} such as determination of the elemental composition using X-ray photoelectron spectroscopy (XPS) will be useful to provide better understanding on the physiochemical properties of CDs and eventually made the isolation of CDs_{Green} possible. Study on masking the effect of interfering metal cations will also be beneficial to further develop present CDs system as sensitive probes for highly specific detection of targeted analytes.

Furthermore, binding isotherms study using the CDs₂₅₀/TRIS system can be further performed at different reaction temperatures. Besides, well-established standard binding isotherms models such as Langmuir, bi-Langmuir and Freundlich isotherms can be applied to further evaluate the binding parameters. Successful immobilization of CDs on solid support is highly desired in order to employ the aforementioned standard binding isotherms models. In this study, immobilization of CDs in alginate beads as solid support has been attempted. However, further characterizations on the pH, stability, coating yield, swelling and release study are yet to be performed.

References

- [1] X.Y. Xu, R. Ray, Y.L. Gu, H.J. Ploehn, L. Gearheart, K. Raker, W.A. Scrivens, Electrophoretic Analysis and Purification of Fluorescent Single-Walled Carbon Nanotube Fragments, *Journal of the American Chemical Society*, 126 (2004) 12736-12737.
- [2] H. Goncalves, P.A.S. Jorge, J.R.A. Fernandes, J.C.G. Esteves da Silva, Hg(II) sensing based on functionalized carbon dots obtained from direct laser ablation, *Sensors and Actuators B*, 145 (2010) 702-707.
- [3] H. Peng, J. Travas-Sejdic, Simple Aqueous Solution Route to Luminescent Carbogenic Dots from Carbohydrate, *Chemistry of Materials*, 21 (2009) 5563-5565.
- [4] D.Y. Pan, J.C. Zhang, Z. Li, M.H. Wu, Hydrothermal Route for Cutting Graphene Sheets into Blue-Luminescent Graphene Quantum Dots, *Advanced Materials*, 22 (2010) 734-738.
- [5] J.G. Zhou, C. Booker, R.Y. Li, X.T. Zhou, S.-K. Sham, X.L. Sun, Z.F. Ding, An Electrochemical Avenue to Blue Luminescent Nanocrystals from Multiwalled Carbon Nanotubes (MWCNTs) *Journal of the American Chemical Society*, 129 (2007) 744-745.
- [6] J. Zhou, Z. Sheng, H. Han, M. Zou, C. Li, Facile synthesis of fluorescent carbon dots using watermelon peel as a carbon source, *Materials Letters*, 66 (2012) 222-224.
- [7] X.W. Tan, A.N.B. Romainor, S.F. Chin, S.M. Ng, Carbon dots production via pyrolysis of sago waste as potential probe for metal ions sensing, *Journal of Analytical and Applied Pyrolysis*, 105 (2014) 157-165.
- [8] Z. Ma, H. Ming, H. Huang, Y. Liu, Z. Kang, One-step ultrasonic synthesis of fluorescent N-doped carbon dots from glucose and their visible-light sensitive photocatalytic ability, *New Journal of Chemistry*, 36 (2012) 861-864.
- [9] S.S. Wee, Y.H. Ng, S.M. Ng, Synthesis of fluorescent carbon dots via simple acid hydrolysis of bovine serum albumin and its potential as sensitive probe for lead (II) ions, *Talanta*, 116 (2013) 71-76.
- [10] Z. Yang, M. Xu, Y. Liu, F. He, F. Gao, Y. Su, H. Wei, Y. Zhang, Nitrogen-doped, carbon-rich, highly photoluminescent carbon dots from ammonium citrate, *Nanoscale*, 6 (2014) 1890-1895.

- [11] D. Chowdhury, N. Gogoi, G. Majumdar, Fluorescent carbon dots obtained from chitosan gel, *RSC Advances*, 2 (2012) 12156-12159.
- [12] K. Jiang, S. Sun, L. Zhang, Y. Lu, A.G. Wu, C.Z. Cai, H.W. Lin, Red, Green, and Blue Luminescence by Carbon Dots: Full-Color Emission Tuning and Multicolor Cellular Imaging, *Angewandte Chemie International Edition*, 54 (2015) 5360-5363.
- [13] X. Wang, K. Qu, B. Xu, J. Ren, X. Qu, Microwave assisted one-step green synthesis of cell-permeable multicolor photoluminescent carbon dots without surface passivation reagents, *Journal of Materials Chemistry*, 21 (2011) 2445-2450.
- [14] S.N. Baker, G.A. Baker, Luminescent Carbon Nanodots: Emergent Nanolights, *Angewandte Chemie International Edition*, 49 (2010) 6726-6744.
- [15] S.J. Zhu, Y.B. Song, X.H. Zhao, J.R. Shao, J.H. Zhang, B. Yang, The photoluminescence mechanism in carbon dots (graphene dots, carbon nanodots and polymer dots): current state and future perspective, *Nano Research*, (2014).
- [16] R. Chaney, The Heavy Elements: Chemistry, Environmental Impact, and Health Effects, *Journal of Environmental Quality*, 20 (1991) 876-876.
- [17] H. Bradl, Heavy metals in the environment: origin, interaction and remediation: origin, interaction and remediation, Academic Press 2005.
- [18] Z.L. He, X.E. Yang, P.J. Stoffella, Trace elements in agroecosystems and impacts on the environment, *Journal of Trace Elements in Medicine and Biology*, 19 (2005) 125-140.
- [19] J.O. Nriagu, A global assessment of natural sources of atmospheric trace metals, *Nature*, 338 (1989) 47-49.
- [20] A. Arruti, I. Fernández-Olmo, Á. Irabien, Evaluation of the contribution of local sources to trace metals levels in urban PM_{2.5} and PM₁₀ in the Cantabria region (Northern Spain), *Journal of Environmental Monitoring*, 12 (2010) 1451-1458.
- [21] E. Sträter, A. Westbeld, O. Klemm, Pollution in coastal fog at Alto Patache, Northern Chile, *Environmental Science and Pollution Research*, 17 (2010) 1563-1573.

- [22] J. Pacyna, Monitoring and assessment of metal contaminants in the air, Toxicology of metals. CRC, Boca Raton, FL, (1996) 9-28.
- [23] S.Y. Lim, W. Shen, Z. Gao, Carbon quantum dots and their applications, Chemical Society Reviews, 44 (2015) 362-381.
- [24] D. Rendell, D.J. Mowthorpe, Fluorescence and phosphorescence spectroscopy, Published on behalf of ACOL, London by Wiley1987.
- [25] An introduction to fluorescence spectroscopy, PerkinElmer, United Kingdom, 2000, pp. 1-36.
- [26] J.R. Lakowicz, Principles of fluorescence spectroscopy, Springer Science & Business Media2013.
- [27] G.G. Shepherd, Spectral imaging of the atmosphere, Academic press2002.
- [28] I. Weeks, G. Svehla, Chemiluminescence Immunoassay Wilson and Wilson's Comprehensive Analytical Chemistry, Elsevier, Amsterdam, 1992.
- [29] C. Dodeigne, L. Thunus, R. Lejeune, Chemiluminescence as diagnostic tool. A review, Talanta, 51 (2000) 415-439.
- [30] W. Baeyens, S. Schulman, A. Calokerinos, Y. Zhao, A.M.G. Campana, K. Nakashima, D. De Keukeleire, Chemiluminescence-based detection: principles and analytical applications in flowing streams and in immunoassays, Journal of pharmaceutical and biomedical analysis, 17 (1998) 941-953.
- [31] M.M. Richter, Electrochemiluminescence (ecl), Chemical Reviews, 104 (2004) 3003-3036.
- [32] B. Mathew, R. Biju, N. Thapalia, An overview of electrochemiluminescent (ECL) technology in laboratory investigations, Kathmandu University medical journal (KUMJ), 3 (2004) 91-93.
- 33 R.D. Gerardi, N.W. Barnett, S.W. Lewis, Analytical applications of tris (2, 2'-bipyridyl) ruthenium (III) as a chemiluminescent reagent, Analytica Chimica Acta, 378 (1999) 1-41.
- [34] J.H. Kenten, Electrochemiluminescence: Ruthenium Complexes, Nonradioactive Analysis of Biomolecules, Springer2000, pp. 271-275.
- [35] H.-H. Perkampus, H.-C. Grinter, T. Threlfall, UV-VIS Spectroscopy and its Applications, Springer1992.
- [36] H.H. Jaffé, M. Orchin, Theory and applications of ultraviolet spectroscopy, (1962).

- [37] G. Gauglitz, Ultraviolet and visible spectroscopy, Ullmann's Encyclopedia of Industrial Chemistry, (1994).
- [38] M.J.K. Thomas, Ultraviolet and Visible Spectroscopy: Analytical Chemistry by Open Learning, John Wiley & Sons, United Kingdom, 1996.
- [39] D.A. Skoog, D.M. West, Principles of instrumental analysis, Saunders College Philadelphia 1980.
- [40] J. Barkauskas, Biological applications of functionalized carbon nanoparticles, Surface Chemistry in Biomedical and Environmental Science, Springer 2006, pp. 265-276.
- [41] X.T. Zheng, A. Ananthanarayanan, K.Q. Luo, P. Chen, Glowing Graphene Quantum Dots and Carbon Dots: Properties, Syntheses, and Biological Applications, *Small*, 11 (2015) 1620-1636.
- [42] H. Liu, T. Ye, C. Mao, Fluorescent carbon nanoparticles derived from candle soot, *Angewandte Chemie International Edition*, 46 (2007) 6473-6475.
- [43] S.F. Chin, S.N.A. Mohd Yazid, S.C. Pang, S.M. Ng, Facile synthesis of fluorescent carbon nanodots from starch nanoparticles, *Materials Letters*, 85 (2012) 50-52.
- [44] J. Peng, W. Gao, B.K. Gupta, Z. Liu, R. Romero-Aburto, L. Ge, L. Song, L.B. Alemany, X. Zhan, G. Gao, Graphene quantum dots derived from carbon fibers, *Nano letters*, 12 (2012) 844-849.
- [45] Z.-A. Qiao, Y. Wang, Y. Gao, H. Li, T. Dai, Y. Liu, Q. Huo, Commercially activated carbon as the source for producing multicolor photoluminescent carbon dots by chemical oxidation, *Chemical Communications*, 46 (2010) 8812-8814.
- [46] Z. Li, W. Zhang, Y. Luo, J. Yang, J.G. Hou, How graphene is cut upon oxidation?, *Journal of the American Chemical Society*, 131 (2009) 6320-6321.
- [47] D. Pan, J. Zhang, Z. Li, M. Wu, Hydrothermal route for cutting graphene sheets into blue-luminescent graphene quantum dots, *Advanced Materials*, 22 (2010) 734-738.
- [48] D. Pan, L. Guo, J. Zhang, C. Xi, Q. Xue, H. Huang, J. Li, Z. Zhang, W. Yu, Z. Chen, Cutting sp² clusters in graphene sheets into colloidal graphene quantum dots with strong green fluorescence, *Journal of Materials Chemistry*, 22 (2012) 3314-3318.

- [49] S. Zhu, J. Zhang, C. Qiao, S. Tang, Y. Li, W. Yuan, B. Li, L. Tian, F. Liu, R. Hu, Strongly green-photoluminescent graphene quantum dots for bioimaging applications, *Chem. Commun.*, 47 (2011) 6858-6860.
- [50] J. Lu, J.-x. Yang, J. Wang, A. Lim, S. Wang, K.P. Loh, One-pot synthesis of fluorescent carbon nanoribbons, nanoparticles, and graphene by the exfoliation of graphite in ionic liquids, *ACS nano*, 3 (2009) 2367-2375.
- [51] Y. Li, Y. Hu, Y. Zhao, G. Shi, L. Deng, Y. Hou, L. Qu, An electrochemical avenue to green-luminescent graphene quantum dots as potential electron-acceptors for photovoltaics, *Advanced Materials*, 23 (2011) 776-780.
- [52] A. Ananthanarayanan, X. Wang, P. Routh, B. Sana, S. Lim, D.H. Kim, K.H. Lim, J. Li, P. Chen, Facile synthesis of graphene quantum dots from 3D graphene and their application for Fe³⁺ sensing, *Advanced Functional Materials*, 24 (2014) 3021-3026.
- [53] Y. Liu, N. Xiao, N. Gong, H. Wang, X. Shi, W. Gu, L. Ye, One-step microwave-assisted polyol synthesis of green luminescent carbon dots as optical nanoprobe, *Carbon*, 68 (2014) 258-264.
- [54] S. Mitra, S. Chandra, T. Kundu, R. Banerjee, P. Pramanik, A. Goswami, Rapid microwave synthesis of fluorescent hydrophobic carbon dots, *RSC Advances*, 2 (2012) 12129-12131.
- 55 R. Liu, D. Wu, . Feng, K. M Ilen, Bottom-up fabrication of photoluminescent graphene quantum dots with uniform morphology, *Journal of the American Chemical Society*, 133 (2011) 15221-15223.
- [56] Y. Dong, J. Shao, C. Chen, H. Li, R. Wang, Y. Chi, X. Lin, G. Chen, Blue luminescent graphene quantum dots and graphene oxide prepared by tuning the carbonization degree of citric acid, *Carbon*, 50 (2012) 4738-4743.
- [57] X. Yan, X. Cui, B. Li, L.-s. Li, Large, solution-processable graphene quantum dots as light absorbers for photovoltaics, *Nano letters*, 10 (2010) 1869-1873.
- [58] X. Yan, X. Cui, L.-s. Li, Synthesis of large, stable colloidal graphene quantum dots with tunable size, *Journal of the American Chemical Society*, 132 (2010) 5944-5945.

- [59] Z. Wang, Y. Qu, X. Gao, C. Mu, J. Bai, Q. Pu, Facile preparation of oligo (ethylene glycol)-capped fluorescent carbon dots from glutamic acid for plant cell imaging, *Materials Letters*, 129 (2014) 122-125.
- [60] X. Jia, J. Li, E. Wang, One-pot green synthesis of optically pH-sensitive carbon dots with upconversion luminescence, *Nanoscale*, 4 (2012) 5572-5575.
- [61] C.W. Lai, Y.H. Hsiao, Y.K. Peng, P.t. Chou, Facile synthesis of highly emissive carbon dots from pyrolysis of glycerol; gram scale production of carbon dots/mSiO₂ for cell imaging and drug release, *Journal of Materials Chemistry*, 22 (2012) 14403-14409.
- [62] L. Tang, R. Ji, X. Cao, J. Lin, H. Jiang, X. Li, K.S. Teng, C.M. Luk, S. Zeng, J. Hao, Deep ultraviolet photoluminescence of water-soluble self-passivated graphene quantum dots, *ACS nano*, 6 (2012) 5102-5110.
- [63] J. Wang, C.F. Wang, S. Chen, Amphiphilic Egg-Derived Carbon Dots: Rapid Plasma Fabrication, Pyrolysis Process, and Multicolor Printing Patterns, *Angewandte Chemie*, 124 (2012) 9431-9435.
- [64] J. Lu, P.S.E. Yeo, C.K. Gan, P. Wu, K.P. Loh, Transforming C60 molecules into graphene quantum dots, *Nature nanotechnology*, 6 (2011) 247-252.
- [65] M. Baker, Nanotechnology imaging probes: smaller and more stable, *Nature Methods*, 7 (2010) 957.
- [66] S. Ray, A. Saha, N.R. Jana, R. Sarkar, Fluorescent carbon nanoparticles: synthesis, characterization, and bioimaging application, *The Journal of Physical Chemistry C*, 113 (2009) 18546-18551.
- [67] Y. Song, S. Zhu, B. Yang, Bioimaging based on fluorescent carbon dots, *RSC Advances*, 4 (2014) 27184-27200.
- [68] Q. Wang, H. Zheng, Y. Long, L. Zhang, M. Gao, W. Bai, Microwave-hydrothermal synthesis of fluorescent carbon dots from graphite oxide, *Carbon*, 49 (2011) 3134-3140.
- [69] H. Yu, H. Zhang, H. Huang, Y. Liu, H. Li, H. Ming, Z. Kang, ZnO/carbon quantum dots nanocomposites: one-step fabrication and superior photocatalytic ability for toxic gas degradation under visible light at room temperature, *New Journal of Chemistry*, 36 (2012) 1031-1035.

- [70] S.-L. Hu, K.-Y. Niu, J. Sun, J. Yang, N.-Q. Zhao, X.-W. Du, One-step synthesis of fluorescent carbon nanoparticles by laser irradiation, *Journal of Materials Chemistry*, 19 (2009) 484-488.
- [71] G. Eda, Y.Y. Lin, C. Mattevi, H. Yamaguchi, H.A. Chen, I. Chen, C.W. Chen, M. Chhowalla, Blue photoluminescence from chemically derived graphene oxide, *Advanced Materials*, 22 (2010) 505-509.
- [72] F. Yang, M. Zhao, B. Zheng, D. Xiao, L. Wu, Y. Guo, Influence of pH on the fluorescence properties of graphene quantum dots using ozonation pre-oxide hydrothermal synthesis, *Journal of Materials Chemistry*, 22 (2012) 25471-25479.
- [73] H. Zhu, X. Wang, Y. Li, Z. Wang, F. Yang, X. Yang, Microwave synthesis of fluorescent carbon nanoparticles with electrochemiluminescence properties, *Chemical Communications*, (2009) 5118-5120.
- [74] J. Zhou, C. Booker, R. Li, X. Zhou, T.-K. Sham, X. Sun, Z. Ding, An electrochemical avenue to blue luminescent nanocrystals from multiwalled carbon nanotubes (MWCNTs), *Journal of the American Chemical Society*, 129 (2007) 744-745.
- [75] Y.-P. Sun, B. Zhou, Y. Lin, W. Wang, K.S. Fernando, P. Pathak, M.J. Meziani, B.A. Harruff, X. Wang, H. Wang, Quantum-sized carbon dots for bright and colorful photoluminescence, *Journal of the American Chemical Society*, 128 (2006) 7756-7757.
- [76] D. Sun, R. Ban, P.H. Zhang, G.H. Wu, J.R. Zhang, J.J. Zhu, Hair fiber as a precursor for synthesizing of sulfur- and nitrogen-co-doped carbon dots with tunable luminescence properties, *Carbon*, 64 (2013) 424-434.
- [77] J.P. Paraknowitsch, Y. Zhang, B. Wienert, A. Thomas, Nitrogen-and phosphorus-co-doped carbons with tunable enhanced surface areas promoted by the doping additives, *Chemical Communications*, 49 (2013) 1208-1210.
- [78] D. Pan, J. Zhang, Z. Li, C. Wu, X. Yan, M. Wu, Observation of pH-, solvent-, spin-, and excitation-dependent blue photoluminescence from carbon nanoparticles, *Chemical Communications*, 46 (2010) 3681-3683.
- [79] M. Xue, Z. Zhan, M. Zou, L. Zhang, S. Zhao, Green synthesis of stable and biocompatible fluorescent carbon dots from peanut shells for multicolor living cell imaging, *New Journal of Chemistry*, (2016).

- [80] L. Cao, X. Wang, M.J. Meziari, F.S. Lu, H.F. Wang, P.G. Luo, Y. Lin, B.A. Harruff, L.M. Veca, D. Murray, S.Y. Xie, Y.P. Sun, Carbon Dots for Multiphoton Bioimaging, *Journal of the American Chemical Society*, 129 (2007) 11318-11319.
- [81] H.T. Li, X.D. He, Z.H. Kang, H. Huang, Y. Liu, J.L. Liu, S.Y. Lian, C.H.A. Tsang, X.B. Yang, S.-T. Lee, Water-Soluble Fluorescent Carbon Quantum Dots and Photocatalyst Design, *Angewandte Chemie International Edition*, 49 (2010) 4430-4434.
- [82] J. Shen, Y. Zhu, C. Chen, X. Yang, C. Li, Facile preparation and upconversion luminescence of graphene quantum dots, *Chem. Commun.*, 47 (2011) 2580-2582.
- [83] A. Salinas-Castillo, M. Ariza-Avidad, C. Pritz, M. Camprubí-Robles, B. Fernández, M.J. Ruedas-Rama, A. Megia-Fernández, A. Lapresta-Fernández, F. Santoyo-Gonzalez, A. Schrott-Fischer, Carbon dots for copper detection with down and upconversion fluorescent properties as excitation sources, *Chemical Communications*, 49 (2013) 1103-1105.
- [84] X. Wen, P. Yu, Y.-R. Toh, X. Ma, J. Tang, On the upconversion fluorescence in carbon nanodots and graphene quantum dots, *Chemical Communications*, 50 (2014) 4703-4706.
- [85] C. Frigerio, D.S. Ribeiro, S.S.M. Rodrigues, V.L. Abreu, J.A. Barbosa, J.A. Prior, K.L. Marques, J.L. Santos, Application of quantum dots as analytical tools in automated chemical analysis: a review, *Analytica chimica acta*, 735 (2012) 9-22.
- [86] L. Zheng, Y. Chi, Y. Dong, J. Lin, B. Wang, Electrochemiluminescence of water-soluble carbon nanocrystals released electrochemically from graphite, *Journal of the American Chemical Society*, 131 (2009) 4564-4565.
- [87] L.L. Li, J. Ji, R. Fei, C.Z. Wang, Q. Lu, J.R. Zhang, L.P. Jiang, J.J. Zhu, A Facile Microwave Avenue to Electrochemiluminescent Two-Color Graphene Quantum Dots, *Advanced Functional Materials*, 22 (2012) 2971-2979.
- [88] C. Xiong, W. Liang, H. Wang, Y. Zheng, Y. Zhuo, Y. Chai, R. Yuan, In situ electro-polymerization of nitrogen doped carbon dots and their application in an electrochemiluminescence biosensor for the detection of intracellular lead ions, *Chemical Communications*, 52 (2016) 5589-5592.

- [89] L.R. Radovic, B. Bockrath, On the chemical nature of graphene edges: origin of stability and potential for magnetism in carbon materials, *Journal of the American Chemical Society*, 127 (2005) 5917-5927.
- [90] S. Kim, S.W. Hwang, M.-K. Kim, D.Y. Shin, D.H. Shin, C.O. Kim, S.B. Yang, J.H. Park, E. Hwang, S.-H. Choi, Anomalous behaviors of visible luminescence from graphene quantum dots: interplay between size and shape, *ACS nano*, 6 (2012) 8203-8208.
- [91] L.L. Li, G.H. Wu, G.H. Yang, J. Peng, J.W. Zhao, J.J. Zhu, Focusing on luminescent graphene quantum dots: current status and future perspectives, *Nanoscale*, 5 (2013) 4015-4039.
- [92] J.C.G. Esteves da Silva, H. Goncalves, Analytical and bioanalytical applications of carbon dots', *Trends in Analytical Chemistry*, *Trends in Analytical Chemistry*, 30 (2011) 1327-1336.
- [93] Q. Xu, Q. Zhou, Z. Hua, Q. Xue, C. Zhang, X. Wang, D. Pan, M. Xiao, Single-particle spectroscopic measurements of fluorescent graphene quantum dots, *ACS nano*, 7 (2013) 10654-10661.
- [94] M. Zhang, L. Bai, W. Shang, W. Xie, H. Ma, Y. Fu, D. Fang, H. Sun, L. Fan, M. Han, Facile synthesis of water-soluble, highly fluorescent graphene quantum dots as a robust biological label for stem cells, *Journal of materials chemistry*, 22 (2012) 7461-7467.
- [95] A.M. Smith, S. Nie, Semiconductor nanocrystals: structure, properties, and band gap engineering, *Accounts of chemical research*, 43 (2009) 190-200.
- [96] A.B. Bourlinos, A. Stassinopoulos, D. Anglos, R. Zboril, M. Karakassides, E.P. Giannelis, Surface Functionalized Carbogenic Quantum Dots, *Small*, 4 (2008) 455-458.
- [97] M.J. Krysmann, A. Kelarakis, P. Dallas, E.P. Giannelis, Formation mechanism of carbogenic nanoparticles with dual photoluminescence emission, *Journal of the American Chemical Society*, 134 (2011) 747-750.
- [98] S. Zhu, L. Wang, N. Zhou, X. Zhao, Y. Song, S. Maharjan, J. Zhang, L. Lu, H. Wang, B. Yang, The crosslink enhanced emission (CEE) in non-conjugated polymer dots: from the photoluminescence mechanism to the cellular uptake mechanism and internalization, *Chemical Communications*, 50 (2014) 13845-13848.

- [99] S.E. Braslavsky, Glossary of terms used in photochemistry, (IUPAC Recommendations 2006), *Pure and Applied Chemistry*, 79 (2007) 293-465.
- [100] A.T.R. Williams, S.A. Winfield, J.N. Miller, Relative fluorescence quantum yields using a computer-controlled luminescence spectrometer, *Analyst*, 108 (1983) 1067-1071.
- [101] A.M. Brouwer, Standards for photoluminescence quantum yield measurements in solution (IUPAC Technical Report), *Pure and Applied Chemistry*, 83 (2011) 2213-2228.
- [102] X. Zhai, P. Zhang, C. Liu, T. Bai, W. Li, L. Dai, W. Liu, Highly luminescent carbon nanodots by microwave-assisted pyrolysis, *Chem. Commun.*, 48 (2012) 7955-7957.
- [103] Y.Q. Dong, H.C. Pang, H.B. Yang, C.X. Guo, J.W. Shao, Y.W. Chi, C.M. Li, T. Yu, Carbon-Based Dots Co-doped with Nitrogen and Sulfur for High Quantum Yield and Excitation-Independent Emission, *Angewandte Chemie International Edition*, 52 (2013) 7800-7804.
- [104] H. Ding, J.-S. Wei, H.-M. Xiong, Nitrogen and sulfur co-doped carbon dots with strong blue luminescence, *Nanoscale*, 6 (2014) 13817-13823.
- [105] D. Qu, M. Zheng, L. Zhang, H. Zhao, Z. Xie, X. Jing, R.E. Haddad, H. Fan, Z. Sun, Formation mechanism and optimization of highly luminescent N-doped graphene quantum dots, *Scientific reports*, 4 (2014).
- [106] S.J. Zhu, J.H. Zhang, S.J. Tang, C.Y. Qiao, L. Wang, H.Y. Wang, X. Liu, Y.F. Li, W.L. Yu, X.F. Wang, H.C. Sun, B. Yang, Surface Chemistry Routes to Modulate the Photoluminescence of Graphene Quantum Dots: From Fluorescence Mechanism to Up-Conversion Bioimaging Applications, *Advanced Functional Materials*, 22 (2012) 4732-4740.
- [107] H. Tetsuka, R. Asahi, A. Nagoya, K. Okamoto, I. Tajima, R. Ohta, A. Okamoto, Optically Tunable Amino-Functionalized Graphene Quantum Dots, *Advanced Materials*, 24 (2012) 5333-5338.
- [108] K.P. Loh, Q. Bao, G. Eda, M. Chhowalla, Graphene oxide as a chemically tunable platform for optical applications, *Nature chemistry*, 2 (2010) 1015-1024.
- [109] S. Zhu, J. Zhang, X. Liu, B. Li, X. Wang, S. Tang, Q. Meng, Y. Li, C. Shi, R. Hu, Graphene quantum dots with controllable surface oxidation, tunable fluorescence and up-conversion emission, *Rsc Advances*, 2 (2012) 2717-2720.

- [110] J. Shen, Y. Zhu, X. Yang, J. Zong, J. Zhang, C. Li, One-pot hydrothermal synthesis of graphene quantum dots surface-passivated by polyethylene glycol and their photoelectric conversion under near-infrared light, *New Journal of Chemistry*, 36 (2012) 97-101.
- [111] X. Wang, L. Cao, S.T. Yang, F. Lu, M.J. Mezziani, L. Tian, K.W. Sun, M.A. Bloodgood, Y.P. Sun, Bandgap-Like strong fluorescence in functionalized carbon nanoparticles, *Angewandte Chemie*, 122 (2010) 5438-5442.
- [112] P. Anilkumar, L. Cao, J.J. Yu, K.N. Tackett, P. Wang, M.J. Mezziani, Y.P. Sun, Crosslinked Carbon Dots as Ultra-Bright Fluorescence Probes, *Small*, 9 (2013) 545-551.
- [113] P. Anilkumar, X. Wang, L. Cao, S. Sahu, J.-H. Liu, P. Wang, K. Korch, K.N. Tackett II, A. Parenzan, Y.-P. Sun, Toward quantitatively fluorescent carbon-based “quantum” dots, *Nanoscale*, 3 (2011) 2023-2027.
- [114] Z.L. Wu, P. Zhang, M.X. Gao, C.F. Liu, W. Wang, F. Leng, C.Z. Huang, One-pot hydrothermal synthesis of highly luminescent nitrogen-doped amphoteric carbon dots for bioimaging from *Bombyx mori* silk–natural proteins, *Journal of Materials Chemistry B*, 1 (2013) 2868-2873.
- [115] W. Li, Z. Zhang, B. Kong, S. Feng, J. Wang, L. Wang, J. Yang, F. Zhang, P. Wu, D. Zhao, Simple and Green Synthesis of Nitrogen-Doped Photoluminescent Carbonaceous Nanospheres for Bioimaging, *Angewandte Chemie International Edition*, 52 (2013) 8151-8155.
- [116] Y. Xu, M. Wu, Y. Liu, X.Z. Feng, X.B. Yin, X.W. He, Y.K. Zhang, Nitrogen-Doped Carbon Dots: A Facile and General Preparation Method, Photoluminescence Investigation, and Imaging Applications, *Chemistry–A European Journal*, 19 (2013) 2276-2283.
- [117] W. Shang, X. Zhang, M. Zhang, Z. Fan, Y. Sun, M. Han, L. Fan, The uptake mechanism and biocompatibility of graphene quantum dots with human neural stem cells, *Nanoscale*, 6 (2014) 5799-5806.
- [118] V. Kumar, V. Singh, S. Umrao, V. Parashar, S. Abraham, A.K. Singh, G. Nath, P.S. Saxena, A. Srivastava, Facile, rapid and upscaled synthesis of green luminescent functional graphene quantum dots for bioimaging, *Rsc Advances*, 4 (2014) 21101-21107.

- [119] X.T. Zheng, A. Than, A. Ananthanaraya, D.-H. Kim, P. Chen, Graphene quantum dots as universal fluorophores and their use in revealing regulated trafficking of insulin receptors in adipocytes, *Acs Nano*, 7 (2013) 6278-6286.
- [120] S.-T. Yang, L. Cao, P.G. Luo, F. Lu, X. Wang, H. Wang, M.J. Mezirani, Y. Liu, G. Qi, Y.-P. Sun, Carbon dots for optical imaging in vivo, *Journal of the American Chemical Society*, 131 (2009) 11308-11309.
- [121] H. He, X. Wang, Z. Feng, T. Cheng, X. Sun, Y. Sun, Y. Xia, S. Wang, J. Wang, X. Zhang, Rapid microwave-assisted synthesis of ultra-bright fluorescent carbon dots for live cell staining, cell-specific targeting and in vivo imaging, *Journal of Materials Chemistry B*, 3 (2015) 4786-4789.
- [122] C. Jiang, H. Wu, X. Song, X. Ma, J. Wang, M. Tan, Presence of photoluminescent carbon dots in Nescafe® original instant coffee: Applications to bioimaging, *Talanta*, 127 (2014) 68-74.
- [123] M. Yuan, R. Zhong, H. Gao, W. Li, X. Yun, J. Liu, X. Zhao, G. Zhao, F. Zhang, One-step, green, and economic synthesis of water-soluble photoluminescent carbon dots by hydrothermal treatment of wheat straw, and their bio-applications in labeling, imaging, and sensing, *Applied Surface Science*, 355 (2015) 1136-1144.
- [124] M. Ghosh, S.K. Sonkar, M. Saxena, S. Sarkar, Carbon Nano-onions for Imaging the Life Cycle of *Drosophila Melanogaster*, *Small*, 7 (2011) 3170-3177.
- [125] T.K. Mandal, N. Parvin, Rapid detection of bacteria by carbon quantum dots, *Journal of biomedical nanotechnology*, 7 (2011) 846-848.
- [126] V.N. Mehta, S. Jha, S.K. Kailasa, One-pot green synthesis of carbon dots by using *Saccharum officinarum* juice for fluorescent imaging of bacteria (*Escherichia coli*) and yeast (*Saccharomyces cerevisiae*) cells, *Materials Science and Engineering: C*, 38 (2014) 20-27.
- [127] X. Jin, X. Sun, G. Chen, L. Ding, Y. Li, Z. Liu, Z. Wang, W. Pan, C. Hu, J. Wang, pH-sensitive carbon dots for the visualization of regulation of intracellular pH inside living pathogenic fungal cells, *Carbon*, 81 (2015) 388-395.
- [128] R.P. Baum, H.R. Kulkarni, Theranostics: from molecular imaging using Ga-68 labeled tracers and PET/CT to personalized radionuclide therapy-the Bad Berka experience, *Theranostics*, 2 (2012) 437-447.

- [129] L. Yang, Z. Wang, J. Wang, W. Jiang, X. Jiang, Z. Bai, Y. He, J. Jiang, D. Wang, L. Yang, Doxorubicin conjugated functionalizable carbon dots for nucleus targeted delivery and enhanced therapeutic efficacy, *Nanoscale*, 8 (2016) 6801-6809.
- [130] C.-W. Lai, Y.-H. Hsiao, Y.-K. Peng, P.-T. Chou, Facile synthesis of highly emissive carbon dots from pyrolysis of glycerol; gram scale production of carbon dots/mSiO₂ for cell imaging and drug release, *Journal of Materials Chemistry*, 22 (2012) 14403-14409.
- [131] Z. Wang, H. Liao, H. Wu, B. Wang, H. Zhao, M. Tan, Fluorescent carbon dots from beer for breast cancer cell imaging and drug delivery, *Analytical Methods*, 7 (2015) 8911-8917.
- [132] X. Huang, F. Zhang, L. Zhu, K.Y. Choi, N. Guo, J. Guo, K. Tackett, P. Anilkumar, G. Liu, Q. Quan, Effect of injection routes on the biodistribution, clearance, and tumor uptake of carbon dots, *ACS nano*, 7 (2013) 5684-5693.
- [133] Y. Choi, S. Kim, M.H. Choi, S.R. Ryoo, J. Park, D.H. Min, B.S. Kim, Highly biocompatible carbon nanodots for simultaneous bioimaging and targeted photodynamic therapy in vitro and in vivo, *Advanced Functional Materials*, 24 (2014) 5781-5789.
- [134] I.L. Christensen, Y.-P. Sun, P. Juzenas, Carbon dots as antioxidants and prooxidants, *Journal of biomedical nanotechnology*, 7 (2011) 667-676.
- [135] C. Yang, R. Ogaki, L. Hansen, J. Kjems, B.M. Teo, Theranostic carbon dots derived from garlic with efficient anti-oxidative effects towards macrophages, *RSC Advances*, 5 (2015) 97836-97840.
- [136] A. Kleinauskas, S. Rocha, S. Sahu, Y.-P. Sun, P. Juzenas, Carbon-core silver-shell nanodots as sensitizers for phototherapy and radiotherapy, *Nanotechnology*, 24 (2013) 325103.
- [137] M. Babaei, M. Ganjalikhani, The potential effectiveness of nanoparticles as radio sensitizers for radiotherapy, *Bioimpacts*, 4 (2014) 15.
- [138] H. Wang, G. Cao, Z. Gai, K. Hong, P. Banerjee, S. Zhou, Magnetic/NIR-responsive drug carrier, multicolor cell imaging, and enhanced photothermal therapy of gold capped magnetite-fluorescent carbon hybrid nanoparticles, *Nanoscale*, 7 (2015) 7885-7895.

- [139] C. Liu, P. Zhang, X. Zhai, F. Tian, W. Li, J. Yang, Y. Liu, H. Wang, W. Wang, W. Liu, Nano-carrier for gene delivery and bioimaging based on carbon dots with PEI-passivation enhanced fluorescence, *Biomaterials*, 33 (2012) 3604-3613.
- [140] L. Hu, Y. Sun, S. Li, X. Wang, K. Hu, L. Wang, X.-j. Liang, Y. Wu, Multifunctional carbon dots with high quantum yield for imaging and gene delivery, *Carbon*, 67 (2014) 508-513.
- [141] X. Qin, A.M. Asiri, K.A. Alamry, A.O. Al-Youbi, X. Sun, Carbon nitride dots can serve as an effective stabilizing agent for reduced graphene oxide and help in subsequent assembly with glucose oxidase into hybrids for glucose detection application, *Electrochimica Acta*, 95 (2013) 260-267.
- [142] P. Shen, Y. Xia, Synthesis-modification integration: one-step fabrication of boronic acid functionalized carbon dots for fluorescent blood sugar sensing, *Analytical chemistry*, 86 (2014) 5323-5329.
- [143] F. Du, Y. Ming, F. Zeng, C. Yu, S. Wu, A low cytotoxic and ratiometric fluorescent nanosensor based on carbon-dots for intracellular pH sensing and mapping, *Nanotechnology*, 24 (2013) 365101.
- [144] Z.L. Wu, M.X. Gao, T.T. Wang, X.Y. Wan, L.L. Zheng, C.Z. Huang, A general quantitative pH sensor developed with dicyandiamide N-doped high quantum yield graphene quantum dots, *Nanoscale*, 6 (2014) 3868-3874.
- [145] B. Xu, C. Zhao, W. Wei, J. Ren, D. Miyoshi, N. Sugimoto, X. Qu, Aptamer carbon nanodot sandwich used for fluorescent detection of protein, *Analyst*, 137 (2012) 5483-5486.
- [146] J. Crawley, S. Zanardelli, C. Chion, D. Lane, The central role of thrombin in hemostasis, *Journal of thrombosis and haemostasis*, 5 (2007) 95-101.
- [147] H. Inuyama, T. Saito, J. Takagi, Y. Saito, Factor X-dependent, thrombin-generating activities on a neuroblastoma cell and their disappearance upon differentiation, *Journal of cellular physiology*, 173 (1997) 406-414.
- [148] H. Li, Y. Zhang, L. Wang, J. Tian, X. Sun, Nucleic acid detection using carbon nanoparticles as a fluorescent sensing platform, *Chemical Communications*, 47 (2011) 961-963.
- 149 J.R. Bloomer, T.A. Waldmann, K.R. McIntire, G. Klatskin, α -Fetoprotein in nonneoplastic hepatic disorders, *Jama*, 233 (1975) 38-41.

- [150] Q. Gao, J. Han, Z. Ma, Polyamidoamine dendrimers-capped carbon dots/Au nanocrystal nanocomposites and its application for electrochemical immunosensor, *Biosensors and Bioelectronics*, 49 (2013) 323-328.
- [151] J. Lu, M. Yan, L. Ge, S. Ge, S. Wang, J. Yan, J. Yu, Electrochemiluminescence of blue-luminescent graphene quantum dots and its application in ultrasensitive aptasensor for adenosine triphosphate detection, *Biosensors and Bioelectronics*, 47 (2013) 271-277.
- [152] H. Zhao, Y. Chang, M. Liu, S. Gao, H. Yu, X. Quan, A universal immunosensing strategy based on regulation of the interaction between graphene and graphene quantum dots, *Chemical Communications*, 49 (2013) 234-236.
- [153] C. Yu, X. Li, F. Zeng, F. Zheng, S. Wu, Carbon-dot-based ratiometric fluorescent sensor for detecting hydrogen sulfide in aqueous media and inside live cells, *Chemical Communications*, 49 (2013) 403-405.
- [154] Q. Huang, S. Hu, H. Zhang, J. Chen, Y. He, F. Li, W. Weng, J. Ni, X. Bao, Y. Lin, Carbon dots and chitosan composite film based biosensor for the sensitive and selective determination of dopamine, *Analyst*, 138 (2013) 5417-5423.
- [155] X. Gao, C. Ding, A. Zhu, Y. Tian, Carbon-dot-based ratiometric fluorescent probe for imaging and biosensing of superoxide anion in live cells, *Analytical chemistry*, 86 (2014) 7071-7078.
- [156] H. Dai, Y. Shi, Y. Wang, Y. Sun, J. Hu, P. Ni, Z. Li, A carbon dot based biosensor for melamine detection by fluorescence resonance energy transfer, *Sensors and Actuators B: Chemical*, 202 (2014) 201-208.
- [157] H. Zhang, H. Ming, S. Lian, H. Huang, H. Li, L. Zhang, Y. Liu, Z. Kang, S.-T. Lee, Fe₂O₃/carbon quantum dots complex photocatalysts and their enhanced photocatalytic activity under visible light, *Dalton Transactions*, 40 (2011) 10822-10825.
- [158] H. Zhang, H. Huang, H. Ming, H. Li, L. Zhang, Y. Liu, Z. Kang, Carbon quantum dots/Ag₃PO₄ complex photocatalysts with enhanced photocatalytic activity and stability under visible light, *Journal of Materials Chemistry*, 22 (2012) 10501-10506.

- [159] H. Yu, Y. Zhao, C. Zhou, L. Shang, Y. Peng, Y. Cao, L.-Z. Wu, C.-H. Tung, T. Zhang, Carbon quantum dots/TiO₂ composites for efficient photocatalytic hydrogen evolution, *Journal of Materials Chemistry A*, 2 (2014) 3344-3351.
- [160] S. Hu, R. Tian, Y. Dong, J. Yang, J. Liu, Q. Chang, Modulation and effects of surface groups on photoluminescence and photocatalytic activity of carbon dots, *Nanoscale*, 5 (2013) 11665-11671.
- [161] Y.-Q. Zhang, D.-K. Ma, Y.-G. Zhang, W. Chen, S.-M. Huang, N-doped carbon quantum dots for TiO₂-based photocatalysts and dye-sensitized solar cells, *Nano Energy*, 2 (2013) 545-552.
- [162] J. Briscoe, A. Marinovic, M. Sevilla, S. Dunn, M. Titirici, Biomass-derived carbon quantum dot sensitizers for solid-state nanostructured solar cells, *Angewandte Chemie International Edition*, 54 (2015) 4463-4468.
- [163] H. Wang, P. Sun, S. Cong, J. Wu, L. Gao, Y. Wang, X. Dai, Q. Yi, G. Zou, Nitrogen-Doped Carbon Dots for "green" Quantum Dot Solar Cells, *Nanoscale research letters*, 11 (2016) 1-6.
- [164] S.N.A.M. Yazid, S.F. Chin, S.C. Pang, S.M. Ng, Detection of Sn (II) ions via quenching of the fluorescence of carbon nanodots, *Microchimica Acta*, 180 (2013) 137-143.
- [165] H. Li, J. Zhai, X. Sun, Sensitive and selective detection of silver (I) ion in aqueous solution using carbon nanoparticles as a cheap, effective fluorescent sensing platform, *Langmuir*, 27 (2011) 4305-4308.
- [166] Y.-L. Zhang, L. Wang, H.-C. Zhang, Y. Liu, H.-Y. Wang, Z.-H. Kang, S.-T. Lee, Graphitic carbon quantum dots as a fluorescent sensing platform for highly efficient detection of Fe³⁺ ions, *Rsc Advances*, 3 (2013) 3733-3738.
- [167] Y. Dong, R. Wang, G. Li, C. Chen, Y. Chi, G. Chen, Polyamine-functionalized carbon quantum dots as fluorescent probes for selective and sensitive detection of copper ions, *Analytical chemistry*, 84 (2012) 6220-6224.
- [168] Y. Chen, Y. Wu, B. Weng, B. Wang, C. Li, Facile synthesis of nitrogen and sulfur co-doped carbon dots and application for Fe (III) ions detection and cell imaging, *Sensors and Actuators B: Chemical*, 223 (2016) 689-696.
- [169] A. Gupta, N.C. Verma, S. Khan, S. Tiwari, A. Chaudhary, C.K. Nandi, Paper strip based and live cell ultrasensitive lead sensor using carbon dots

synthesized from biological media, *Sensors and Actuators B: Chemical*, 232 (2016) 107-114.

[170] X. Wang, X. Shen, B. Li, G. Jiang, X. Zhou, H. Jiang, One-step facile synthesis of novel β -amino alcohol functionalized carbon dots for the fabrication of a selective copper ion sensing interface based on the biuret reaction, *RSC Advances*, 6 (2016) 18326-18332.

[171] C. Yuan, B. Liu, F. Liu, M.-Y. Han, Z. Zhang, Fluorescence "Turn On" detection of mercuric ion based on bis (dithiocarbamate) copper (II) complex functionalized carbon nanodots, *Analytical chemistry*, 86 (2014) 1123-1130.

[172] J. He, H. Zhang, J. Zou, Y. Liu, J. Zhuang, Y. Xiao, B. Lei, Carbon dots-based fluorescent probe for "off-on" sensing of Hg (II) and I⁻, *Biosensors and Bioelectronics*, 79 (2016) 531-535.

[173] F. Yan, D. Shi, T. Zheng, K. Yun, X. Zhou, L. Chen, Carbon dots as nanosensor for sensitive and selective detection of Hg 2⁺ and L-cysteine by means of fluorescence "Off-On" switching, *Sensors and Actuators B: Chemical*, 224 (2016) 926-935.

[174] Z.-h. Gao, Z.-z. Lin, X.-m. Chen, Z.-z. Lai, Z.-y. Huang, Carbon dots-based fluorescent probe for trace Hg 2⁺ detection in water sample, *Sensors and Actuators B: Chemical*, 222 (2016) 965-971.

[175] Y. Zhang, P. Cui, F. Zhang, X. Feng, Y. Wang, Y. Yang, X. Liu, Fluorescent probes for "off-on" highly sensitive detection of Hg 2⁺ and L-cysteine based on nitrogen-doped carbon dots, *Talanta*, 152 (2016) 288-300.

[176] Z. Wu, M. Feng, X. Chen, X. Tang, N-dots as a photoluminescent probe for the rapid and selective detection of Hg 2⁺ and Ag⁺ in aqueous solution, *Journal of Materials Chemistry B*, 4 (2016) 2086-2089.

[177] Z.-h. Gao, Z.-z. Lin, X.-m. Chen, H.-p. Zhong, Z.-y. Huang, A fluorescent probe based on N-doped carbon dots for highly sensitive detection of Hg 2⁺ in aqueous solutions, *Analytical Methods*, 8 (2016) 2297-2304.

[178] R. Patidar, B. Rebarry, G.R. Bhadu, P. Paul, Fluorescent carbon nanoparticles as label-free recognizer of Hg 2⁺ and Fe 3⁺ through effective fluorescence quenching in aqueous media, *Journal of Luminescence*, (2016).

- [179] Z. Fu, M. Yao, X. Niu, F. Cui, Facile synthesis of highly luminescent co-doped carbon nanodots for rapid, sensitive, and label-free detection of Hg²⁺, *Sensors and Actuators B: Chemical*, 226 (2016) 486-494.
- [180] J. Hou, T. Zhou, L. Wang, P. Zhang, L. Ding, Template-free microwave-assisted fabrication of carbon dots/Zn(OH)₂ composites for separation and enhancing chemical sensing, *Sensors and Actuators B: Chemical*, 230 (2016) 615-622.
- [181] X. Hou, F. Zeng, F. Du, S. Wu, Carbon-dot-based fluorescent turn-on sensor for selectively detecting sulfide anions in totally aqueous media and imaging inside live cells, *Nanotechnology*, 24 (2013) 335502.
- [182] F. Du, F. Zeng, Y. Ming, S. Wu, Carbon dots-based fluorescent probes for sensitive and selective detection of iodide, *Microchimica Acta*, 180 (2013) 453-460.
- [183] E.F. Simões, J.C.E. da Silva, J.M. Leitão, Carbon dots from tryptophan doped glucose for peroxy nitrite sensing, *Analytica chimica acta*, 852 (2014) 174-180.
- [184] L. Zhang, Y. Han, J. Zhu, Y. Zhai, S. Dong, Simple and sensitive fluorescent and electrochemical trinitrotoluene sensors based on aqueous carbon dots, *Analytical chemistry*, 87 (2015) 2033-2036.
- [185] A. Cayuela, C. Carrillo-Carrión, M.L. Soriano, W.J. Parak, M. Valcárcel, One-step synthesis and characterization of N-doped carbon nanodots for sensing in organic media, *Analytical chemistry*, 88 (2016) 3178-3185.
- [186] S. Pang, Y. Zhang, C. Wu, S. Feng, Fluorescent carbon dots sensor for highly sensitive detection of guanine, *Sensors and Actuators B: Chemical*, 222 (2016) 857-863.
- [187] J. Hou, H. Li, L. Wang, P. Zhang, T. Zhou, H. Ding, L. Ding, Rapid microwave-assisted synthesis of molecularly imprinted polymers on carbon quantum dots for fluorescent sensing of tetracycline in milk, *Talanta*, 146 (2016) 34-40.
- [188] M. Ganiga, J. Cyriac, FRET based ammonia sensor using carbon dots, *Sensors and Actuators B: Chemical*, 225 (2016) 522-528.

- [189] Q. Zhang, C. Zhang, Z. Li, J. Ge, C. Li, C. Dong, S. Shuang, Nitrogen-doped carbon dots as fluorescent probe for detection of curcumin based on the inner filter effect, *RSC Advances*, 5 (2015) 95054-95060.
- [190] H. Xu, X. Yang, G. Li, C. Zhao, X. Liao, Green synthesis of fluorescent carbon dots for selective detection of tartrazine in food samples, *Journal of agricultural and food chemistry*, 63 (2015) 6707-6714.
- [191] Z. Song, F. Quan, Y. Xu, M. Liu, L. Cui, J. Liu, Multifunctional N, S co-doped carbon quantum dots with pH-and thermo-dependent switchable fluorescent properties and highly selective detection of glutathione, *Carbon*, 104 (2016) 169-178.
- [192] X. Liu, X. Hu, Z. Xie, P. Chen, X. Sun, J. Yan, S. Zhou, In situ bifunctionalized carbon dots with boronic acid and amino groups for ultrasensitive dopamine detection, *Analytical Methods*, 8 (2016) 3236-3241.
- [193] R. Purbia, S. Paria, A simple turn on fluorescent sensor for the selective detection of thiamine using coconut water derived luminescent carbon dots, *Biosensors and Bioelectronics*, 79 (2016) 467-475.
- [194] S. Chandra, P. Das, S. Bag, D. Laha, P. Pramanik, Synthesis, functionalization and bioimaging applications of highly fluorescent carbon nanoparticles, *Nanoscale*, 3 (2011) 1533-1540.
- [195] A. Sachdev, I. Matai, S.U. Kumar, B. Bhushan, P. Dubey, P. Gopinath, A novel one-step synthesis of PEG passivated multicolour fluorescent carbon dots for potential biolabeling application, *RSC Advances*, 3 (2013) 16958-16961.
- [196] J. Peng, w. Gao, B.K. Gupta, Z. Liu, R. Romero-Aburto, L.H. Ge, L. Song, L.B. Alemany, X.B. Zhan, G.H. Gao, S.A. Vithayathil, B.A. Kaiparettu, A.A. Marti, T. Hayashi, J.J. Zhu, P.M. Ajayan, Graphene Quantum Dots Derived from Carbon Fibers, *Nano Letters*, 12 (2012) 844-849.
- [197] S.K. Bhunia, A. Saha, A.R. Maity, S.C. Ray, N.R. Jana, Carbon Nanoparticle-based Fluorescent Bioimaging Probes, *Scientific Reports*, 3 (2013) 1473.
- [198] J.R. Lakowicz, *Principles of Fluorescence Spectroscopy*, Third edition ed., Springer Science, USA, 2006.

- [199] S.J. Zhuo, M.W. Shao, S.-T. Lee, Upconversion and Downconversion Fluorescent Graphene Quantum Dots: Ultrasonic Preparation and Photocatalysis, *ACS Nano*, 2 (2012) 1059-1064.
- [200] L. Zhou, B. He, J. Huang, Amphibious fluorescent carbon dots: one-step green synthesis and application for light-emitting polymer nanocomposites, *Chemical Communications*, 49 (2013) 8078-8080.
- [201] Z.-C. Yang, M. Wang, A.M. Yong, S.Y. Wong, X.-H. Zhang, H. Tan, A.Y. Chang, X. Li, J. Wang, Intrinsically fluorescent carbon dots with tunable emission derived from hydrothermal treatment of glucose in the presence of monopotassium phosphate, *Chemical Communications*, 47 (2011) 11615-11617.
- [202] Y.P. Sun, B. Zhou, Y. Lin, W. Wang, K.A.S. Fernando, P. Pathak, M.J. Meziani, B.A. Harruff, X. Wang, H.F. Wang, P.G. Luo, H. Yang, M.E. Kose, B.L. Chen, L.M. Veca, S.Y. Xie, Quantum-Sized Carbon Dots for Bright and Colorful Photoluminescence, *Journal of the American Chemical Society*, 128 (2006) 7756-7757.
- [203] P.C. Hsu, H.T. Chang, Synthesis of high-quality carbon nanodots from hydrophilic compounds: role of functional groups, *Chemical Communications*, 48 (2012) 3984-3986.
- [204] L. Song, E. Hennink, I.T. Young, H.J. Tanke, Photobleaching kinetics of fluorescein in quantitative fluorescence microscopy, *Biophysical journal*, 68 (1995) 2588.
- [205] H. Huang, J.J. Lv, D.L. Zhou, N. Bao, Y. Xu, A.J. Wang, J.J. Feng, One-pot green synthesis of nitrogen-doped carbon nanoparticles as fluorescent probes for mercury ions, *RSC Advances*, 3 (2013) 21691-21696.
- [206] B. Cao, C. Yuan, B. Liu, C. Jiang, G. Guan, M.Y. Han, Ratiometric fluorescence detection of mercuric ion based on the nanohybrid of fluorescence carbon dots and quantum dots, *Analytica Chimica Acta*, 786 (2013) 146-152.
- [207] W.G. Kong, H.Z. Wu, Z.Y. Ye, R.F. Li, T.N. Xu, B.P. Zhang, Optical properties of pH-sensitive carbon-dots with different modifications, *Journal of Luminescence*, 148 (2014) 238-242.

- [208] Z. Zhang, J. Hao, J. Zhang, B. Zhang, J. Tang, Protein as the source for synthesizing fluorescent carbon dots by a one-pot hydrothermal route, *RSC Advances*, 2 (2012) 8599-8601.
- [209] C. Yang, R.P. Thomsen, R. Ogaki, J. Kjems, B.M. Teo, Ultrastable green fluorescence carbon dots with a high quantum yield for bioimaging and use as theranostic carriers, *Journal of Materials Chemistry B*, 3 (2015) 4577-4584.
- [210] C. Wang, Z. Xu, H. Cheng, H. Lin, M.G. Humphrey, C. Zhang, A hydrothermal route to water-stable luminescent carbon dots as nanosensors for pH and temperature, *Carbon*, 82 (2015) 87-95.
- [211] S. Bourbigot, S. Chlebicki, V. Mamleev, Thermal degradation of cotton under linear heating, *Polymer degradation and stability*, 78 (2002) 57-62.
- [212] C. Zhu, J. Zhai, S. Dong, Bifunctional fluorescent carbon nanodots: green synthesis via soy milk and application as metal-free electrocatalysts for oxygen reduction, *Chemical Communications*, 48 (2012) 9367-9369.
- [213] R.K. Agrawal, Kinetics of reactions involved in pyrolysis of cellulose I. The three reaction model, *The Canadian Journal of Chemical Engineering*, 66 (1988) 403-412.
- [214] J.A. Conesa, J. Caballero, A. Marcilla, R. Font, Analysis of different kinetic models in the dynamic pyrolysis of cellulose, *Thermochimica Acta*, 254 (1995) 175-192.
- [215] Z.-H. Wen, X.-B. Yin, Excitation-independent carbon dots, from photoluminescence mechanism to single-color application, *RSC Advances*, 6 (2016) 27829-27835.
- [216] L-glutamic acid, National Center for Biotechnology Information, PubChem Compound Database.
- [217] Z. Luo, Y. Lu, L.A. Somers, A.C. Johnson, High yield preparation of macroscopic graphene oxide membranes, *Journal of the American Chemical Society*, 131 (2009) 898-899.
- [218] D. Kozawa, Y. Miyauchi, S. Mouri, K. Matsuda, Exploring the origin of blue and ultraviolet fluorescence in graphene oxide, *The journal of physical chemistry letters*, 4 (2013) 2035-2040.

- [219] H. Zheng, Q. Wang, Y. Long, H. Zhang, X. Huang, R. Zhu, Enhancing the luminescence of carbon dots with a reduction pathway, *Chem. Commun.*, 47 (2011) 10650-10652.
- [220] L. Ilium, Chitosan and its use as a pharmaceutical excipient, *Pharmaceutical research*, 15 (1998) 1326-1331.
- [221] A. Boccaccini, S. Keim, R. Ma, Y. Li, I. Zhitomirsky, Electrophoretic deposition of biomaterials, *Journal of The Royal Society Interface*, 7 (2010) S581-S613.
- [222] M. Rinaudo, Chitin and chitosan: properties and applications, *Progress in polymer science*, 31 (2006) 603-632.
- [223] S. Paul, A.K. Ghoshal, B. Mandal, Kinetics of absorption of carbon dioxide into aqueous solutions of 2-amino-2-hydroxymethyl-1, 3-propanediol, *Separation and Purification Technology*, 68 (2009) 422-427.
- [224] H. Sigel, K.H. Scheller, B. Prijs, Metal ion/buffer interactions. Stability of alkali and alkaline earth ion complexes with triethanolamine (tea), 2-amino-2 (hydroxymethyl)-1, 3-propanediol (tris) and 2-[bis (2-hydroxyethyl)-amino] 2 (hydroxymethyl)-1, 3-propanediol (Bistris) in aqueous and mixed solvents, *Inorganica Chimica Acta*, 66 (1982) 147-155.
- [225] R.L. Dotson, Characterization and studies of some four, five and six coordinate transition and representative metal complexes of tris-(hydroxymethyl)-aminomethane, *Journal of Inorganic and Nuclear Chemistry*, 34 (1972) 3131-3138.
- [226] Y.-S. Xia, C.-Q. Zhu, Use of surface-modified CdTe quantum dots as fluorescent probes in sensing mercury (II), *Talanta*, 75 (2008) 215-221.
- [227] L. Zhou, Y. Lin, Z. Huang, J. Ren, X. Qu, Carbon nanodots as fluorescence probes for rapid, sensitive, and label-free detection of Hg 2+ and biothiols in complex matrices, *Chemical communications*, 48 (2012) 1147-1149.
- [228] X. Qin, W. Lu, A.M. Asiri, A.O. Al-Youbi, X. Sun, Microwave-assisted rapid green synthesis of photoluminescent carbon nanodots from flour and their applications for sensitive and selective detection of mercury (II) ions, *Sensors and Actuators B: Chemical*, 184 (2013) 156-162.

- [229] R. Zhang, W. Chen, Nitrogen-doped carbon quantum dots: facile synthesis and application as a “turn-off” fluorescent probe for detection of Hg²⁺ ions, *Biosensors and Bioelectronics*, 55 (2014) 83-90.
- [230] F.Y. Yan, Y. Zou, M. Wang, X.L. Mu, N. Yang, L. Chen, Highly photoluminescent carbon dots-based fluorescent chemosensors for sensitive and selective detection of mercury ions and application of imaging in living cells, *Sensors and Actuators B: Chemical*, 192 (2014) 488-495.
- [231] C. Han, R. Wang, K. Wang, H. Xu, M. Sui, J. Li, K. Xu, Highly fluorescent carbon dots as selective and sensitive “on-off-on” probes for iron (III) ion and apoferritin detection and imaging in living cells, *Biosensors and Bioelectronics*, 83 (2016) 229-236.
- [232] E.S. Costa-Júnior, E.F. Barbosa-Stancioli, A.A. Mansur, W.L. Vasconcelos, H.S. Mansur, Preparation and characterization of chitosan/poly (vinyl alcohol) chemically crosslinked blends for biomedical applications, *Carbohydrate Polymers*, 76 (2009) 472-481.
- [233] M. Thommes, Physical adsorption characterization of nanoporous materials, *Chemie Ingenieur Technik*, 82 (2010) 1059-1073.
- [234] R. Sanjeev, V. Jagannadham, R.V. Vrat, Implications of a novel interpretation of the isosbestic point, *Chemistry in New Zealand*, (2012).
- [235] D. Wang, L. Wang, X. Dong, Z. Shi, J. Jin, Chemically tailoring graphene oxides into fluorescent nanosheets for Fe³⁺ ion detection, *Carbon*, 50 (2012) 2147-2154.
- [236] S. Liu, J. Tian, L. Wang, Y. Luo, X. Sun, A general strategy for the production of photoluminescent carbon nitride dots from organic amines and their application as novel peroxidase-like catalysts for colorimetric detection of H₂O₂ and glucose, *Rsc Advances*, 2 (2012) 411-413.
- [237] Z. Qian, C. Wang, G. Du, J. Zhou, C. Chen, J. Ma, J. Chen, H. Feng, Multicolour fluorescent graphene oxide by cutting carbon nanotubes upon oxidation, *CrystEngComm*, 14 (2012) 4976-4979.
- [238] H. Li, Z. Kang, Y. Liu, S.-T. Lee, Carbon nanodots: synthesis, properties and applications, *Journal of materials chemistry*, 22 (2012) 24230-24253.

- [239] X. Wang, L. Cao, F.S. Lu, M.J. Mezziani, H.T. Li, G. Qi, B. Zhou, B.A. Harruff, F. Kermarrec, Y.-P. Sun, Photoinduced electron transfers with carbon dots, *Chemical Communications*, (2009) 3774-3776.
- [240] J. Xu, S. Sahu, L. Cao, C.E. Bunker, G. Peng, Y. Liu, K.S. Fernando, P. Wang, E.A. Gulians, M.J. Mezziani, Efficient fluorescence quenching in carbon dots by surface-doped metals-disruption of excited state redox processes and mechanistic implications, *Langmuir*, 28 (2012) 16141-16147.
- [241] C.-L. Li, C.-C. Huang, A.P. Periasamy, P. Roy, W.-C. Wu, C.-L. Hsu, H.-T. Chang, Synthesis of photoluminescent carbon dots for the detection of cobalt ions, *RSC Advances*, 5 (2015) 2285-2291.
- [242] B.B. Campos, R. Contreras-Cáceres, T.J. Badosz, J. Jiménez-Jiménez, E. Rodríguez-Castellón, J.C.E. da Silva, M. Algarra, Carbon dots as fluorescent sensor for detection of explosive nitrocompounds, *Carbon*, 106 (2016) 171-178.
- [243] H.M. Goncalves, A.J. Duarte, J.C.E. da Silva, Optical fiber sensor for Hg (II) based on carbon dots, *Biosensors and Bioelectronics*, 26 (2010) 1302-1306.
- [244] L. Henke, P.A. Piunno, A.C. McClure, U.J. Krull, Covalent immobilization of single-stranded DNA onto optical fibers using various linkers, *Analytica Chimica Acta*, 344 (1997) 201-213.
- [245] B. Gupta, S. Sharma, A long-range fiber optic pH sensor prepared by dye doped sol-gel immobilization technique, *Optics communications*, 154 (1998) 282-284.
- [246] G.J. Mohr, O.S. Wolfbeis, Optical sensors for a wide pH range based on azo dyes immobilized on a novel support, *Analytica chimica acta*, 292 (1994) 41-48.
- [247] M. Kierstan, C. Bucke, The immobilization of microbial cells, subcellular organelles, and enzymes in calcium alginate gels, *Biotechnology and Bioengineering*, 19 (1977) 387-397.
- [248] D. Poncelet, R. Lencki, C. Beaulieu, J. Halle, R. Neufeld, A. Fournier, Production of alginate beads by emulsification/internal gelation. I. Methodology, *Applied Microbiology and Biotechnology*, 38 (1992) 39-45.
- [249] R. Aravindhan, N.N. Fathima, J.R. Rao, B.U. Nair, Equilibrium and thermodynamic studies on the removal of basic black dye using calcium

alginate beads, *Colloids and Surfaces A: Physicochemical and Engineering Aspects*, 299 (2007) 232-238.

250 J. Kuljanin, I. Janković, J. Nedeljković, D. Prstojević, V. Marinković, Spectrophotometric determination of alendronate in pharmaceutical formulations via complex formation with Fe (III) ions, *Journal of pharmaceutical and biomedical analysis*, 28 (2002) 1215-1220.

[251] B.S. Berlett, R.L. Levine, E.R. Stadtman, Use of isosbestic point wavelength shifts to estimate the fraction of a precursor that is converted to a given product, *Analytical biochemistry*, 287 (2000) 329-333.

[252] J. Cornard, J. Merlin, Spectroscopic and structural study of complexes of quercetin with Al (III), *Journal of Inorganic Biochemistry*, 92 (2002) 19-27.

[253] J.H. Yoe, A.L. Jones, Colorimetric determination of iron with disodium-1, 2-dihydroxybenzene-3, 5-disulfonate, *Industrial & Engineering Chemistry Analytical Edition*, 16 (1944) 111-115.

[254] M.A. Lawrence, M.J. Celestine, E.T. Artis, L.S. Joseph, D.L. Esquivel, A.J. Ledbetter, D.M. Cropek, W.L. Jarrett, C.A. Bayse, M.I. Brewer, Computational, electrochemical, and spectroscopic studies of two mononuclear cobaloximes: the influence of an axial pyridine and solvent on the redox behaviour and evidence for pyridine coordination to cobalt (i) and cobalt (ii) metal centres, *Dalton Transactions*, (2016).

[255] R.L. Dotson, Electronic-, ESR-spectra, bonding, and structural schemes for some four-and five-coordinate mono-and Bi-nuclear copper (II) and cobalt (II) complexes of tris-(hydroxymethyl)-aminomethane, *Inorganic and Nuclear Chemistry Letters*, 9 (1973) 215-225.

[256] H.M. Leite, H.D. Moya, N. Coichev, E.A. Neves, The interaction of 2-amino-2-hydroxymethyl-1, 3-propanediol with cobalt (II) and manganese (II) ions, *Journal of Coordination Chemistry*, 49 (2000) 251-259.

[257] J.L. Hall, J.A. Swisher, D.G. Brannon, T.M. Liden, Copper (II) Ion and Nickel (II) Ion Complexes with 2-Amino-2-(hydroxymethyl)-1, 3-propanediol. Reactions with Sodium Hydroxide, *Inorganic Chemistry*, 1 (1962) 409-413.

[258] L. Bologni, A. Sabatini, A. Vacca, Complex formation equilibria between 2-amino-2 (hydroxymethyl)-1, 3,-propanediol (tris, tham) and nickel (II), copper (II),

zinc (II) and hydrogen ions in aqueous solutions, *Inorganica Chimica Acta*, 69 (1983) 71-75.

[259] J.R. Lakowicz, G. Weber, Quenching of fluorescence by oxygen. Probe for structural fluctuations in macromolecules, *Biochemistry*, 12 (1973) 4161-4170.

[260] X.-Z. Feng, Z. Lin, L.-J. Yang, C. Wang, C.-I. Bai, Investigation of the interaction between acridine orange and bovine serum albumin, *Talanta*, 47 (1998) 1223-1229.

[261] J. Min, X. Meng-Xia, Z. Dong, L. Yuan, L. Xiao-Yu, C. Xing, Spectroscopic studies on the interaction of cinnamic acid and its hydroxyl derivatives with human serum albumin, *Journal of Molecular Structure*, 692 (2004) 71-80.

[262] J. Jin, X. Zhang, Spectrophotometric studies on the interaction between pazufloxacin mesilate and human serum albumin or lysozyme, *Journal of Luminescence*, 128 (2008) 81-86.

[263] R.L. Levine, Fluorescence-quenching studies of the binding of bilirubin to albumin, *Clinical Chemistry*, 23 (1977) 2292-2301.

[264] K. Foo, B. Hameed, Insights into the modeling of adsorption isotherm systems, *Chemical Engineering Journal*, 156 (2010) 2-10.

[265] D. Karadag, Y. Koc, M. Turan, M. Ozturk, A comparative study of linear and non-linear regression analysis for ammonium exchange by clinoptilolite zeolite, *Journal of Hazardous Materials*, 144 (2007) 432-437.

[266] S. Menard, Coefficients of determination for multiple logistic regression analysis, *The American Statistician*, 54 (2000) 17-24.

[267] S.W. Ueng, L.J. Yuan, N. Lee, S.S. Lin, E.C. Chan, J.H. Weng, In vivo study of biodegradable alginate antibiotic beads in rabbits, *Journal of orthopaedic research*, 22 (2004) 592-599.

[268] P. Del Gaudio, P. Colombo, G. Colombo, P. Russo, F. Sonvico, Mechanisms of formation and disintegration of alginate beads obtained by prilling, *International journal of pharmaceutics*, 302 (2005) 1-9.

[269] N.M. Velings, M.M. Mestdagh, Physico-chemical properties of alginate gel beads, *Polymer Gels and Networks*, 3 (1995) 311-330.

[270] I.-L. Andresen, O. Smidsørod, Temperature dependence of the elastic properties of alginate gels, *Carbohydrate Research*, 58 (1977) 271-279.

[271] A. Nussinovitch, Hydrocolloid applications: gum technology in the food and other industries, (1997).